

Report

**R-21-21**

January 2024



# Characterisation of porewater of core samples from borehole KFR121

## Chemical composition in out-diffusion experiment solutions and stable isotopes

Florian Eichinger  
Joy Iannotta

SVENSK KÄRNBRÄNSLEHANTERING AB

SWEDISH NUCLEAR FUEL  
AND WASTE MANAGEMENT CO

Box 3091, SE-169 03 Solna  
Phone +46 8 459 84 00  
skb.se

SVENSK KÄRNBRÄNSLEHANTERING



ISSN 1402-3091

**SKB R-21-21**

ID 1997940

January 2024

# **Characterisation of porewater of core samples from borehole KFR121**

## **Chemical composition in out-diffusion experiment solutions and stable isotopes**

Florian Eichinger, Joy Iannotta  
Hydroisotop GmbH

*Keywords:* Matrix Porewater, Diffusion Coefficients, Water Contents, Water-Loss Porosity.

This report concerns a study which was conducted for Svensk Kärnbränslehantering AB (SKB). The conclusions and viewpoints presented in the report are those of the authors. SKB may draw modified conclusions, based on additional literature sources and/or expert opinions.

This report is published on [www.skb.se](http://www.skb.se)

© 2024 Svensk Kärnbränslehantering AB



## Abstract

Porewater investigations and determinations of petrophysical parameters were successfully conducted on 10 core samples taken from borehole KFR121 at depths between 71 and 350 m borehole length.

The main objectives of the conducted investigations are (a) the characterisation of porewater chemistry and isotopic signature in the encountered bedrock and (b) the determination of petrophysical properties such as water content, water-loss porosity and pore- and effective diffusion coefficients.

The gravimetrically determined water contents vary along the depth profile between 0.08 and 0.38 wt.%, corresponding to water-loss porosities between 0.22 and 0.94 Vol.%. Gravimetrically determined water contents agreed well with those determined by isotope diffusive exchange experiments. The bulk, wet density values are between 2.61 and 2.69 g/cm<sup>3</sup>.

Pore diffusion coefficients were determined by 1-dimensional diffusion modelling based on the fitting of Cl-elution curves, set up by taking periodic sub-samples from out-diffusion experiments. Elution curves could not be fitted by a single pore diffusion coefficient. All cores showed a faster diffusion in the outer rim of the cores and a slower diffusion in the inner parts. The average pore diffusion coefficients (10 °C) vary between  $0.4 \times 10^{-10}$  and  $0.6 \times 10^{-10}$  m<sup>2</sup>/s, corresponding to effective diffusion coefficients between  $0.9 \times 10^{-13}$  and  $4.3 \times 10^{-13}$  m<sup>2</sup>/s.

Porewater Cl- and Br-concentrations were calculated using out-diffusion concentrations and the gravimetrically determined mass of porewater. They vary between 532 and 1453 mg/kg H<sub>2</sub>O for Cl, and 2.1 and 6.9 mg/kg H<sub>2</sub>O for Br, resulting in Br·1000/Cl mass ratios between 3.4 and 5.4.

Porewater stable water isotope,  $\delta^{18}\text{O}$  and  $\delta^2\text{H}$  signatures, were determined by isotope diffusive exchange experiments. Along the depth profile encountered by borehole KFR121, porewater  $\delta^{18}\text{O}$  signatures vary between -6.57 and -13.54 ‰ V-SMOW, and  $\delta^2\text{H}$  signatures between -59.9 and -121.5 ‰ V-SMOW.

The influence of drilling fluid contamination on the porewater Cl- and Br-concentration as well as on the porewater isotope signatures was evaluated for the first time by the analyses of uranine concentrations of the out-diffusion solutions. The applied drilling fluid was traced with uranine and its concentration was analysed in the in- and outflow water. The proportions of drilling fluid on the total volume of porewater varied between 3.5 Vol.% and 21.7 Vol.%. Hence, porewater tracer concentrations and isotope signatures could be corrected for drilling fluid contamination.

## Sammanfattning

Porvattenundersökningar och bestämningar av petrofysiska parametrar genomfördes framgångsrikt på 10 kärnprov tagna från borrhål KFR121 mellan 71 m och 350 m borrhålslängd.

Huvudsyftet med de genomförda undersökningarna är (a) karakteriseringen av porvattenkemi och isotopsignatur i den kristallina berggrunden och (b) bestämning av petrofysiska egenskaper såsom vattenhalt, vattenförlustporositet (konnekterad porositet) och por- och effektiva diffusionskoefficienter.

De gravimetriskt bestämda vattenhalterna varierar längs borrhålet mellan 0,08 och 0,38 viktprocent, vilket motsvarar vattenförlustporositeter mellan 0,22 och 0,94 volymprocent. De gravimetriskt bestämda vattenhalterna stämde väl överens med de som bestämdes genom isotopdiffusiva utbytesexperimenten. Bulk-/våtdensiteter är mellan 2,61 och 2,69 g/cm<sup>3</sup>.

Pordiffusionskoefficienter bestämdes genom 1-dimensionell diffusionsmodellering baserad på anpassningen av Cl-elueringskurvor, uppställda genom att ta periodiska delprover från utdiffusionsexperiment. Elueringskurvor kunde inte anpassas med en enda pordiffusionskoefficient. Alla kärnor visade en snabbare diffusion i kärnornas yttre kant och en långsammare diffusion i de inre delarna. De genomsnittliga pordiffusionskoefficienterna (10 °C) varierar mellan  $0,4 \times 10^{-10}$  och  $0,6 \times 10^{-10}$  m<sup>2</sup>/s, motsvarande effektiva diffusionskoefficienter mellan  $0,9 \times 10^{-13}$  och  $4,3 \times 10^{-13}$  m<sup>2</sup>/s.

Porvatten Cl- och Br-koncentrationer beräknades med koncentrationer från utdiffusionsförsöken relaterade till mängden porvatten bestämd med gravimetri. De varierar mellan 532 och 1 453 mg/kg H<sub>2</sub>O för Cl och 2,1 och 6,9 mg/kg H<sub>2</sub>O för Br, vilket resulterar i Br·1 000/Cl massförhållanden mellan 3,4 och 5,4.

Även porvattnets δ<sup>18</sup>O och δ<sup>2</sup>H sammansättning bestämdes. Detta gjordes genom isotopdiffusionsexperiment. Längs den djupprofil som borrhålet KFR121 möter varierar porvatten δ<sup>18</sup>O signaturer mellan -6,57 och 13,54 ‰ V SMOW, och δ<sup>2</sup>H signaturer mellan -59,9 och -121,5 ‰ V-SMOW.

Borrvätskekontamineringens inverkan på porvattnets Cl- och Br-koncentration samt porvattnets isotopsignatur utvärderades för första gången genom analyser av uraninkoncentrationer i utdiffusionslösningarna. Det spolvatten som användes vid borrning märktes med uranin och dess koncentration analyserades i in- och utflödesvattnet från borrningen. Andelen spolvatten av den totala volymen porvatten varierade mellan 3,5 volymprocent och 21,7 volymprocent. Följaktligen kunde koncentrationer av spårämnen och isotopsignaturer i porvattnet korrigeras för förorening av spolvatten.

# Contents

<b>1</b>	<b>Introduction</b>	7
<b>2</b>	<b>Sampling and Sample Preparation</b>	9
<b>3</b>	<b>Experimental Set-ups and Analytical Methods</b>	11
3.1	Water content and water-loss porosity	11
3.2	Porewater extraction methods	12
3.2.1	Out-diffusion experiments	12
3.2.2	Isotope diffusive exchange experiments	13
3.2.3	Quantification of the influence of drilling fluid	14
<b>4</b>	<b>Petrophysical Rock Properties</b>	15
4.1	Water Content	15
4.2	Bulk density	18
4.3	Water-loss Porosity	18
<b>5</b>	<b>Chemical composition of out-diffusion experiment solutions and time series samples</b>	19
5.1	Out-diffusion test solutions	19
5.2	Elemental Elution Curves	21
<b>6</b>	<b>Elemental time series and pore diffusion coefficient of chloride</b>	33
6.1	Modelling of pore diffusion coefficients	33
<b>7</b>	<b>Porewater chloride and bromide concentrations</b>	37
7.1	Quantification of drilling fluid contamination	37
7.2	Porewater Cl- and Br-concentration	38
<b>8</b>	<b>Porewater stable isotope signatures</b>	41
<b>9</b>	<b>Uncertainties</b>	43
9.1	Uncertainties of water content determination and their control	43
9.1.1	Potential Experimental Artefacts	43
9.1.2	Potential Artefacts Induced by the Drilling Process	44
9.2	Uncertainties in bulk density determination	45
9.3	Uncertainties in the porewater Cl-, Br- and chlorine isotope determination and their control	46
9.4	Uncertainties in the determination of porewater stable isotope compositions and their control	46
<b>10</b>	<b>Summary</b>	49
	<b>References</b>	51
<b>Appendix 1</b>	Comparison of porewater results of core samples taken from borehole KFR121 with results obtained from boreholes KFM22 and KFM23	53
<b>Appendix 2</b>	Determination of <sup>36</sup> Cl/Cl ratios of porewater chloride extracted from core samples from borehole KFR121	59
<b>Appendix 3</b>	Error Calculations and Analytical Raw Data	61



# 1 Introduction

Porewater in low-permeability crystalline bedrock resides in the connected inter- and intragranular pore space of the rock matrix and forms a significant water reservoir within bedrock suites, which interacts by diffusion with fracture groundwater.

The characterisation of the porewater composition and the solute transport processes in the rock matrix contribute important information for the long-term safety assessment of deep geological repositories for radioactive waste. Thus, knowledge of the porewater composition will allow better constraints on the processes affecting the near-field of a repository. In designs where repository construction is restricted to bedrock of low permeability, the first water to interact with the repository barrier materials (e.g., bentonite, Cu-canister) will be the porewater. This interaction could result in changes of the physical and chemical properties of the various barrier materials. Knowledge of the porewater composition and its evolution over recent geological time – particularly during the last thousand to hundreds of thousands of years, in accordance with the expected lifespan of a geological repository – is considered to be of high importance.

In combination with the knowledge gained about solute transport in the rock matrix, the characterisation of porewater also contributes to a better understanding of processes related to the far-field environment around the repository. Thus, it provides valuable information about matrix diffusion as a potential retardation factor for radionuclides and allows better constraints to be placed on the palaeohydrogeological history of a repository site. Due to the exchange by diffusion between fracture groundwater and matrix porewater, released radionuclides may be temporally immobilised by matrix diffusion, and possible subsequent sorption on mineral surfaces. For radionuclides susceptible to sorption, the accessible surface areas are greatly enhanced by matrix diffusion compared to the accessible surface area on fracture surfaces alone. Matrix diffusion has the potential to increase solute transport times in the transport modelling to the biosphere from the repository.

In contrast to fracture groundwater, porewater cannot be sampled by conventional groundwater sampling techniques. The chemical and isotopic composition of porewater has, therefore, to be derived by indirect extraction techniques based on rock material. In most of these indirect extraction techniques – especially in case of rocks of a porosity below about 2 Vol.% – the original porewater concentrations are diluted and need to be back-calculated to in situ concentrations. This requires a well-defined value for the connected porosity – accessible to different solutes under in situ conditions. The derivation of such porosity values, as well as solute concentrations, is prone to various perturbations during drilling, core sampling, storage and experiments in the laboratory. The obtained data have to be carefully evaluated for potential perturbations induced by drilling activities, rock stress release and sample treatment in the laboratory in order to derive values that are representative of in situ conditions. This requires detailed knowledge about the rock composition, the rock texture, and the local stress field, because porewater composition is dependent on these factors as well.

Matrix porewater of ten core samples taken from 71 m to 349 m borehole length in the borehole KFR121 drilled at the Forsmark investigation site, was investigated for its chemical and isotopic composition using different methods. Additionally, the crystalline rock core samples were characterised for their petrophysical properties, including water content, water-loss porosity, bulk density and pore diffusion coefficient.



## 2 Sampling and Sample Preparation

A total of 10 samples were taken from borehole KFR121 between June 04, 2020 and June 14, 2020 for the characterisation of porewater (Table 2-1).

Core samples were taken between 71 m and 350 m borehole length. The borehole KFR121 was drilled with an inclination of  $-52.4^\circ$ . Converting the sampling depths to vertical depths, core samples for porewater investigations originate from depths between  $-53$  m and  $-275$  m a.s.l. (Table 2-1).

Sampling was conducted by SKB according to the instructions provided by Hydroisotop GmbH. After recovery from the borehole, the cores were photographed and immediately packed in a plastic bag, evacuated and sealed airtight. This procedure was repeated for a second plastic bag and a final Al-coated plastic layer. The samples were stored in a refrigerator on site and then sent to Hydroisotop, Germany, in a cooler.

The samples arrived in the lab between June 05 and June 18, 2020. All samples were well packed and arrived in the lab with preserved vacuum in all three layers. At Hydroisotop the samples were stored in the fridge at  $4^\circ\text{C}$  and prepared between June 10 and June 23, 2020.

The assigned samples were unpacked and immediately wrapped into Parafilm™ and cut by dry-sawing into full-diameter sections. After sawing, the surfaces of the obtained pieces were cleaned with paper towels and again wrapped into Parafilm™. The entire sample preparation was conducted as rapidly as possible (within 10 minutes) after opening the sealed bags, in order to minimise evaporation.

The analytical program conducted on each sample is summarised in Table 2-2.

**Table 2-1. Overview of the core samples taken from borehole KFR121 for porewater investigations.**

Sample ID	Borehole length			Core length m	Date arrived
	from m	to m	ave m		
KFR121 71.04–71.40	71.04	71.40	71.2	0.36	05.06.20
KFR121 124.60–124.97	124.60	124.97	124.8	0.37	09.06.20
KFR121 150.25–150.66	150.25	150.66	150.5	0.41	18.06.20
KFR121 163.83–164.19	163.83	164.19	164.0	0.36	18.06.20
KFR121 175.42–175.75	175.42	175.75	175.6	0.33	18.06.20
KFR121 187.58–187.94	187.58	187.94	187.8	0.36	18.06.20
KFR121 196.40–196.81	196.40	196.81	196.6	0.41	18.06.20
KFR121 234.33–234.75	234.33	234.75	234.5	0.42	18.06.20
KFR121 331.38–331.79	331.38	331.79	331.6	0.41	18.06.20
KFR121 349.57–349.95	349.57	349.95	349.8	0.38	18.06.20

**Table 2-2. Overview of the analytical porewater program conducted on core samples from borehole KFR121.**

Sample ID	Ave. depth m BHL	Date prepared	Diffusive isotope exchange experiments			Out-diffusion experiments						Grav. WC	
			Exp. set-up	Isotope analyses	Grav. WC	Exp. set-up	Time series	Analyses ions	Grav. WC	Density	Modelling $D_p$	Extra pieces	
KFR121 71.04–71.40	71.2	10.06.20	X	X	X	X	X	X	X	X	X	X	X
KFR121 124.60–124.97	124.8	10.06.20	X	X	X	X	X	X	X	X	X	X	X
KFR121 150.25–150.66	150.5	22.06.20	X	X	X	X	X	X	X	X	X	X	X
KFR121 163.83–164.19	164.0	22.06.20	X	X	X	X	X	X	X	X	X	X	X
KFR121 175.42–175.75	175.6	22.06.20	X	X	X	X	X	X	X	X	X	X	X
KFR121 187.58–187.94	187.8	22.06.20	X	X	X	X	X	X	X	X	X	X	X
KFR121 196.40–196.81	196.6	22.06.20	X	X	X	X	X	X	X	X	X	X	X
KFR121 234.33–234.75	234.5	22.06.20	X	X	X	X	X	X	X	X	X	X	X
KFR121 331.38–331.79	331.6	23.06.20	X	X	X	X	X	X	X	X	X	X	X
KFR121 349.57–349.95	349.8	23.06.20	X	X	X	X	X	X	X	X	X	X	X

### 3 Experimental Set-ups and Analytical Methods

Porewater investigations were performed on different types of samples that were subjected to different types of extraction and exchange experiments. This included out-diffusion experiments to characterise porewater using chemical tracers, isotope diffusive exchange experiments for the porewater  $\delta^{18}\text{O}$  and  $\delta^2\text{H}$  composition, and the determination of the water content and water-loss porosity on the respective samples.

Unless otherwise specified, the analytical work has been conducted at Hydroisotop GmbH, Germany. Experimental and analytical raw data are given in Appendix 1.

#### 3.1 Water content and water-loss porosity

The water content was determined on core material used for out-diffusion experiments (755–825 g), as well as on the core pieces used for the isotope diffusive exchange technique (182–323 g). Water contents were also determined on the lid pieces of the cores (60–164 g).

The degree of sample saturation upon arrival in the laboratory was assessed by the condition of the sample bags and of the core surface (wet vs. dry).

For water content measurements, drill-core pieces were placed in a crystallisation dish, weighed and subsequently dried at 105 °C until stable weight conditions. Before taking the initial wet weight of the full diameter core sections, the surface was allowed to dry on the balance until stable weight was achieved for  $\approx 10$  sec. During the following drying process, weighing was carried out weekly until the sample weight remained constant ( $\pm 0.002$  g) for at least 14 days.

Water contents were determined on core pieces used for out-diffusion experiments, with weights between 755–825 g and on the two cut uneven head pieces with weights between 60 and 164 g. Drying times varied between 91 and 120 days for large sized out-diffusion cores and between 35 and 105 days for the head pieces.

Gravimetric water contents were further determined on crushed core sections used for the single isotope diffusive exchange experiments after equilibration. Their masses varied between 182 and 323 g and drying times ranged between 28 and 112 days.

The calculation of the water-loss porosity (i.e., the connected porosity) from the gravimetric water content requires a measure of the grain density. In rocks of low porosity, the bulk wet density can be used as a proxy for the grain density. A measure for the bulk wet density of the rocks used for out-diffusion and aqueous extraction experiments was obtained from volume and saturated mass of the core samples. The volume was calculated from measurements of height and diameter of the core samples using a Vernier Caliper, with an error of  $\pm 0.01$  mm.

From known sample volume and wet mass, the bulk, wet and dry density is obtained by

$$\rho_{\text{bulk,wet}} = \frac{m_{\text{rock,wet}}}{V_{\text{rock}}}, \quad \rho_{\text{bulk,dry}} = \frac{m_{\text{rock,dry}}}{V_{\text{rock}}} \quad \text{Equation 3-1}$$

and the water-loss (connected) porosity,  $\phi_{\text{WL}}$ , can be calculated according to

$$\phi_{\text{WL}} = \text{WC}_{\text{wet}} * \frac{\rho_{\text{bulk,wet}}}{\rho_{\text{water}}} = \frac{m_{\text{pw}} \times 100}{r^2 \times h \times \pi \times \rho_{\text{water}}} \quad \text{Equation 3-2}$$

where  $\text{WC}_{\text{wet}}$  is the water content based on the wet weight of the rock sample and  $\rho_{\text{bulk,wet}}$  the bulk wet density of the rock. In a first approximation, the density of water,  $\rho_{\text{water}}$  is assumed to be 1 g/cm<sup>3</sup>.

Due to the low water content of the investigated crystalline rocks, the water content and water-loss porosity determined by the wet weight and bulk, wet density of the sample is essentially equal to those values calculated using the dry weight and bulk, dry density.

As shown by Gaussian error propagation (cf. Appendix 2) the error of the water content and the water-loss porosity depends predominately on the accuracy of the determination of the mass of porewater measured after unpacking (i.e., on the measured initial wet weight) and the final dry weight of the cores.

## 3.2 Porewater extraction methods

### 3.2.1 Out-diffusion experiments

Out-diffusion experiments were performed on intact full disc core samples with a diameter of 4.49–4.51 cm and a length of 18.1–19.4 cm by immersion into ultrapure water. The volume of test water varied between 172 and 188 ml. During the experiments the two water reservoirs, i.e., porewater and test water, were allowed to exchange until equilibrium. Equilibrium with respect to chloride is reached, when the Cl-concentration has been constant within the analytical error range ( $\pm 5\%$ ) over a minimum of 14 days.

After placing the core sample in the PE-vessel, the vessel was sealed and put in a vibrating water bath (40 rpm) at a constant temperature of 45 °C to accelerate diffusion. The PE-vessels were covered by a vapour-tight lid, which is equipped with two Swagelock™ valves and PEEK™ sampling lines. The core, the experiment container and the test water were weighed before and after the experiment to ensure that no loss of test water occurred during the entire experiment. At specific time intervals of initially a few days, and later a few weeks, 0.5 ml of solution were sampled using a PVC-syringe to determine the chloride concentration as a function of time. The experimental time depended on the equilibration grade in the individual experiments. All out-diffusion experiments were ended between 122 and 135 days.

After equilibrium with respect to chloride was achieved, the vessels were removed from the water bath and cooled to room temperature. Subsequently, the cylinder, the core and the remaining test water was weighed and the supernatant solution was filtered (0.45 µm) and analysed immediately for pH, sp. el. conductivity (EC) and alkalinity (acid capacity 4.3 and base capacity 8.2), and later for major cations and anions and certain trace elements and isotopes.

The major cations (Na, K, Ca, Mg, Sr) and anions (F, Cl, NO<sub>3</sub>, Br, SO<sub>4</sub>) of the final test solutions and Cl of the time series of the out-diffusion experiments were analysed by ion chromatography using a Thermo Scientific Dionex Integrion HPLC. The relative analytical error of these analyses is  $\pm 5\%$  based on multiple measurements of external check standard solutions (1s). The final test solutions with a volume of app. 100 ml were analysed undiluted and in different dilutions (1:10 and if necessary 1:20). The time series samples were analysed within days after sampling.

The alkalinity titration, pH and EC measurements were performed using Metrohm titration systems and a WTW LF325 probe.

Aluminium and silica concentrations of out-diffusion test solutions were analysed at Görtler analytical services GmbH, Germany, using a Thermo Fischer ICP-MS system with a detection limit of 0.0001 mg/l and an analytical uncertainty of 5 %.

Chloride and bromide concentrations of the experiment solution can be converted to porewater concentrations by applying mass balance calculations if equilibrium between test water and porewater is achieved. With knowledge of the mass of porewater in the rock sample, the chloride and bromide concentration of the porewater can be calculated according to:

$$C_{pw} = \frac{(m_{pw} + m_{TWi} - \sum^n m_s) * C_{TW\infty} - (m_{TWi} * C_{TWi}) + \sum^n m_s * C_s}{m_{pw}} \quad \text{Equation 3-3}$$

where  $C_{pw}$  = porewater concentration;  $m_{pw}$  = mass of porewater;  $m_{TWi}$  = initial mass of test water;  $C_{TWi}$  = initial Cl-concentration of test water;  $m_s$  = mass of sub sample used for time series;  $C_s$  = Cl-concentration of sub sample used for time series.

The term  $\Sigma m_s \cdot C_s$  (Equation 3-3) describes the amount of Cl removed from the initial experiment solution for Cl time-series samples. A correction for chloride and bromide in the initial experiment solution ( $m_{TWi} \cdot C_{TWi}$ ) is necessary if this solution is not entirely free of chloride and bromide.

The unit for the porewater concentration is given in mg/kg<sub>H<sub>2</sub>O</sub> (and not mg/l) because it is derived on a mass basis rather than a volumetric basis. This is due to the fact that the density of the porewater is not known beforehand, because it depends, inter alia, on the in situ salinity of the water, which is unknown.

### 3.2.2 Isotope diffusive exchange experiments

The isotope diffusive exchange technique to determine the water isotope composition,  $\delta^{18}\text{O}$  and  $\delta^2\text{H}$ , of the porewater and the mass of porewater was originally developed by Rogge (1997) and Rubel et al. (2002) for sedimentary rocks and later adapted for crystalline rocks by Waber and Smellie (2005, 2006) and Eichinger et al. (2006). In this method, initially saturated rock material is placed into two vapour-tight containers together with different test waters of known isotope composition. The porewater and test water is then allowed to isotopically equilibrate via the vapour phase without any direct contact between the core material and the test water. The porewater isotope composition and the water content of the rock sample can then be derived by isotope mass balance relationships. It has been shown that the uncertainty of the derived isotope composition largely depends on the ratio of porewater to test water used in the experiments (e.g., Rubel et al. 2002). For crystalline rocks, this ratio was optimised by using larger volumes of rock and smaller volumes of test water in the experiments (e.g., Waber and Smellie 2005, 2006, Eichinger et al. 2006).

For the present samples, 1.5 ml of test water were placed in a Petri dish in the centre of a glass vessel and surrounded by hand crushed core pieces of 4–6 cm<sup>3</sup> in size and with a total mass of 182 to 323 g. After an equilibration time of 60 days, the two test waters were removed and analysed by Cavity Ring Down Spectroscopy using a Picarro L 2130-I Analyser. The results for the test waters are reported relative to the V-SMOW standard with a precision of  $\pm 0.15$  ‰ for  $\delta^{18}\text{O}$  and  $\pm 1.5$  ‰ for  $\delta^2\text{H}$ .

Test water and core material were weighed before and after the experiment to assess if test water was lost on the container walls and/or rock material due to evaporation and/or condensation. To minimise condensation, 0.3 mol of NaCl were dissolved in the test water to lower its water vapour pressure. For every sample, two experiments were performed, one using test water with an isotope composition close to that expected in the porewater (“LAB-sample”) and one using test water with an isotope composition far from that expected for the porewater (“ICE-sample”).

The test water used for the LAB-sample was normal laboratory tap water, while that for the ICE-sample was water from an ice core drilled in Antarctica and provided by the University of Bern (Dr. Roland Purtschert). The equilibration time in the three reservoirs – rock porewater, test water and the air inside the container as a diaphragm – depends on the volume of the container, the size of the rock pieces and the distance of the rock pieces to the test water (see Rogge 1997). Based on the estimations of the minimum time period required for complete isotopic equilibration (cf. Eichinger et al. 2006), an experimental time of 60 days was chosen.

The isotope diffusive exchange technique delivers the  $\delta^{18}\text{O}$  and  $\delta^2\text{H}$  values and the mass of the porewater present in the connected pore space of the rock sample. These parameters are calculated from the analytical results obtained for the two test water solutions using mass balance relationships according to:

$$m_{pw} * c_{pw}|_{t=0} + m_{tw} * c_{tw}|_{t=0} = (m_{pw} + m_{tw}) * c_{tw}|_{t=\infty} \quad \text{Equation 3-4}$$

where  $m$  = mass,  $c$  = isotope ratios expressed in the  $\delta$  notation,  $pw$  = porewater,  $tw$  = test water;  $t = 0$  means the isotope concentrations at the beginning, and  $t = \infty$  at the end of the experiment.

The water content of the applied samples is calculated by transformation of Equation 3-4 to

$$WC_{IsoEx} = \left[ \frac{m_{TW(Std2)} \times m_{Rock(Std1)} \times (C_{TW^0(Std2)} - C_{TW^\infty(Std2)}) + m_{TW(Std1)} \times m_{Rock(Std2)} \times (C_{TW^\infty(Std1)} - C_{TW^0(Std1)})}{m_{Rock(Std1)} \times m_{Rock(Std2)} \times (C_{TW^\infty(Std2)} - C_{TW^\infty(Std1)})} \right] \times 100 \quad \text{Equation 3-5}$$

where  $m_{Rock}$  = mass of rock,  $Std 1$  = test solution 1 and  $Std 2$  = test solution 2.

Equation 3-6 can be set up for oxygen and hydrogen isotope ratios of the test water, resulting in two independent values for the mass of porewater.

The  $\delta^{18}\text{O}$ - and  $\delta^2\text{H}$ -values of the porewater are calculated by transformation of Equation 3-4 to

$$C_{PW} = \frac{C_{TW^0(Std1)} \times m_{TW(Std2)} \times m_{Rock(Std1)} \times (C_{TW^z(Std2)} - C_{TW^0(Std2)}) - C_{TW^z(Std2)} \times m_{TW(Std1)} \times m_{Rock(Std2)} \times (C_{TW^z(Std1)} - C_{TW^0(Std1)})}{m_{TW(Std2)} \times m_{Rock(Std1)} \times (C_{TW^z(Std2)} - C_{TW^0(Std2)}) - m_{TW(Std1)} \times m_{Rock(Std2)} \times (C_{TW^z(Std1)} - C_{TW^0(Std1)})} \quad \text{Equation 3-6}$$

The errors of the calculated  $\delta^{18}\text{O}$ ,  $\delta^2\text{H}$  and the mass of porewater are computed for each sample using Gauss' law of error propagation.

### 3.2.3 Quantification of the influence of drilling fluid

Porewater tracer concentrations and isotopic signatures can be influenced by the ingress of drilling fluid during the drilling process by the creation of a drilling disturbed zone or stress release. The drilling fluid applied for the drilling of borehole KFR121 was traced with Uranine. During the out-diffusion experiments, the potential intake of drilling fluid exchanges also with the test solution. So, the test solution of the ten out-diffusion experiments was analysed for their Uranine concentrations using a Shimadzu LC20AD HPLC. Afterwards the proportion of drilling fluid was calculated by using the mass of porewater and final Uranine concentrations according to Equation 3-7

$$m(DF) = \frac{V_{TW} + V_{PW}}{c(Uranine)_{TW,final}} \quad \text{Equation 3-7}$$

where  $m(DF)$  = mass of drilling fluid,  $V_{TW}$  = volume of test water,  $V_{PW}$  = volume of porewater determined gravimetrically,  $c(Uranine)_{TW,final}$  = Uranine concentration of final test water,  $c(Uranine)_{DF}$  = Uranine concentration of the drilling fluid.

The Uranine concentration was measured on site on the in- and out-flow water during different drilling steps (cf. Table 7-1). The concentrations of Uranine in the inflow and outflow vary and so a minimum and maximum drilling fluid contamination was determined. According to the proportion of drilling fluid, the porewater Cl-, and Br-concentrations and stable isotope signatures were corrected. The applied drilling fluid is produced from Forsmark tap water with an average Cl-concentration of 8.7 mg/l, Br-concentration of 0.015 mg/l and stable water isotope signatures of  $-9.45\text{‰}$  V-SMOW for  $\delta^{18}\text{O}$  and  $-73.8\text{‰}$  V-SMOW for  $\delta^2\text{H}$  (data are taken from the SKB database). Elemental concentrations and stable isotope signatures of the in- and outflow drilling fluids do not exist.

## 4 Petrophysical Rock Properties

The petrophysical properties determined on the drillcore samples from borehole KFR121 include the water content derived by different methods on different core pieces, the bulk wet and dry density, and the water-loss porosity. All water content measurements were conducted on originally saturated samples.

### 4.1 Water Content

Gravimetric water contents were determined on different aliquots of the ten core samples taken between 71 and 350 m borehole length.

#### **Gravimetric water contents determined on out-diffusion cores**

Gravimetric water contents on large sized 755 g to 825 g core pieces were determined by the weights taken before and after their long-term immersion in deionised water during out-diffusion experiments.

The gravimetric water contents determined on the out-diffusion cores vary between 0.08 wt.% and 0.36 wt.% (Table 4-1). The differences of the core samples determined before (b.e.) and after the experiments (a.e.), which vary between 0.008 g and 0.051 g, result in water content variations of maximum 0.01 wt.% (Table 4-1, Figure 4-1). These differences are within the error ranges determined by Gaussian error propagation. The water contents determined by taking the wet ( $WC_{wet}$ ) and dry weight ( $WC_{dry}$ ) are similar within the first two decimal places due to the low water masses in the investigated cores (Table 4-1).

**Table 4-1. Gravimetric water contents of out-diffusion core samples from borehole KFR121 calculated by the mass of cores determined before (b.e.) and after (a.e.) experiments using wet ( $WC_{wet}$ ) and dry masses ( $WC_{dry}$ ) of the individual core pieces; the error of the water content is determined by Gaussian error propagation (Appendix 2).**

Sample ID	Depth m BHL	mass core			mass porewater		$WC_{grav,wet}$		$WC_{grav,dry}$		Error $WC_{grav}$ wt.%
		wet b.e. g	wet a.e. g	$\Delta m_{core}$ g	$m_{core}$ b.e. g	$m_{core}$ a.e. g	$m_{core}$ b.e. wt.%	$m_{core}$ a.e. wt.%	$m_{core}$ b.e. wt.%	$m_{core}$ a.e. wt.%	
KFR121 71.04–71.40	71.2	786.890	786.874	-0.016	1.268	1.252	0.16	0.16	0.16	0.16	0.01
KFR121 124.60–124.97	124.8	776.026	776.011	-0.015	2.254	2.239	0.29	0.29	0.29	0.29	0.01
KFR121 150.25–150.66	150.5	825.508	825.559	0.051	0.886	0.937	0.11	0.11	0.11	0.11	0.01
KFR121 163.83–164.19	164.0	780.309	780.322	0.013	0.637	0.65	0.08	0.08	0.08	0.08	0.01
KFR121 175.42–175.75	175.6	788.053	788.038	-0.015	0.861	0.846	0.11	0.11	0.11	0.11	0.01
KFR121 187.58–187.94	187.8	780.832	780.849	0.017	1.046	1.063	0.13	0.14	0.13	0.14	0.01
KFR121 196.40–196.81	196.6	802.280	802.292	0.012	0.675	0.687	0.08	0.09	0.08	0.09	0.01
KFR121 234.33–234.75	234.5	799.855	799.847	-0.008	1.25	1.242	0.16	0.16	0.16	0.16	0.01
KFR121 331.38–331.79	331.6	755.140	755.104	-0.036	2.704	2.668	0.36	0.35	0.36	0.35	0.01
KFR121 349.57–349.95	349.8	790.287	790.323	0.036	1.873	1.909	0.24	0.24	0.24	0.24	0.01

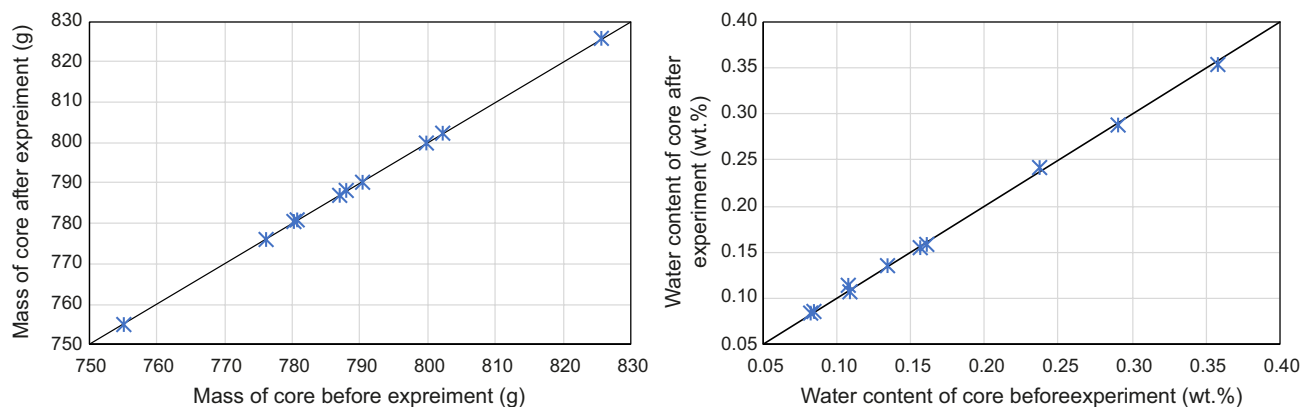


**Figure 4-1.** Left: Mass of core samples from borehole KFR121 before and after the out-diffusion experiments; the uncertainty of the core mass is  $\pm 0.05$  g; right: Water content calculated from the wet mass before and after the out-diffusion experiments of core sections from borehole KFR121; the error of the water content is determined by Gaussian error propagation (Appendix 2).

### Gravimetric water contents determined on head pieces

During sample preparation, the head pieces with weights between 60 g and 164 g were cut, weighed and dried at 105 °C to obtain a first estimate about the water contents of the investigated core samples.

The gravimetric water contents determined on the head pieces of the core samples from borehole KFR121 vary between 0.07 wt.% and 0.40 wt.%, with weighted  $WC_{\text{grav}}$  values between  $0.08 \pm 0.01$  wt.% and  $0.38 \pm 0.04$  wt.% (Table 4-2).

The water contents determined by taking the wet ( $WC_{\text{wet}}$ ) and dry weight ( $WC_{\text{dry}}$ ) are similar within the first two decimal places due to the low water masses in the investigated cores.

The water contents determined on the two head pieces of the different core samples vary partly significant (up to  $\pm 0.10$  wt.%, Table 4-2), which is most likely due to mineralogical heterogeneities.

**Table 4-2. Gravimetric water contents of head pieces of core samples from borehole KFR121; the weighted values are calculated by using the individual masses.**

Sample ID	Depth m BHL	Subsample A		Subsample B		mass <sub>total</sub> g	WC <sub>weighted</sub> wt.%	St dev wt.%
		mass g	WC wt.%	mass g	WC wt.%			
KFR121 71.04–71.40	71.2	62.45	0.12	91.59	0.21	154.04	0.17	0.06
KFR121 124.60–124.97	124.8	112.84	0.17	97.76	0.32	210.60	0.24	0.10
KFR121 150.25–150.66	150.5	103.06	0.11	74.05	0.10	177.11	0.10	0.01
KFR121 163.83–164.19	164.0	132.66	0.17	64.23	0.07	196.89	0.14	0.07
KFR121 175.42–175.75	175.6	148.99	0.16	60.48	0.11	209.47	0.15	0.04
KFR121 187.58–187.94	187.8	130.13	0.18	71.14	0.14	201.27	0.16	0.03
KFR121 196.40–196.81	196.6	94.31	0.08	64.30	0.08	158.61	0.08	0.00
KFR121 234.33–234.75	234.5	136.75	0.17	94.88	0.13	231.63	0.15	0.02
KFR121 331.38–331.79	331.6	153.65	0.40	87.35	0.34	241.00	0.38	0.04
KFR121 349.57–349.95	349.8	136.05	0.22	164.93	0.33	300.98	0.28	0.08

### Water contents determined by isotope diffusive exchange

Gravimetric water contents were determined on crushed core pieces with weights between 182 g and 323 g used for the isotope diffusive exchange experiments.

The gravimetric water contents determined on rock pieces used for isotope diffusive exchange experiments ( $WC_{\text{IsoEx,grav}}$ ) vary between 0.03 wt.% and 0.38 wt.% with weighted  $WC_{\text{IsoEx,grav}}$  values ranging from  $0.09 \pm 0.09$  wt.% to  $0.32 \pm 0.06$  wt.% (Table 4-3). The water contents determined on the different aliquots (LAB, ICE) vary partly significantly due to mineralogical heterogeneities.

The water contents determined by the isotope diffusive exchange technique ( $WC_{IsoEx}$ ) for core samples from borehole KFR121 vary between  $0.09 \pm 0.01$  wt.% and  $0.27 \pm 0.02$  wt.% (Table 4-3).

The water contents determined by isotope diffusive exchange are mostly in good agreement with those determined gravimetrically (Table 4-3, Figure 4-2). Few samples show slightly higher water contents determined by isotope diffusive exchange compared to the gravimetric water contents (Table 4-3, Figure 4-2).

**Table 4-3. Water contents determined gravimetrically on core samples from borehole KFR121 used for isotope diffusive exchange experiments ( $WC_{grav,IDE}$ ) and determined independently by isotope diffusive exchange experiments ( $WC_{IDE,ave}$ ); the gravimetric water contents determined on the rock pieces used in the experiments with LAB- and ICE-water are weighted taking their weights into account; the error of the water content is determined by Gaussian error propagation (Appendix 2).**

Sample ID	Depth m BHL	$WC_{grav}$ (LAB)		$WC_{grav}$ (ICE)		$mass_{tot}$ g	$WC_{grav,IDE}$ weighted wt. %	error wt. %	$WC_{IDE,ave}$ wt. %	error wt. %
		mass g	WC wt. %	mass g	WC wt. %					
KFR121 71.04–71.40	71.2	230.42	0.11	230.81	0.11	461.23	0.11	0.01	0.10	0.01
KFR121 124.60–124.97	124.8	221.97	0.16	222.34	0.27	444.30	0.21	0.08	0.18	0.02
KFR121 150.25–150.66	150.5	302.84	0.12	301.19	0.11	604.03	0.12	0.01	0.11	0.01
KFR121 163.83–164.19	164.0	218.44	0.11	218.95	0.08	437.39	0.10	0.02	0.09	0.01
KFR121 175.42–175.75	175.6	214.40	0.12	214.67	0.10	429.07	0.11	0.02	0.12	0.01
KFR121 187.58–187.94	187.8	227.80	0.13	226.77	0.11	454.58	0.12	0.02	0.12	0.01
KFR121 196.40–196.81	196.6	323.06	0.03	323.04	0.16	646.10	0.09	0.09	0.09	0.01
KFR121 234.33–234.75	234.5	293.24	0.14	292.76	0.14	586.01	0.14	0.01	0.13	0.01
KFR121 331.38–331.79	331.6	219.26	0.38	218.49	0.26	437.75	0.32	0.08	0.27	0.02
KFR121 349.57–349.95	349.8	182.31	0.29	182.23	0.29	364.54	0.29	0.02	0.24	0.02

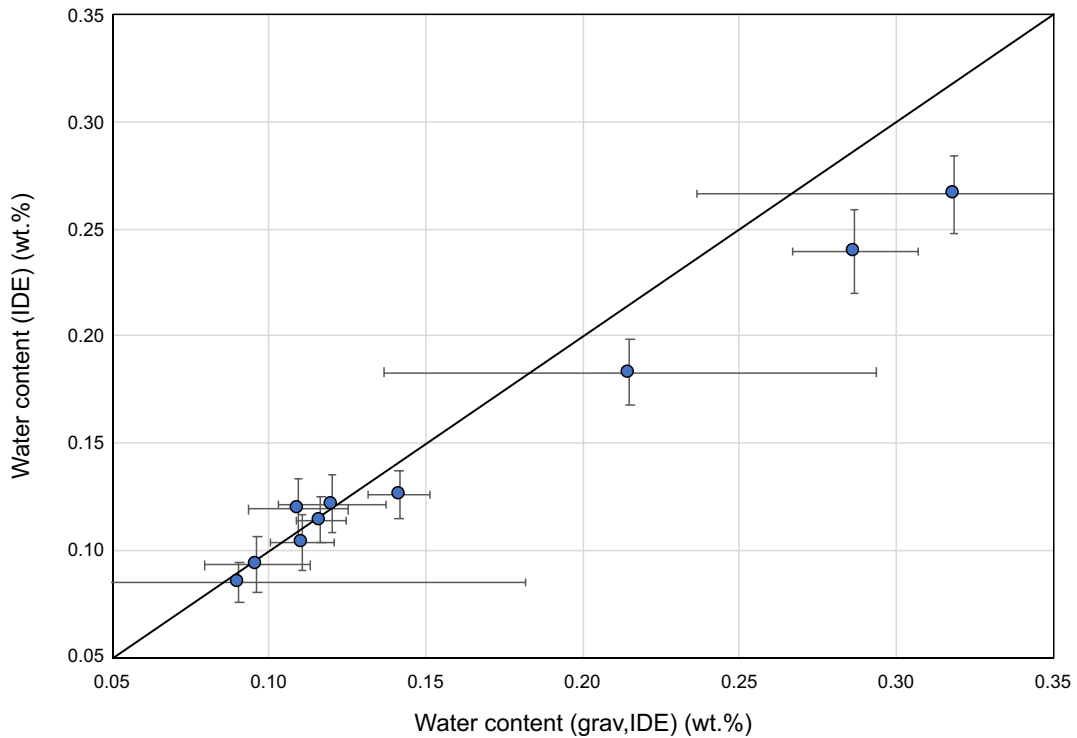


**Figure 4-2. Comparison of water contents determined by isotope diffusive exchange (IDE) and gravimetrically (grav, IDE) by wet weight; the error of the water content is determined by Gaussian error propagation.**

## 4.2 Bulk density

The bulk dry and wet density is calculated according to Equation 3-1 (Section 3.1) using the dry and wet mass of the full diameter cylindrical cores used for out-diffusion experiments and the volume of the core samples determined by measuring the height and core diameter by a Vernier Calliper.

Bulk dry and wet density values of the core samples from borehole KFR121 are similar, differing by a maximum of 0.01 g/cm<sup>3</sup>, due to the low water content of the samples, and vary between 2.61 and 2.69 g/cm<sup>3</sup> (Table 4-4).

**Table 4-4. Bulk wet and dry density determined on core samples from borehole KFR121 used for out-diffusion experiments.**

Sample ID	Depth m BHL	m (core a.e.) wet g	m (core) dry g	diameter core cm	height core cm	Volume core ccm	bulk, wet density g/ccm	bulk, dry density g/ccm
KFR121 71.04–71.40	71.2	786.92	785.62	4.50	18.51	294.39	2.67	2.67
KFR121 124.60–124.97	124.8	776.08	773.77	4.49	18.70	296.09	2.62	2.61
KFR121 150.25–150.66	150.5	825.66	824.62	4.50	19.44	309.18	2.67	2.67
KFR121 163.83–164.19	164.0	780.37	779.67	4.51	18.29	292.18	2.67	2.67
KFR121 175.42–175.75	175.6	788.08	787.19	4.51	18.43	294.42	2.68	2.67
KFR121 187.58–187.94	187.8	780.93	779.79	4.50	18.28	290.73	2.69	2.68
KFR121 196.40–196.81	196.6	802.36	801.61	4.51	18.65	297.94	2.69	2.69
KFR121 234.33–234.75	234.5	799.88	798.61	4.50	18.88	300.27	2.66	2.66
KFR121 331.38–331.79	331.6	755.27	752.44	4.51	18.07	288.67	2.62	2.61
KFR121 349.57–349.95	349.8	790.48	788.41	4.51	18.98	303.21	2.61	2.60

## 4.3 Water-loss Porosity

The water-loss (connected) porosity was calculated according to Equation 3-2 (Section 3.1) using the water content calculated by the dry and wet weight and the bulk dry/wet density of the samples. Water-loss porosities are calculated for core sections used for the out-diffusion experiments, for which the water content and the bulk dry/wet density were determined. Water-loss porosities calculated using the wet/dry mass and wet/dry density are similar within two decimals (Table 4-5).

Water-loss porosity values of core samples taken between 71 and 350 m BHL from borehole KFR121 vary between 0.22 ± 0.02 Vol.% and 0.94 ± 0.04 Vol.% (Table 4-5).

**Table 4-5. Water-loss (WL) porosity values of out-diffusion core samples calculated by water contents determined by taking the wet and dry weight and the bulk wet/dry density; errors are calculated by Gaussian error propagation.**

Sample ID	Depth m BHL	WCwet wt. %	WCdry wt. %	Bulk, wet density g/ccm	Bulk, dry density g/ccm	VL-porosity (wet) Vol. %	VL-porosity (dry) Vol. %	error Vol. %
KFR121 71.04–71.40	71.2	0.16	0.16	2.67	2.67	0.43	0.43	0.02
KFR121 124.60–124.97	124.8	0.29	0.29	2.62	2.61	0.76	0.76	0.04
KFR121 150.25–150.66	150.5	0.11	0.11	2.67	2.67	0.29	0.29	0.02
KFR121 163.83–164.19	164.0	0.08	0.08	2.67	2.67	0.22	0.22	0.02
KFR121 175.42–175.75	175.6	0.11	0.11	2.68	2.67	0.29	0.29	0.02
KFR121 187.58–187.94	187.8	0.13	0.13	2.69	2.68	0.36	0.36	0.02
KFR121 196.40–196.81	196.6	0.08	0.08	2.69	2.69	0.23	0.23	0.02
KFR121 234.33–234.75	234.5	0.16	0.16	2.66	2.66	0.42	0.42	0.02
KFR121 331.38–331.79	331.6	0.36	0.36	2.62	2.61	0.94	0.94	0.04
KFR121 349.57–349.95	349.8	0.24	0.24	2.61	2.60	0.62	0.62	0.03

## 5 Chemical composition of out-diffusion experiment solutions and time series samples

### 5.1 Out-diffusion test solutions

Out-diffusion experiments were performed on the 10 core samples taken from borehole KFR121. During the experiments the investigated rock samples were immersed in test water with a temperature of 45 °C for 122 to 135 days. The concentrations of dissolved constituents in the test solutions originate from (a) porewater, which exchanges and mixes with test water and (b) water-rock interactions, releasing reactive elements in the test water.

The core sections varied in diameter between 44.9 mm and 45.1 mm, with lengths between 181 mm and 194 mm. The corresponding volume of the sections varied between 288 cm<sup>3</sup> and 309 cm<sup>3</sup> and the saturated mass was between 755 g and 825 g. In the out-diffusion experiments, the mass ratio of experiment solution to rock samples was between 0.22 and 0.24 (Table 5-1).

During the out-diffusion experiments, a continuous exchange between porewater and test water takes place until equilibrium conditions with respect to conservative, non-reactive compounds are achieved. The exchange appears to occur mainly by diffusion (cf. Chapter 6). For chemically conservative elements, such as chloride and bromide, for which the porewater is the only source, the porewater concentration can be calculated using the gravimetrically determined porewater mass of the rock sample. For reactive elements and compounds, such as Ca, Mg, Na, K, Sr, Si, Al, F, SO<sub>4</sub> and HCO<sub>3</sub>, the contribution of mineral dissolution reactions during the experiment has to be taken into account. Those reactions are evaluated by the determination of the concentrations of the non-conservative elements taken in time-series (cf. Chapter 6.1).

The pH-value of the experiment solutions varies between 7.2 and 8.0 with a total mineralisation between 65 mg/L and 187 mg/L (EC = 90–222 µS/cm, Table 5-1). It should be noted that the total mineralisation obtained for the experiment solutions depends on the water content of the sample and the water/rock ratio used in the experiment and does not directly reflect differences in porewater salinity.

The experimental solutions contain Na (14.0–27.1 mg/L), Ca (1.3–25.2 mg/L), K (1.0–2.2 mg/L), HCO<sub>3</sub> (35.0–125 mg/L), Cl (3.2–16.4 mg/L), F (0.56–6.6 mg/L) and SO<sub>4</sub> (0.97–2.8 mg/L) in varying proportions and concentrations (Table 5-1, Figure 5-1). Bromide is present in the test solutions with concentrations ranging between < 0.01 mg/L and 0.06 mg/L. Magnesium concentrations vary between < 0.1 mg/L and 0.85 mg/L in the test solutions.

Based on the out-diffusion test solutions, samples are characterized by Na- and HCO<sub>3</sub>-dominated solutions with varying proportions of F and Cl between 71 and 164 m BHL, followed by Na-Ca-HCO<sub>3</sub> type solutions with different proportions of Cl and F between 175 and 331 m BHL and a Ca-Na-HCO<sub>3</sub> type solution for the deepest sample at 349 m BHL (Table 5-1, Figure 5-1).

Silicon (expressed as Si) is present in concentrations between 6.2 and 9.9 mg/L, Aluminium with concentrations between 0.03 and 0.14 mg/L. The concentrations of Sr are below detection limit in all test solutions.

**Table 5-1. Analytical results of test solutions of out-diffusion experiments using core samples from borehole KFR121.**

Sample		KFR121 71.04–71.40	KFR121 124.60–124.97	KFR121 150.25–150.66	KFR121 163.83–164.19	KFR121 175.42–175.75	KFR121 187.58–187.94	KFR121 196.40–196.81	KFR121 234.33–234.75	KFR121 331.38–331.79	KFR121 349.57–349.95
Ratio Exp.Water : Rock		71.2	124.8	150.5	164.0	175.6	187.8	196.6	234.5	331.6	349.8
Ratio TW:PW		0.23	0.24	0.22	0.23	0.22	0.23	0.23	0.24	0.23	0.24
		145.6	83.3	207.0	285.9	205.8	173.3	273.5	150.5	92.1	1204.9
<b>Miscellaneous properties</b>											
pH	-log(H <sup>+</sup> )	7.4	7.7	8.0	7.2	7.3	7.8	7.5	7.4	7.9	7.8
Electr. conductivity	μS/cm	131	222	126	103	118	155	90	102	201	176
Sample temperature	°C	22.9	22.6	22.6	22.5	22.9	23.1	23	22.9	23.5	23.2
Uranine	mg/l	0.066	0.12	0.18	0.14	0.15	0.14	0.16	0.15	0.13	0.086
<b>Dissolved constituents cations</b>											
Sodium (Na <sup>+</sup> )	mg/l	25.5	25.0	26.7	20.1	15.9	27.1	14.0	17.2	20.7	11.5
Potassium (K <sup>+</sup> )	mg/l	1.5	1.5	1.1	1.3	2.0	1.9	2.2	1.7	1.4	1.0
Calcium (Ca <sup>+2</sup> )	mg/l	3.0	24.6	1.3	2.3	8.1	6.7	4.1	3.8	19.8	25.2
Magnesium (Mg <sup>+2</sup> )	mg/l	0.28	0.50	< 0.1	0.22	0.57	0.45	0.41	0.34	0.85	0.34
Strontium (Sr <sup>+2</sup> )	mg/l	< 0.1	< 0.1	< 0.1	< 0.1	< 0.1	< 0.1	< 0.1	< 0.1	< 0.1	< 0.1
Aluminium (Al <sup>+3</sup> )	mg/l	0.067	0.072	0.14	0.11	0.033	0.066	0.046	0.09	0.093	0.10
Silicium (Si <sup>+4</sup> )	mg/l	8.4	6.3	6.9	7.8	7.7	6.2	6.9	9.9	6.5	6.4
<b>Anions</b>											
Flouride (F <sup>-</sup> )	mg/l	4.4	0.71	6.6	5.4	3.7	3.6	3.8	5.8	0.63	0.56
Chloride (Cl <sup>-</sup> )	mg/l	9.1	7.1	5.7	4.0	4.0	6.0	3.2	4.4	16.4	5.9
Bromide (Br <sup>-</sup> )	mg/l	0.03	0.03	0.02	< 0.01	< 0.01	< 0.01	< 0.01	0.02	0.06	< 0.01
Nitrate (NO <sub>3</sub> <sup>-</sup> )	mg/l	< 0.1	0.93	< 0.1	< 0.1	< 0.1	< 0.1	< 0.1	< 0.1	< 0.1	< 0.1
Sulphate (SO <sub>4</sub> <sup>-2</sup> )	mg/l	2.8	2.4	0.97	1.3	1.5	2.4	0.98	1.2	1.0	1.6
Total Alkalinity as HCO <sub>3</sub> <sup>-</sup>	mg/l	50.8	125	42.7	40.0	50.8	75.2	36.7	35.0	96.7	96.7
<b>Parameters calculated from analytical data</b>											
Sum of analysed constituents	mg/l	97	187	85	75	87	123	65	69	157	143
Charge balance	%	-2.18	1.21	1.07	-1.88	0.97	-1.30	-0.51	-0.96	-2.63	-0.07
<b>Water type</b>		Na-HCO <sub>3</sub> - (Cl)-(F)	Na-Ca-HCO <sub>3</sub>	Na-HCO <sub>3</sub> -F- (Cl)	Na-HCO <sub>3</sub> -F- (Cl)	Na-Ca-HCO <sub>3</sub> - (F)	Na-(Ca)- HCO <sub>3</sub> -(F)-(Cl)	Na-(Ca)- HCO <sub>3</sub> -F	Na-(Ca)- HCO <sub>3</sub> -F-(Cl)	Na-Ca- HCO <sub>3</sub> -Cl	Ca-Na-HCO <sub>3</sub>

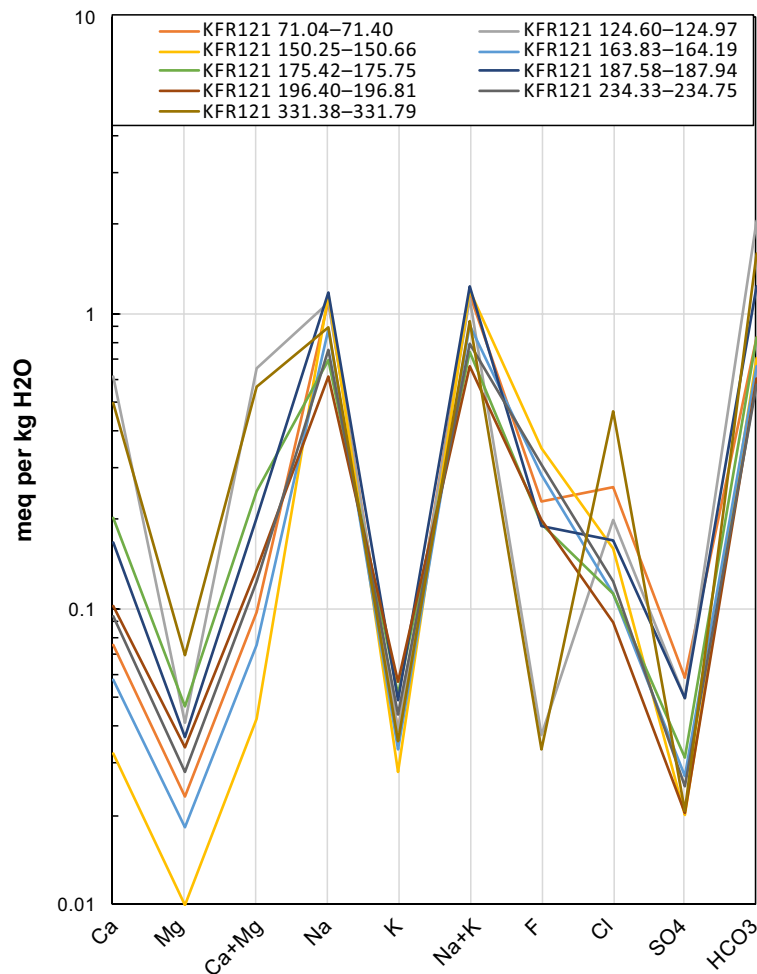


Figure 5-1. Schoeller diagram of experiment solutions from out-diffusion experiments.

## 5.2 Elemental Elution Curves

Non-destructive out-diffusion experiments are performed based on the concept of chemical exchange between porewater residing in the rock matrix and a test solution of known composition surrounding the rock sample. The experimental setup is maintained until specific conditions between the two solution reservoirs are attained. Because of the closed system character of out-diffusion experiments, the specific conditions to be achieved between the two solution reservoirs are equilibrium for any solutes for which the porewater is the only source, and which are only subjected to transport processes (i.e., Cl and Br).

For the present study, improved analytical techniques allowed continuous monitoring of all major solute concentrations in the eluate solutions during out-diffusion. This allows definition of mineral reactions and – at a later stage – possible determination of solute specific transport (e.g., ion-specific accessible porosity) in the matrix of crystalline rocks.

Porewater chloride and bromide concentrations are calculated based on the final concentrations in the out-diffusion test solutions and the water content of the individual core samples (cf. Section 3). The approach to equilibrium was monitored by periodically taking sub-samples and analysing them for their Cl- and Br-concentrations. The criterion for attainment of equilibrium conditions is defined by a difference of less than 5 % in Cl-concentrations between the last sub-sample and the final test solution at the end of the experiment. This corresponds to the analytical uncertainty of the Cl measurements. Sub-samples were collected as a function of time for all out-diffusion experiments.

Out-diffusion experiments were run for 122 to 135 days. Equilibrium with respect to Cl was attained for all samples with respect to the above mentioned criteria after 48 – 63 days (Figure 5-2).

Bromide elution curves could not be set-up for all samples, because of partly very low Br-concentrations in the test solutions. The Br-concentrations of the final test solutions could be determined due to the larger sample volume, which is sufficient for IC analyses.

Sodium, which is the main cation in the test solutions does not reach equilibrium in all out-diffusion experiments (Figure 5-2). This indicates that its concentration is influenced probably by the interaction of test water with rock forming plagioclases.

The fluoride concentrations are also increasing during the experimental time or reach equilibrium after 120–135 days of equilibration, what indicates the intake of fluoride by the dissolution of fluorite ( $\text{CaF}_2$ ).

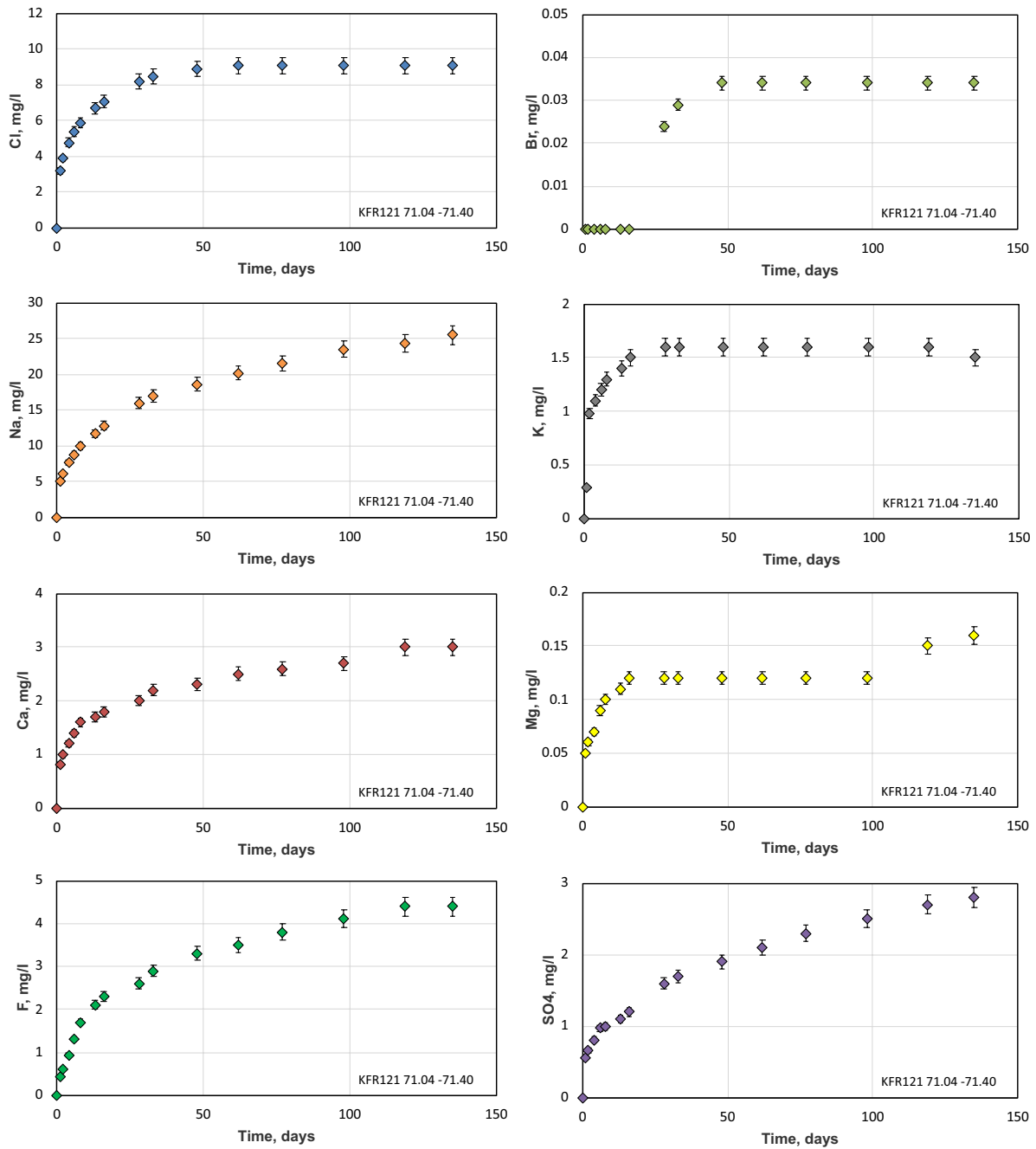


**Figure 5-2.** Elution curves of different main anions and cations set-up by the periodic sampling of test solutions of out-diffusion experiments applying core samples from borehole KFR121; the errors are the analytical uncertainty of  $\pm 5\%$ .

Sulphate shows a similar behaviour with increasing concentrations during the experimental time for most of the samples or a late equilibrium. This indicates the dissolution of sulphide minerals and the oxidation to  $\text{SO}_4$ .

In several experiments calcium also increases during the experimental time and does not reach equilibrium (Figure 5-2), what can be explained by the dissolution of calcite or plagioclase.

In most of the test solutions, magnesium does also not reach equilibrium. This might be caused by the dissolution of Mg-bearing minerals and implies that Mg cannot be taken as conservative tracer for this study.

Potassium, in contrast, achieves equilibrium in all test solutions.

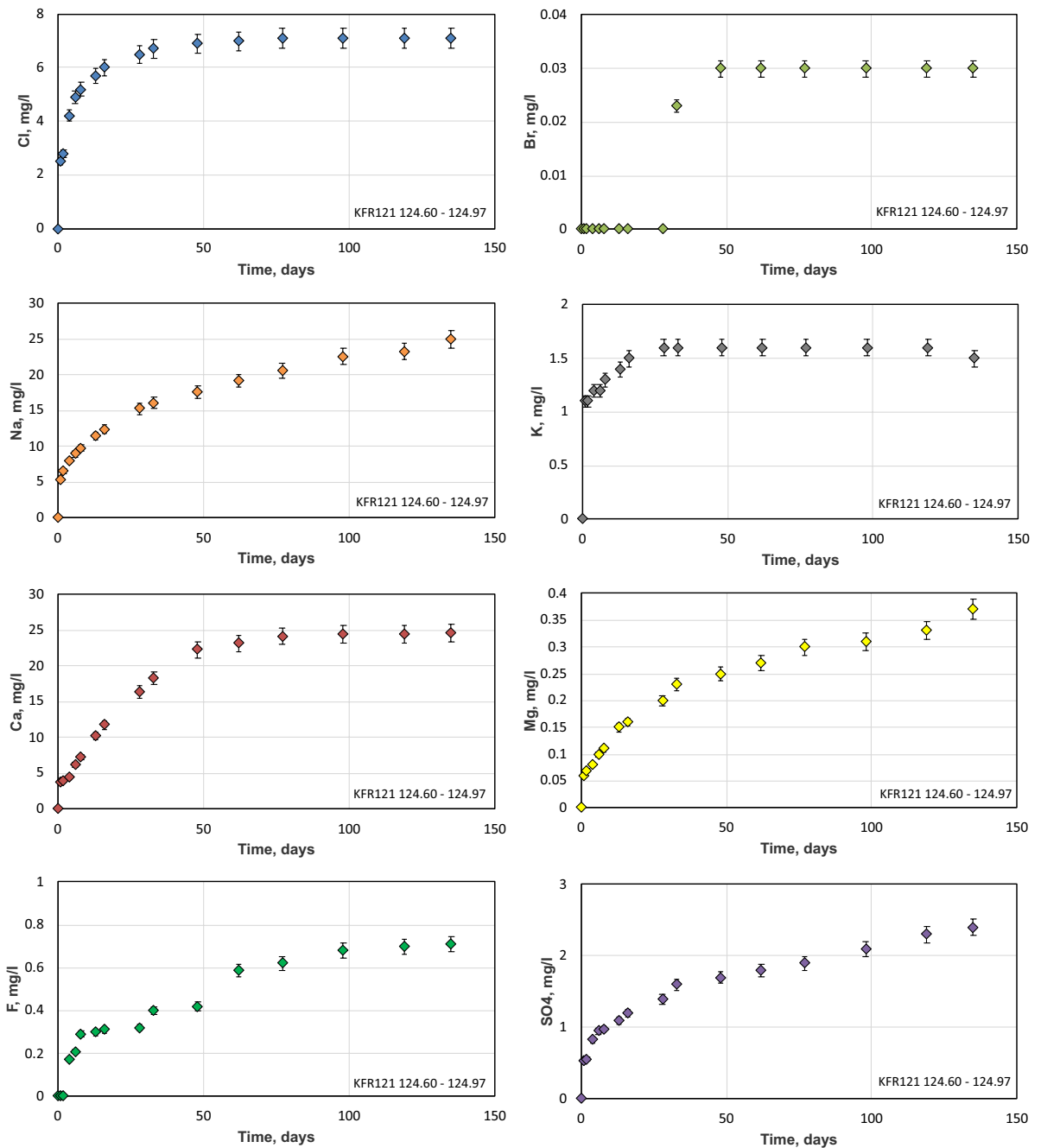


Figure 5-2. Continued.

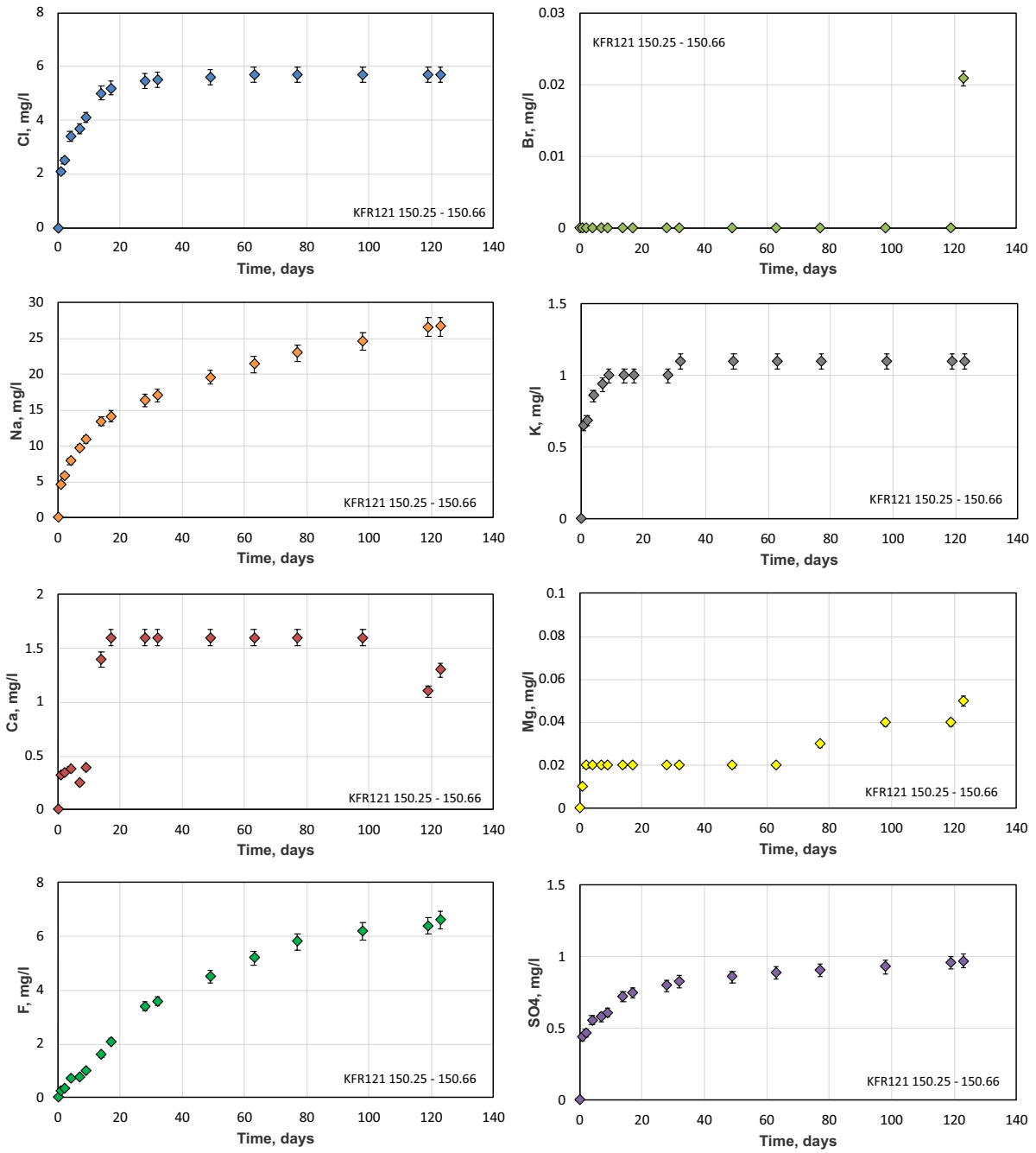


Figure 5-2. Continued.

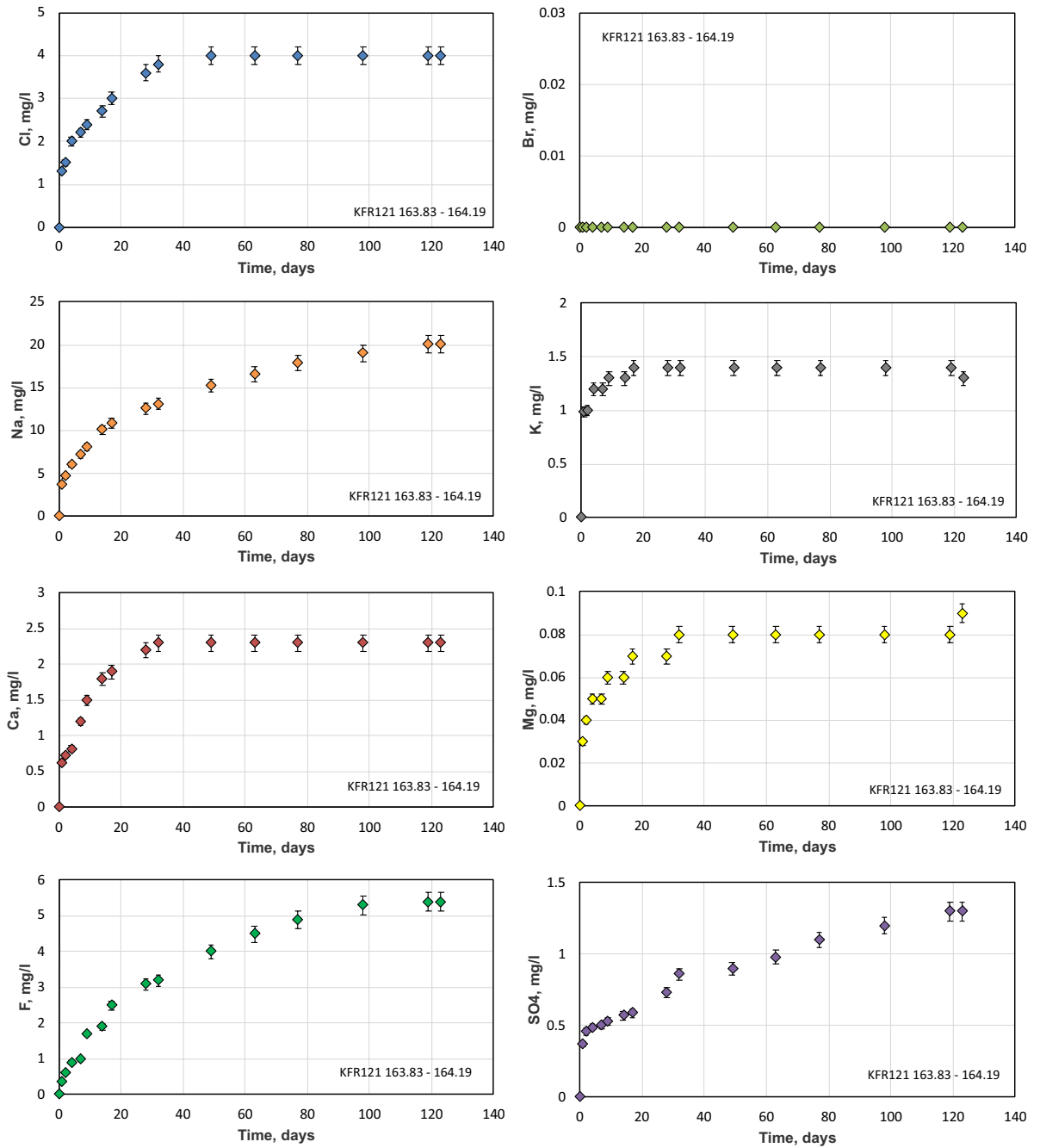


Figure 5-2. Continued.

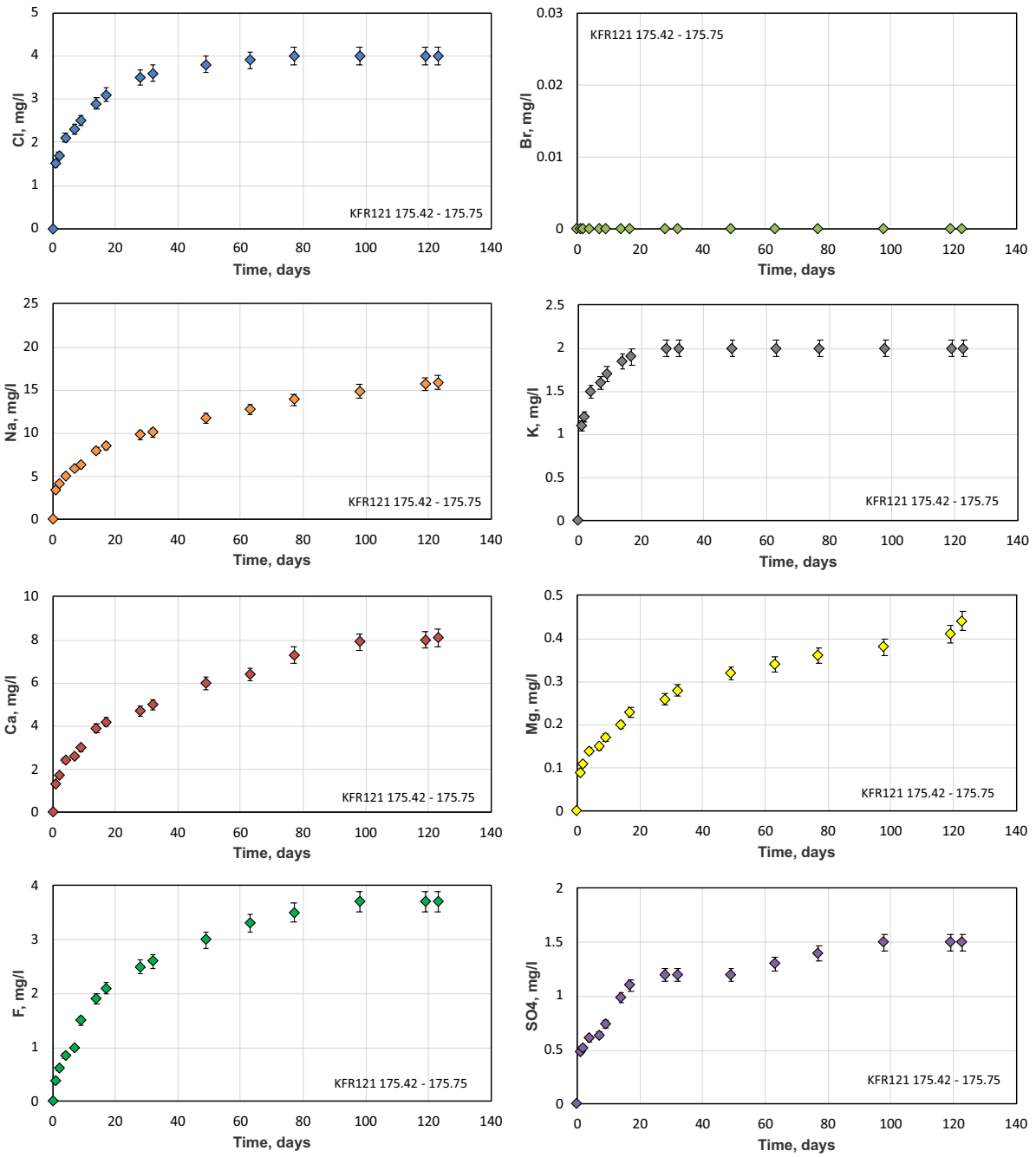


Figure 5-2. Continued.

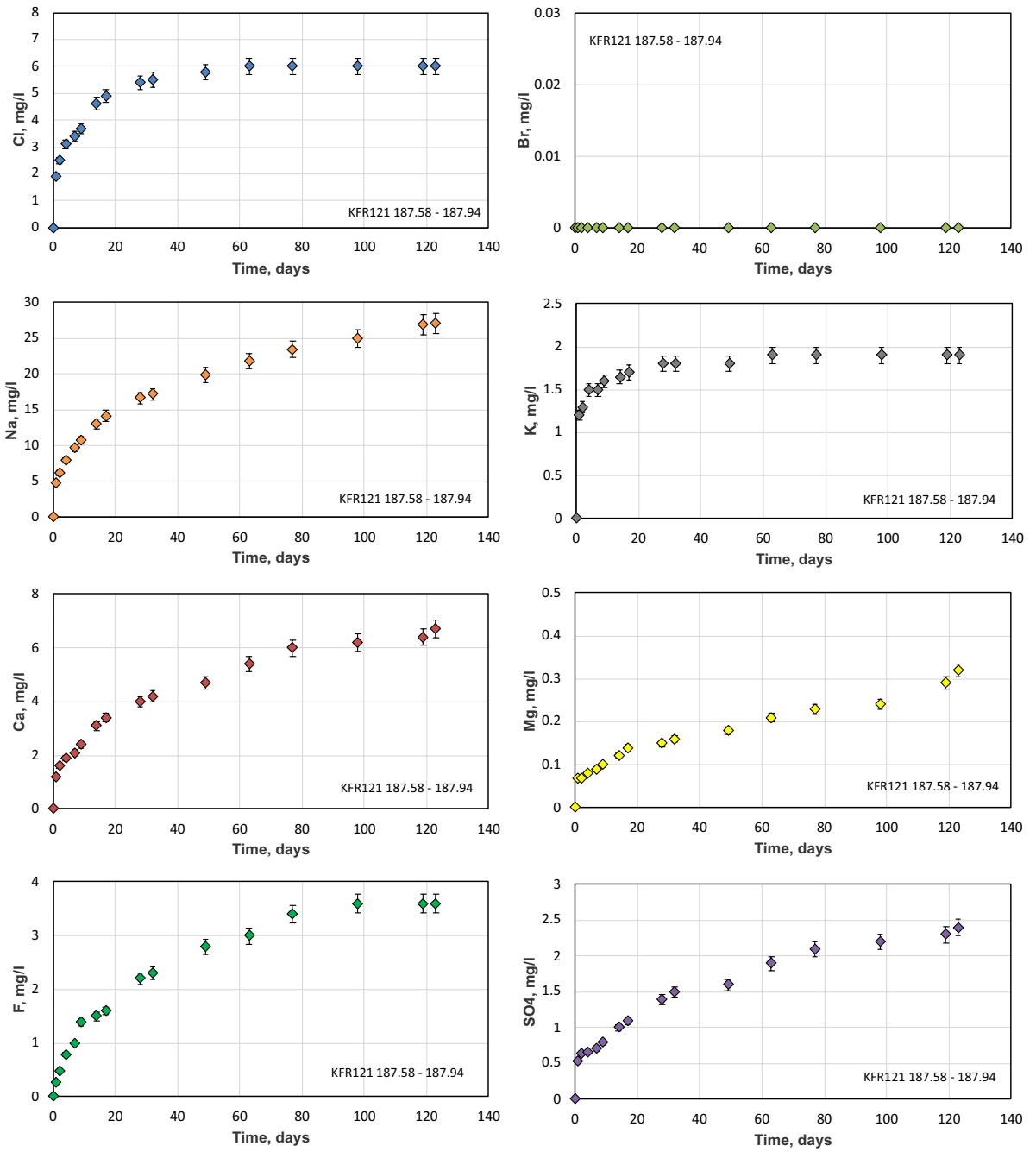


Figure 5-2. Continued.

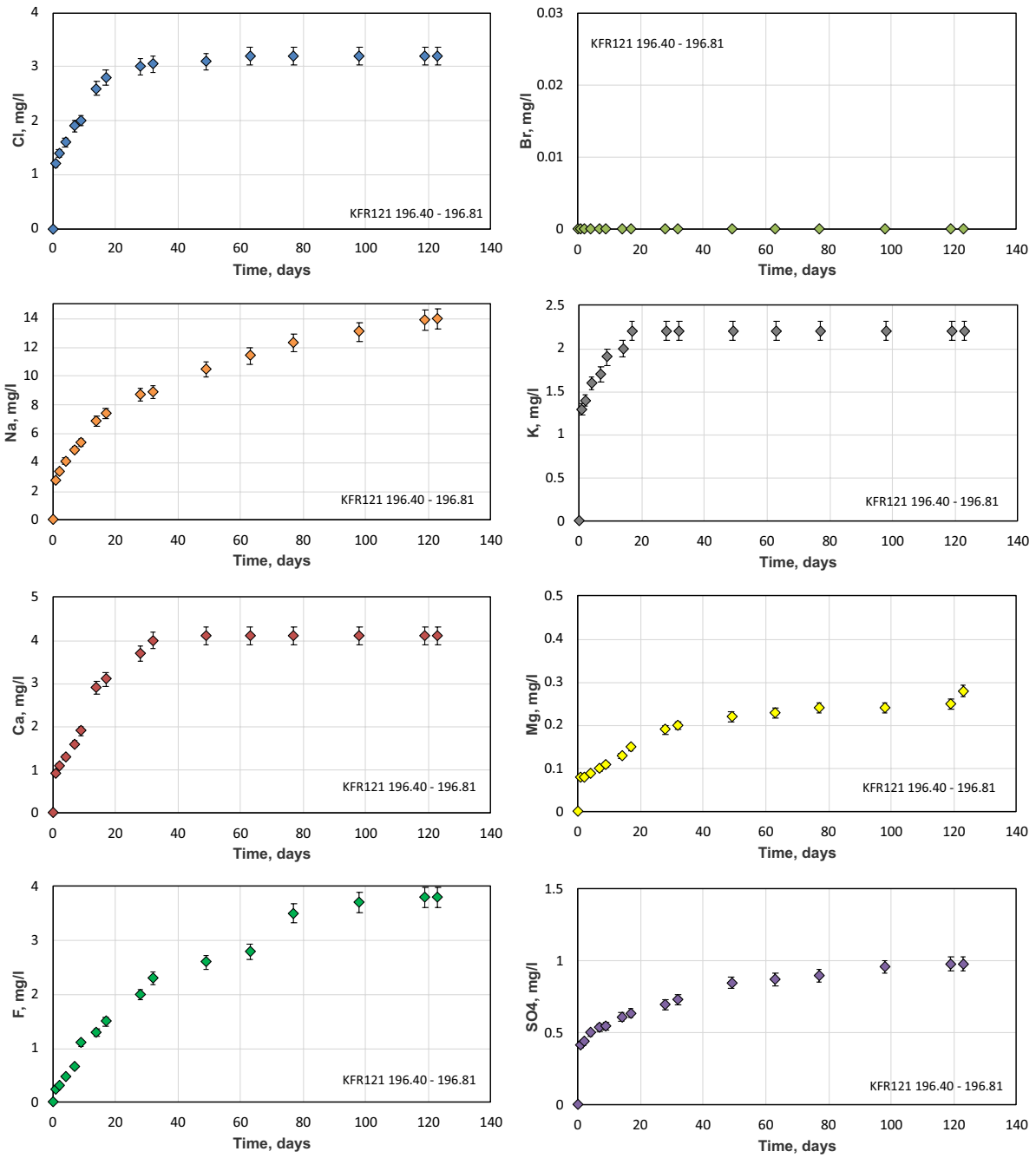


Figure 5-2. Continued.

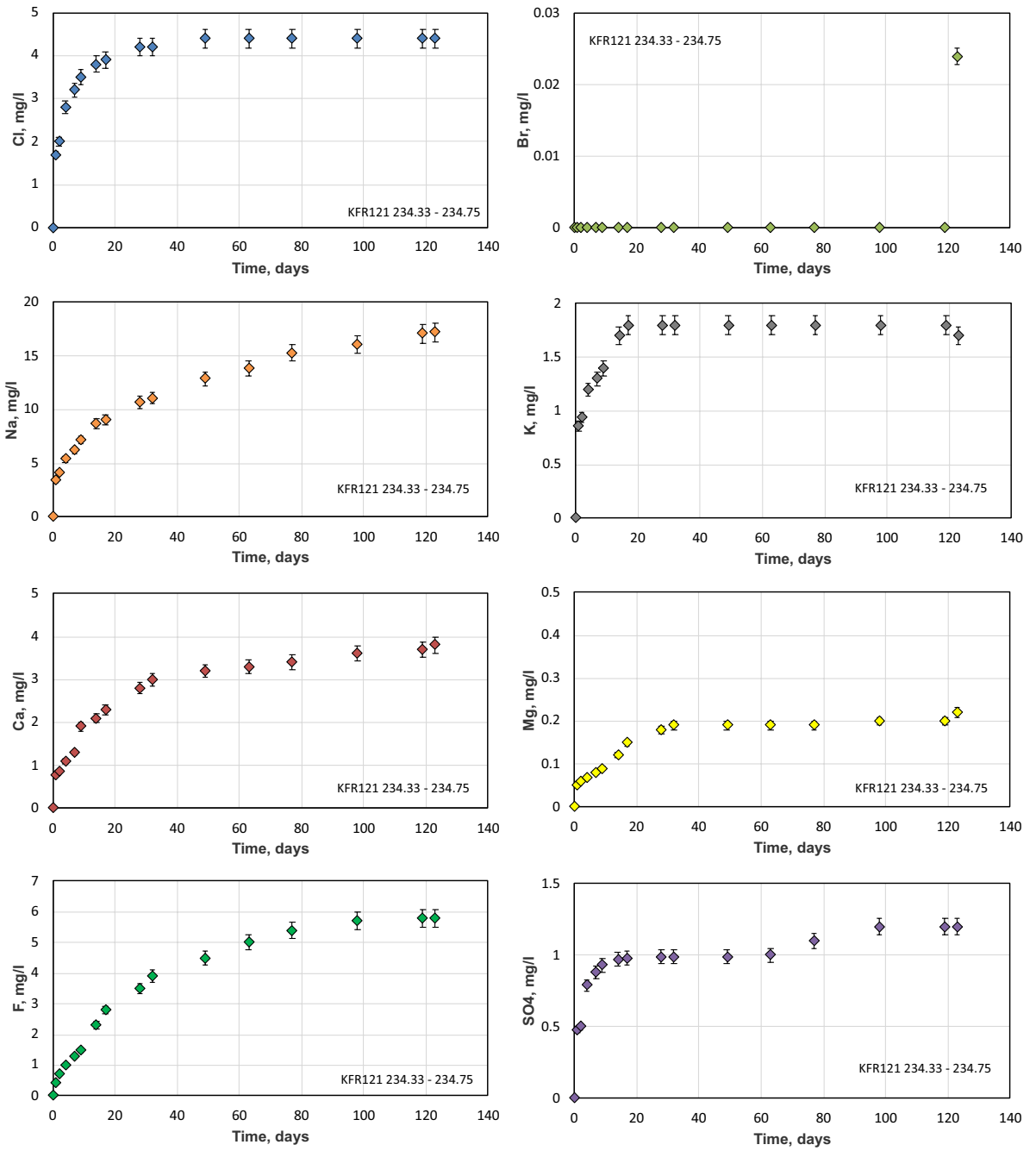


Figure 5-2. Continued.

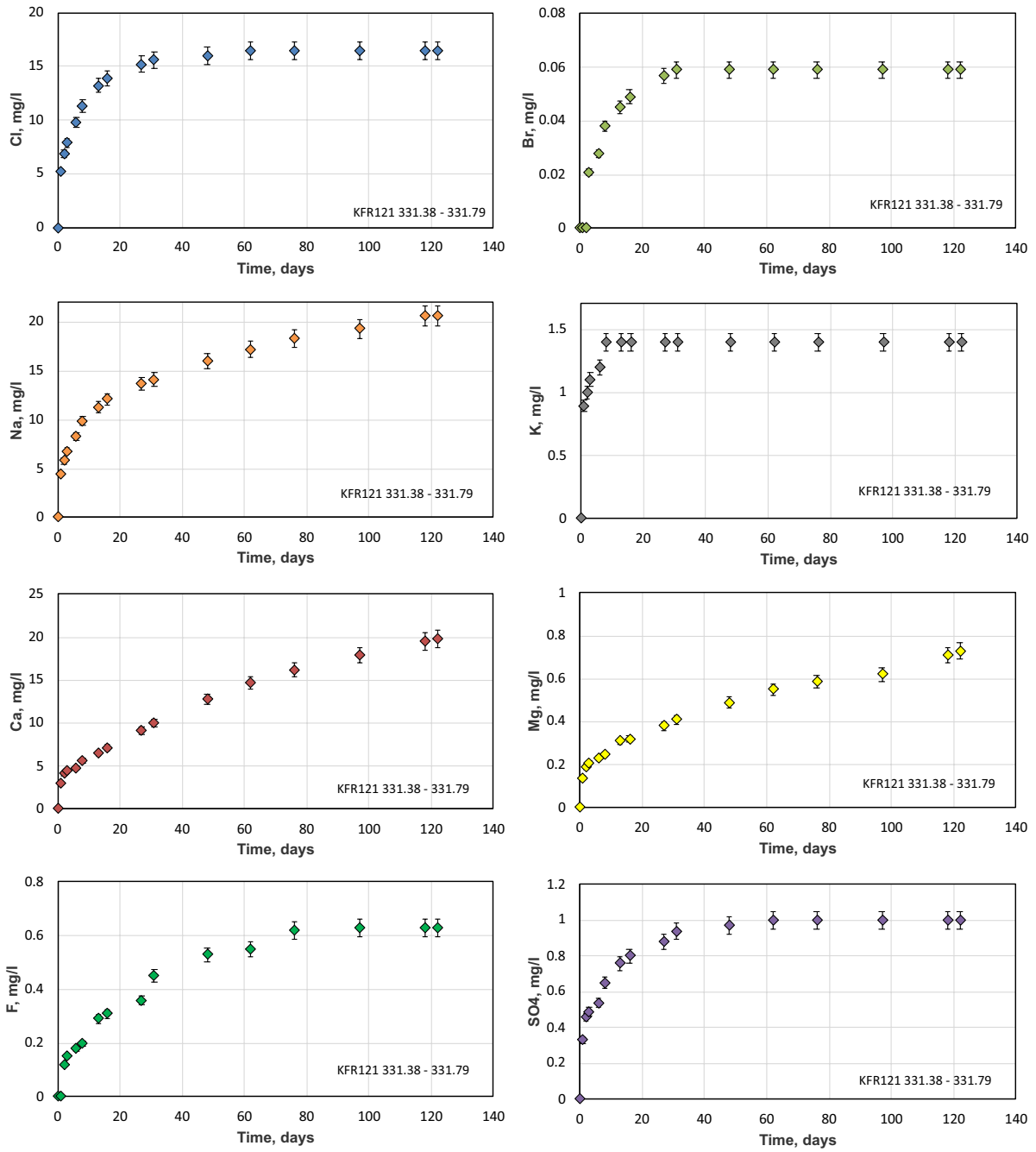


Figure 5-2. Continued.

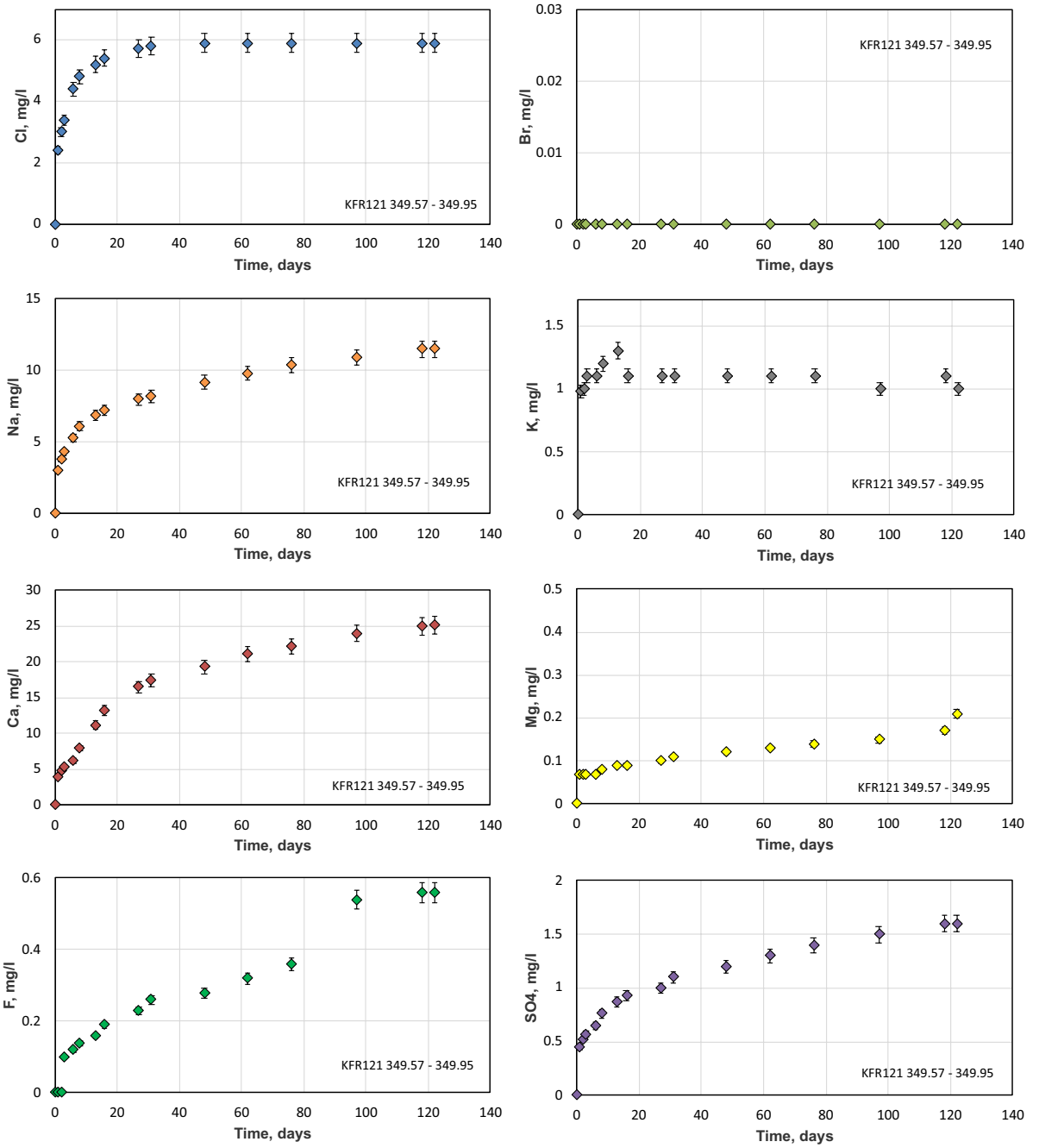


Figure 5-2. Continued.



## 6 Elemental time series and pore diffusion coefficient of chloride

### 6.1 Modelling of pore diffusion coefficients

Chloride pore diffusion coefficients were derived by modelling the chloride breakthrough curves obtained from the out-diffusion experiments of all 10 samples from borehole KFR121. The chloride breakthrough curves are deduced from the Cl contents in the small-sized subsamples that were collected periodically during the out-diffusion experiments (cf. Sections 3.2.1, 5.2). The pore diffusion coefficient is obtained by fitting the observed data with an analytical solution for one-dimensional radial diffusion out of the cylinder into a well-mixed solution reservoir (Crank 1975). The applied model (T. Gimmi, RWI, University of Bern) is restricted to homogeneous hydraulic properties (porosity, diffusion coefficient) across the core cylinder, and cannot consider heterogeneous properties due to rock anisotropy or induced effects, such as a drilling disturbed zone and/or stress release (Meier et al. 2015).

The pore diffusion coefficient,  $D_p$ , of a solute in a geological media mainly depends on the shape and size of water conducting pores (constrictivity) and on the pathways given by the connected pore network (tortuosity, cf. e.g., Ohlsson and Neretnieks 1995). It can be defined as:

$$D_p = D_w \frac{\delta_D}{\tau^2} \quad \text{Equation 6-1}$$

where  $D_p$  = pore-diffusion coefficient in  $\text{m}^2/\text{s}$ ;  $D_w$  = diffusion coefficient in pure water in  $\text{m}^2/\text{s}$ ;  $\delta_D$  = constrictivity;  $\tau$  = tortuosity; the term  $\delta_D/\tau^2$  is called the geometry factor.

In a first assumption the pore diffusion coefficient of a given species,  $D_p$ , can be converted to the effective diffusion coefficient of this species,  $D_e$ , according to:

$$D_e = D_p \Phi_{WC} \quad \text{Equation 6-2}$$

where  $D_e$  is the effective diffusion coefficient in  $\text{m}^2/\text{s}$  and  $\Phi_{WC}$  the species-accessible porosity.

The shape of the Cl elution curves obtained for all core samples from borehole KFR121 suggests a heterogeneous transport system from the rim to the centre of the core (Figure 6-1). The initial slopes are steep (in the transient state) during the first five to ten days of out-diffusion, and become more moderate later in the experiment.

The quality of the  $D_p$  fits is controlled by the difference ( $\Delta_{\text{meas-mod}}$ ) of the measured and modelled Cl-concentration at equal time and shown graphically by logarithmic plots (Figure 6-1). To determine the lowest  $\Delta_{\text{meas-mod}}$  values, a stepwise adjustment of the single points was conducted and the  $\Delta_{\text{meas-mod}}$  values were calculated for every measured point. The determination of the best fits per sampling point indicates a gradual decrease of the modelled pore diffusion coefficients as diffusion progresses deeper into the cores.

The modelled  $D_p$  values, which were determined at 45 °C, are additionally converted to 10 °C by the Stoke-Einstein equation (Lide 1994).

For the investigated core samples, the influence of the disturbed zone results in a pore diffusion coefficient that is a factor 2 to 4 higher than that of the inner core (Table 6-1).

The average pore diffusion coefficients ( $D_p$ ) of the 10 crystalline core samples vary between 0.4 and  $0.6 \times 10^{-10} \text{ m}^2/\text{s}$  (10 °C), resulting in effective diffusion coefficients ( $D_e$ ) between 0.9 and  $4.3 \times 10^{-13} \text{ m}^2/\text{s}$  (10 °C, Table 6-1).

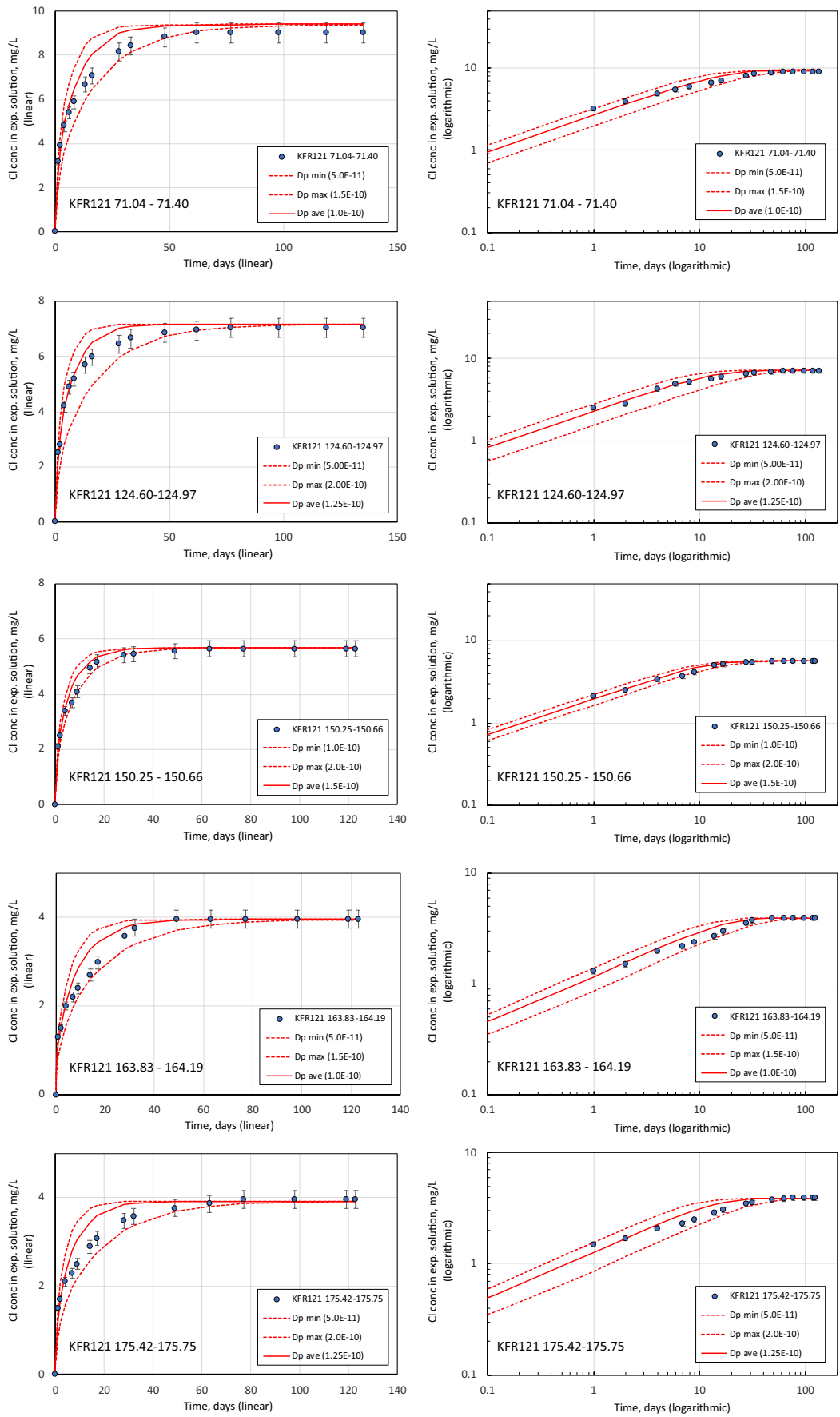


**Figure 6-1.** Maximum ( $D_p(\text{max})$ ) and minimum ( $D_p(\text{min})$ ) pore diffusion coefficients (45 °C) determined by a best fit of Cl elution curves in linear and logarithmic time and concentration scale; the solid lines mark the average diffusion coefficients (45 °C,  $D_p(\text{ave})$ ).

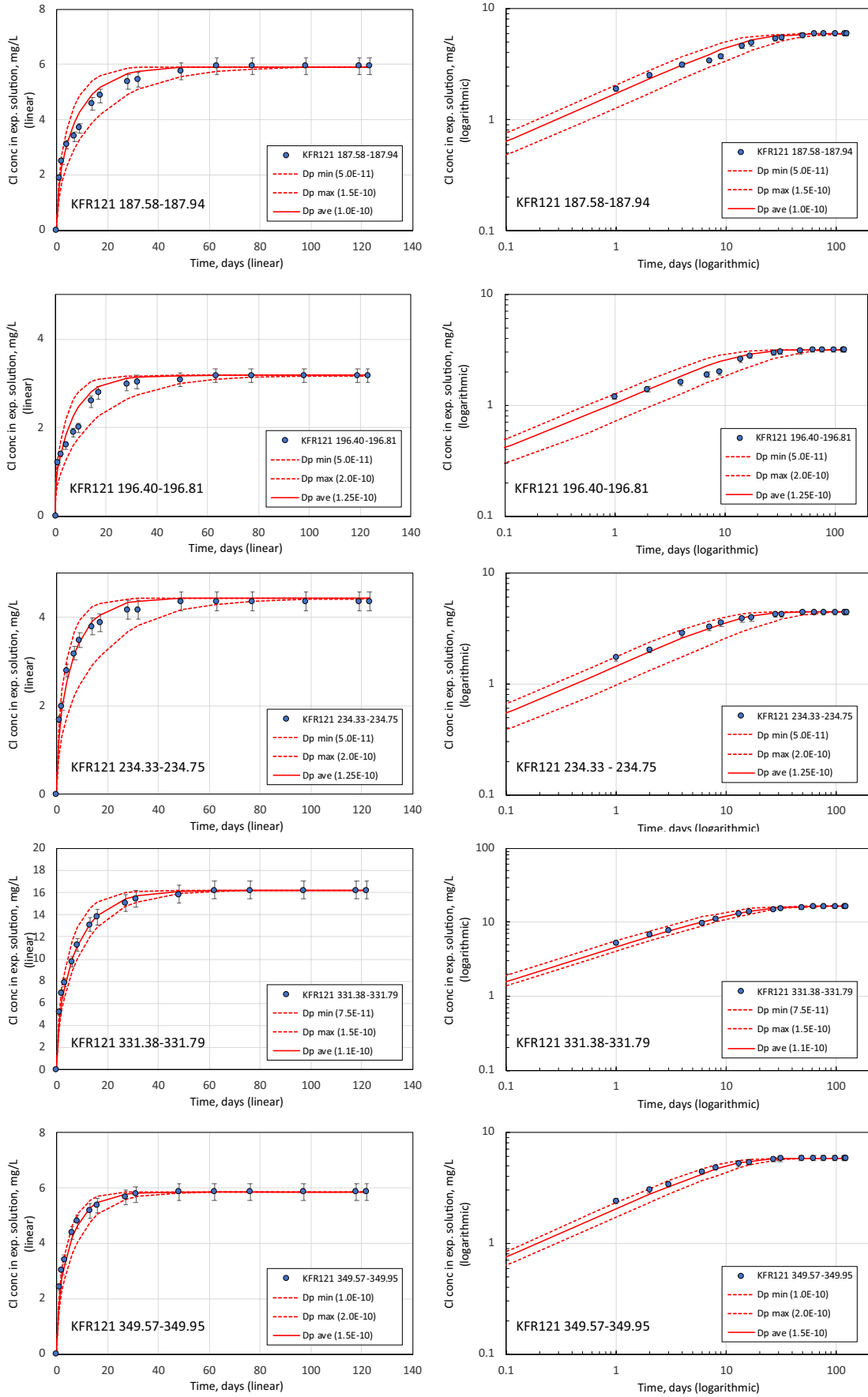


Figure 6-1. Continued.

**Table 6-1. Minimum (min), maximum (max) and average (avg) pore and effective diffusion coefficients determined by 1-dimensional modelling of Cl-elution curves of out-diffusion experiments conducted on core samples from borehole KFR121 at 45 °C and calculated by the Stoke-Einstein equation for 10 °C.**

Sample ID	Depth m BHL	WL-Porosity Vol. %	D(P)-E-10 (45 °C)			D(P)-E-10 (10 °C)			D(e)-E-13 (10 °C)		
			min m <sup>2</sup> /s	max m <sup>2</sup> /s	ave m <sup>2</sup> /s	min m <sup>2</sup> /s	max m <sup>2</sup> /s	ave m <sup>2</sup> /s	min m <sup>2</sup> /s	max m <sup>2</sup> /s	ave m <sup>2</sup> /s
KFR121 71.04–71.40	71.2	0.43	0.5	1.5	1.0	0.2	0.6	0.4	0.9	2.6	1.7
KFR121 124.60–124.97	124.8	0.76	0.5	2.0	1.3	0.2	0.8	0.5	1.5	6.2	3.9
KFR121 150.25–150.66	150.5	0.29	1.0	2.0	1.5	0.4	0.8	0.6	1.2	2.3	1.7
KFR121 163.83–164.19	164.0	0.22	0.5	1.5	1.0	0.2	0.6	0.4	0.4	1.3	0.9
KFR121 175.42–175.75	175.6	0.29	0.5	2.0	1.3	0.2	0.8	0.5	0.6	2.3	1.4
KFR121 187.58–187.94	187.8	0.36	0.5	1.5	1.0	0.2	0.6	0.4	0.7	2.2	1.5
KFR121 196.40–196.81	196.6	0.23	0.5	2.0	1.3	0.2	0.8	0.5	0.5	1.8	1.1
KFR121 234.33–234.75	234.5	0.42	0.5	2.0	1.3	0.2	0.8	0.5	0.8	3.4	2.1
KFR121 331.38–331.79	331.6	0.94	0.75	1.5	1.1	0.3	0.6	0.5	2.9	5.7	4.3
KFR121 349.57–349.95	349.8	0.62	1.0	2.0	1.5	0.4	0.8	0.6	2.5	5.0	3.8

## 7 Porewater chloride and bromide concentrations

The conservative behaviour of chloride and bromide, the absence of Cl and Br bearing minerals in the rock and the non-destructive character of the out-diffusion method make the porewater the only source for dissolved Cl and Br in the experimental solution. This allows calculation of the Cl- and Br-concentration in the porewater using mass balance according to Equation 3-3 (Section 3.2.1), given that equilibrium in the out-diffusion experiments is achieved. As shown by their chloride and bromide elution curves, this latter condition is fulfilled for all samples within the applied constraints (cf. Section 5.2).

### 7.1 Quantification of drilling fluid contamination

Porewater Cl- and Br-concentrations determined by out-diffusion experiments can be influenced by the ingress of drilling fluid in newly created pore space created by the drilling process (drilling disturbed zone) and by the release of the lithostatic pressure regime (stress release).

Waber et al. (2011) evaluated the influence of drilling fluid on the porewater Cl-concentration of granodioritic drillcore material from 560 m below surface at Forsmark by using artificial traced drilling fluid. In their study the combined effects of stress release and the drilling process resulted in a maximum contamination of the derived porewater Cl-concentration of about 8 %. Similar results were obtained by Meier et al. (2015), which found maximum contamination effects on porewater Cl-concentrations on granitic gneisses from Olkiluoto by drilling fluid between 0.9 and 8.9 %.

The applied drilling fluid was traced with uranine, which concentration was periodically measured in the in- and outflowing water.

The uranine concentrations were analysed in the final out-diffusion solutions and the proportion of drilling fluid was calculated according to Equation 3-7 (Section 3.2.3).

The uranine concentrations of the applied drilling fluid vary widely between 0.109 mg/L and 0.319 mg/L (Table 7-1), those of the out-flow taken during different drilling stages between 0.062 mg/L and 0.184 mg/L (Table 7-1). The uranine concentrations of the out-flow are of a factor 1.1 to 4.3 lower than the in-flow drilling fluid. The concentration decrease is caused by the influence of inflowing groundwater.

For the evaluation of the proportion of drilling fluid in the investigated core samples, the inflow uranine concentrations were taken into account, because they reflect the fluid, which is in direct contact during the actual drilling process.

For the production of drilling fluid tap water was used. Ion concentrations were not analysed on inflow and outflow drilling fluid. Hence, Cl- and Br-concentrations of tap water from the Sicada data base were taken, which are 8.7 mg/L for Cl and 0.015 mg/L for Br (average of the samples 16067 and 16173).

The proportions of drilling fluid of the total porewater in the investigated naturally saturated core samples vary between 3.5 and 21.7 Vol.% (Table 7-1). This numbers can be considered as conservative, because uranine can also sorb on the surface of the cores and falsify the results. A depth dependency of drilling fluid contamination cannot be observed. Considering stress release as a main process for the ingress of drilling fluid, an increase with increasing depth can be expected.

A correlation of drilling fluid contamination with petrographical and mineralogical properties of the investigated rocks was not subject of this study.

The drilling fluid contaminations estimated by uranine are for six samples higher and for four samples in the similar range than those investigated by Waber et al. (2011) using NaI traced drilling fluid.

**Table 7-1. Calculated proportions of drilling fluid (DF) in the investigated naturally saturated core samples; uranine concentrations of inflow and outflow drilling fluids collected at different drilling stages of borehole KFR121 are provided by SKB, uranine concentrations of out-diffusion test solutions (O.D. TW) are analysed by HPLC at Hydroisotop.**

Sample ID	Drilling Fluid Data						
	Depth PW sample	Drilling Depth	Uranine conc. Inflow	Uranine conc. Outflow	Uranine conc. O.D. TW	Water Content	Propotion DP of PW
	m BHL	m BHL	mg/L	mg/L	µg/L	wt. %	%
KFR121 71.04–71.40	71.2	83.6	0.194	0.184	0.066	0.14	5.5
KFR121 124.60–124.97	124.8	122.6	0.319	0.080	0.119	0.26	3.5
KFR121 150.25–150.66	150.5	149.6	0.269	0.062	0.177	0.11	12.9
KFR121 163.83–164.19	164.0	176.6	0.200	0.170	0.140	0.09	17.3
KFR121 175.42–175.75	175.6	176.6	0.200	0.170	0.145	0.11	14.4
KFR121 187.58–187.94	187.8	176.6	0.200	0.170	0.137	0.13	11.9
KFR121 196.40–196.81	196.6	215.6	0.204	0.155	0.157	0.09	20.4
KFR121 234.33–234.75	234.5	248.5	0.109	0.102	0.150	0.15	21.7
KFR121 331.38–331.79	331.6	332.5	0.190	0.083	0.130	0.35	4.6
KFR121 349.57–349.95	349.8	362.53	0.192	0.125	0.086	0.26	4.1

## 7.2 Porewater Cl- and Br-concentration

Porewater Cl-concentrations of porewater extracted from core samples taken between 71 and 350 m borehole length vary between 532 and 1 453 mg/kg H<sub>2</sub>O (uncorrected) and between 555 and 1 538 mg/kg H<sub>2</sub>O corrected for drilling fluid contamination (Table 7-2, Figure 7-1). For the samples with a drilling fluid contamination > 17 Vol.% (n = 3) the corrected Cl-concentrations are beyond the error calculations of the uncorrected values (Table 7-2, Figure 7-1).

Porewater Br-concentrations vary along the depth profile of borehole KFR121 between 2.1 and 6.9 mg/kg H<sub>2</sub>O (uncorrected) and between 2.2 and 7.3 mg/kg H<sub>2</sub>O corrected for drilling fluid contamination (Table 7-2, Figure 7-1). All uncorrected porewater Br-concentrations agree within the error with the corrected concentrations, except of one sample (DF contamination = 22 Vol.%), which shows a slightly higher corrected concentration (Table 7-2, Figure 7-1).

Porewater Br·1000/Cl mass ratios vary between 3.4 and 5.4 along the depth profile of borehole KFR121 (Table 7-2, Figure 7-1). They plot on or above the seawater dilution line on the Chloride versus Bromide diagram (Figure 7-2).

**Table 7-2. Porewater Cl- and Br-concentrations (uncorrected and corrected for drilling fluid contamination) and Br·1000/Cl mass ratios; the errors of porewater Cl- and Br-concentrations and Br·1000/Cl mass ratios are calculated by Gaussian error propagation (Appendix 2).**

Sample ID	Depth	Cl(PW)	error	Br(PW)	error	Br·1000/Cl	error	DF Contamination	Cl(PW) corrected	Br(PW) corrected
	m b.l.	mg/kgH <sub>2</sub> O	mg/kgH <sub>2</sub> O	mg/kgH <sub>2</sub> O	mg/kgH <sub>2</sub> O	mg/mg	mg/mg	%	mg/kgH <sub>2</sub> O	mg/kgH <sub>2</sub> O
KFR121 71.04–71.40	71.2	1453	135	6.9	0.6	4.7	0.6	5.5	1538	7.3
KFR121 124.60–124.97	124.8	656	47	3.5	0.3	5.4	0.3	3.5	679	3.6
KFR121 150.25–150.66	150.5	1093	100	5.9	0.5	5.4	0.5	12.9	1254	6.8
KFR121 163.83–164.19	164.0	953	106	3.3	0.4	3.5	0.4	17.3	1150	4.0
KFR121 175.42–175.75	175.6	767	92	3.5	0.4	4.5	0.4	14.4	895	4.0
KFR121 187.58–187.94	187.8	1012	99	3.9	0.4	3.8	0.4	11.9	1148	4.4
KFR121 196.40–196.81	196.6	816	120	2.8	0.4	3.4	0.4	20.4	1023	3.5
KFR121 234.33–234.75	234.5	674	68	3.4	0.3	5.0	0.3	21.7	859	4.3
KFR121 331.38–331.79	331.6	1078	76	5.6	0.4	5.2	0.4	4.6	1129	5.9
KFR121 349.57–349.95	349.8	532	41	2.1	0.2	3.9	0.2	4.1	555	2.2

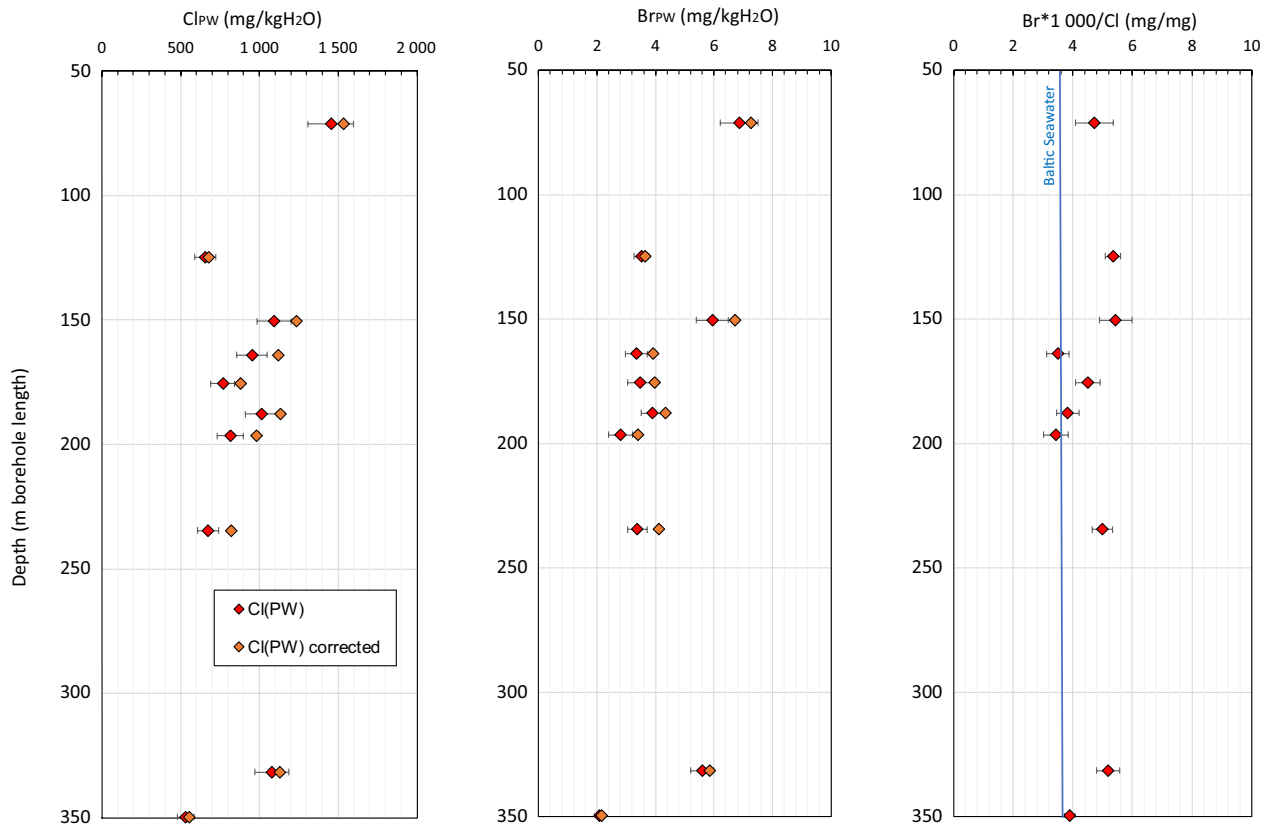


**Figure 7-1.** Porewater chloride and bromide concentrations and Br-1 000/Cl mass ratios extracted from cores from borehole KFR121 as function of depth.

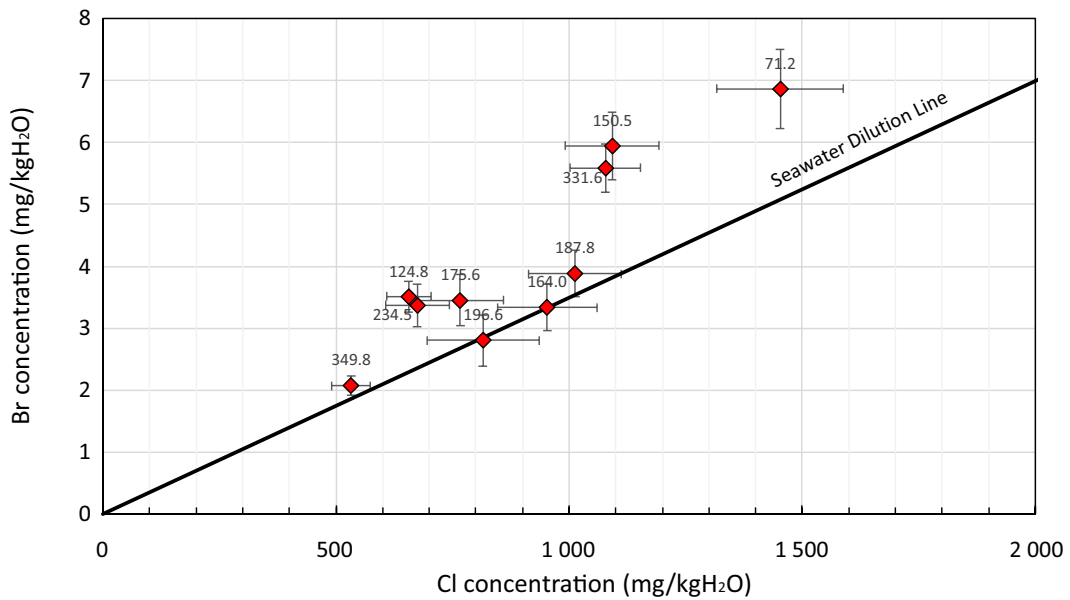


**Figure 7-2.** Chloride versus bromide concentrations of porewater from cores from borehole KFR121; the black line indicates the seawater dilution line; the numbers mark the sampling depths along borehole.



## 8 Porewater stable isotope signatures

Isotope diffusive exchange experiments have been carried out on ten core samples (20 individual experiments) from borehole 121. The  $\delta^{18}\text{O}$  and  $\delta^2\text{H}$  values of porewater are calculated according to Equation 3-6 (cf. Section 3.2.2), expressed relative to the standard V-SMOW, and are listed in Table 8-1 and graphically shown in Figures 8-1 and 8-2. The calculated porewater isotope signatures, which are based on the isotope analyses of the test waters, are carefully evaluated for potential artefacts, mainly due to evaporation of test water during the experiment, test water storage and handling. Evaporation of porewater during storage and handling was minimised by careful handling of the core samples (cf. Section 3.2.2).

These processes might result in large discrepancies between the gravimetric water content and that calculated from isotope mass balance or isotope signatures that are out of any natural range and/or a large error on the calculated porewater isotope signatures. Such differences were not observed in this study (cf. Section 4.1).

Evaporation within the experiment was monitored by keeping track of all individual weights before and after the experiments. None of the experiments suffered evaporation > 2 % of the total water mass in the experiments (= mass of porewater determined gravimetrically + mass of test water) during the time of equilibration.

Porewater stable isotope signatures were also corrected for drilling fluid contamination according to Equation 3-7 (Section 3.2.3). The  $\delta^{18}\text{O}$  and  $\delta^2\text{H}$  isotope signatures of tap water, which were used for the corrections are according to the Sicada data base  $-9.45\text{‰}$  and  $-73.8\text{‰}$  V-SMOW (average of the samples 16067 and 16173). Stable isotopes were not analysed directly on the in- and outflow drilling fluid.

Porewater stable oxygen and hydrogen isotope signatures of core samples taken between 71 and 350 m borehole length vary between  $-6.57\text{‰}$  and  $-15.54\text{‰}$  V-SMOW for  $\delta^{18}\text{O}$  and between  $-59.9\text{‰}$  and  $-121.5\text{‰}$  V-SMOW for  $\delta^2\text{H}$ , respectively (Table 8-1, Figure 8-1). The isotope signatures corrected for drilling fluid contamination vary between  $-6.40\text{‰}$  and  $-19.86\text{‰}$  V-SMOW for  $\delta^{18}\text{O}$  and between  $-59.0\text{‰}$  and  $-155.2\text{‰}$  V-SMOW for  $\delta^2\text{H}$ , respectively (Table 8-1, Figure 8-1). For samples with determined drilling fluid contaminations > 13 Vol.% (n = 5), the corrected isotope signatures are beyond the errors of the uncorrected values, showing more depleted signatures (Table 8-1, Figure 8-1).

The porewater of cores from KFR121 (corrected and uncorrected) plot on a wide range on or close the meteoric water line on the  $\delta^{18}\text{O}$  versus  $\delta^2\text{H}$  diagram (Figure 8-2).

**Table 8-1.  $\delta^{18}\text{O}$  and  $\delta^2\text{H}$  values of porewater (uncorrected and corrected for drilling fluid contamination) of core samples from borehole KFR121; the errors are calculated by Gaussian error propagation.**

Sample ID	Depth	$\delta^{18}\text{O}$	$s(\delta^{18}\text{O})$	$\delta^2\text{H}$	$s(\delta^2\text{H})$	DF cont.	$\delta^{18}\text{O}$ corr.	$\delta^2\text{H}$ corr.
	m b.l.	‰ V-SMOW	‰ V-SMOW	‰ V-SMOW	‰ V-SMOW		%	‰ V-SMOW
KFR121 71.04–71.40	71.2	-6.57	1.70	-59.9	7.7	6	-6.40	-59.0
KFR121 124.60–124.97	124.8	-12.75	0.78	-98.1	4.0	4	-13.21	-101.7
KFR121 150.25–150.66	150.5	-13.21	0.91	-101.7	4.5	13	-15.17	-116.8
KFR121 163.83–164.19	164.0	-12.77	1.47	-103.0	7.2	17	-15.44	-124.5
KFR121 175.42–175.75	175.6	-12.97	1.19	-102.2	5.9	14	-15.15	-119.4
KFR121 187.58–187.94	187.8	-14.58	1.05	-117.1	5.1	12	-16.55	-132.9
KFR121 196.40–196.81	196.6	-12.58	1.15	-98.2	5.6	20	-15.80	-123.4
KFR121 234.33–234.75	234.5	-15.54	0.77	-121.5	7.8	22	-19.86	-155.2
KFR121 331.38–331.79	331.6	-13.54	0.57	-107.8	5.6	5	-14.19	-112.9
KFR121 349.57–349.95	349.8	-11.49	0.79	-88.7	7.9	4	-11.98	-92.5

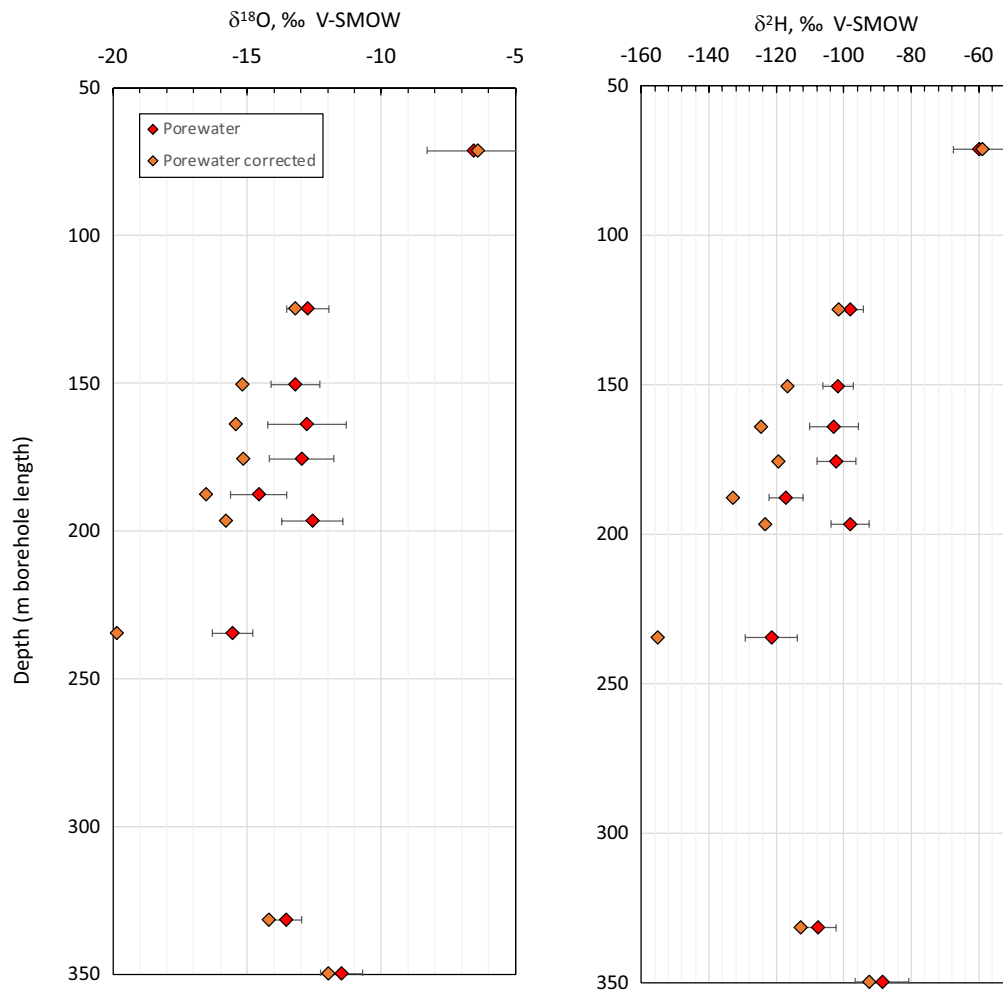


**Figure 8-1.**  $\delta^{18}\text{O}$  and  $\delta^2\text{H}$  porewater signatures (uncorrected and corrected for drilling fluid contamination) as function of depth along borehole KFR121; errors are calculated by Gaussian error propagation.

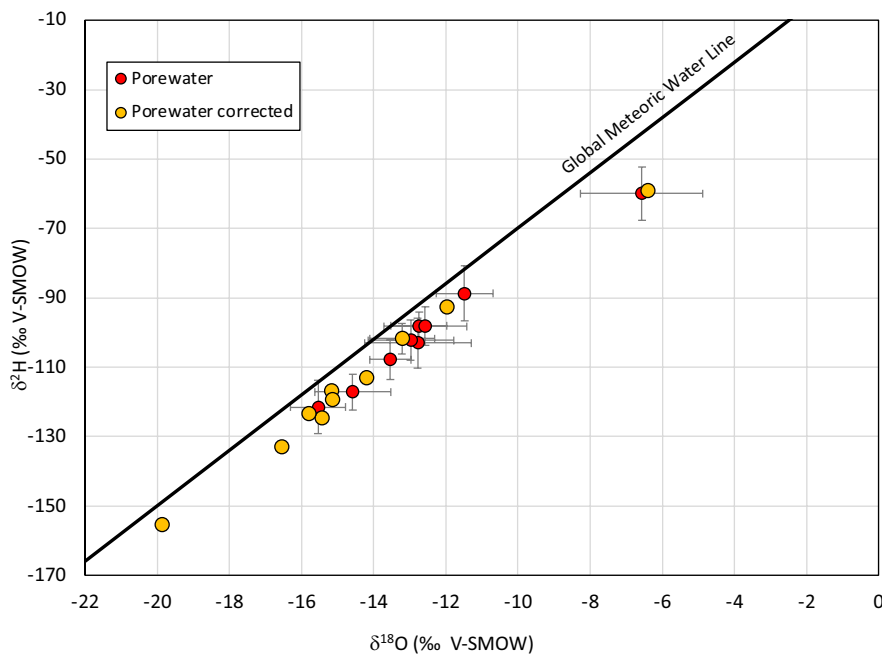


**Figure 8-2.**  $\delta^{18}\text{O}$  versus  $\delta^2\text{H}$  values of porewater (uncorrected and corrected for drilling fluid contamination); the black line marks the global meteoric water line; the errors of the stable isotope ratios are calculated by Gaussian error propagation.

## 9 Uncertainties

Porewater chemical and isotopic concentrations of low-permeable crystalline rocks are determined by indirect methods. The exact determination is based on the mass of porewater, which is determined on naturally saturated samples. Besides analytical uncertainties related to analytics and experiments, the obtained porewater compositions can be influenced by natural and drilling related effects. The individual uncertainties and their control are listed and explained as follows:

### 9.1 Uncertainties of water content determination and their control

The determination of the water content can be disturbed by several processes and artefacts, which can be divided in drilling induced and experimental artefacts. The determination of the water content is an essential parameter for the determination of the concentrations of dissolved constituents in porewater.

#### 9.1.1 Potential Experimental Artefacts

For the exact determination of the water content, it is necessary to determine the initial wet weight of the core samples as present right after recovery from the borehole and the final dry mass of core after the experiments. Potential experimentally induced artefacts modifying the water content of a rock sample from that under *in situ* conditions include:

- evaporation during the packing and transport,
- creation of artificial pore space and entrance of water during preparation of core samples,
- overestimation of the amount of porewater due to a dehydration of hydrated minerals during drying,
- incomplete drying of the core pieces and
- overestimation of the amount of porewater due to water sorbed on the core surfaces.

These artefacts can be controlled by well-defined logistics in the field and a well-defined analytical lab protocol.

#### ***Control of evaporation during packing and transport***

Non-destructive porewater studies, as they have to be applied for crystalline rocks, are based on naturally saturated core samples. Therefore, it is necessary to preserve the natural saturation state and prevent the samples from any evaporation effects during packing and transport. Such effects are minimised by the specially developed packing procedure, which guarantees a short atmospheric exposure time and a complete barrier against evaporation during the transport. The time between packing and preparation of the samples in the laboratory is no longer than one week.

Potential evaporation during transport is controlled by comparing the weights of the core samples before wrapping and after unwrapping the sample in the lab. Intact vacuum in the single bags and wet core surfaces after arrival in the lab are good indications for the preservation of the saturated state between the time of core recovery and sample preparation.

#### ***Creation of artificial pore space and entrance of water during the preparation of core pieces***

Additional pore space can be formed during sawing of samples and the ingress of water in the newly created pore space. The degree of artefacts induced by preparation (i.e. sawing) depends on the sample size. Based on gravimetric water loss of resaturated samples with different thicknesses, Tullborg and Larson (2006) found that porosity values (which are proportional to the water contents at equal density) of thin slices of medium-grained granite samples (0.3 and 20 mm) are up to 50 % higher than porosity values of thicker (60 mm) core pieces. They attribute the increase of porosity – and hence the water

content – to the artificial connection of unconnected pores, which are not accessible to water in the 60 mm pieces, and to the generation of newly created pores and microcracks which penetrate through the thinly sliced core pieces.

The influence of preparation artefacts due to sawing can be minimised by using large-sized full diameter core samples. The length of the naturally saturated core pieces used in the present study for the determination of the gravimetric water content were between 8 and 20 cm and hence even exceed the sample thicknesses used by Tullborg and Larson (2006).

### **Control of complete drying of crystalline core samples**

The completeness of the drying process is controlled by a regular monitoring of the core weights. The final dry weight is recorded, when the weight differences are  $\leq 0.002$  g over a time period of at least two weeks.

### **Control of the influence of on the core surface-sorbed water**

Due to the use of drilling fluid, all core samples prepared for water content measurements have wetted surfaces. The water sorbed on the core surface (here referred as surface water), which is used as an indicator for possible evaporation, is not part of the matrix porewater and leads to an overestimation of the water content. Drillcore samples are cut out of the bedrock. The area around the core, which is moistened by drilling fluid, is not present *in situ* and hence this artificially created water volume cannot be taken into account as part of the natural mass of porewater.

With respect to the exact determination of the water content, the ideal procedure is to dry the surface water from the cores before the initial weight of the saturated sample is taken. Experience from multiple sample preparations showed that the surfaces of the cores are dried after 2 minutes without evaporation of porewater under normal room conditions (Eichinger 2009). During drying of the surface of the cores under the atmosphere, the weights should be monitored and recorded.

## **9.1.2 Potential Artefacts Induced by the Drilling Process**

### ***Influence of stress release***

Rock samples recovered from deep boreholes are affected by the release of stress that they are exposed under *in situ* conditions. This results in a decrease of the elastic moduli of rock building minerals. Due to anisotropy in the mechanical properties of mineral grains, this process leads to the generation of microcracks and an increase of pore apertures. Thus, the physical porosity of rock samples may be increased. As a consequence, drilling fluid might penetrate in the newly created pore space, which might lead to an increase of the measured water content of the samples.

Perturbations related to stress release are commonly identified in drill core samples. The microcracks, which are caused by stress release are open and of tensile nature with closing pressures approximately equal to the *in situ* vertical stress. Microcracking induced by stress release depends on a variety of parameters. The magnitude of stress release is controlled by the sampling depth as the increasing overload results in higher vertical stresses and the present shear stresses, which depend on the local and regional horizontal and sub-horizontal stress distributions within the bedrock. Microcracking induced by stress release has been described from samples between 200 and 11 000 m b.s. (e.g. Kowallis and Wang, 1983, Meglis et al. 1991, Morrow et al. 1994, Jacobsson et al. 2007). The effects of stress release also depend on the sample lithology and texture. Morrow et al. (1994) found a correlation between the degree of microcracking induced by stress release and the quartz content of samples from the KTB borehole and the Kola superdeep borehole. The results of Meglis et al. (1991) from scientific boreholes in New York and Connecticut suggest that the orientation of stress-release microcracks is controlled by the foliation of the drill core samples. The magnitude of stress release also strongly depends on the local stress field. This could possibly explain the discrepancy between stress release induced microcracks observed at shallow depths (e.g. Kowallis and Wang 1983, Meglis et al. 1991) and studies from the Kola superdeep borehole, which suggest that microcracking induced by stress release is negligible down to a depth of 800 to 1 000 m b.s. (Gorbatsevich 2003).

Quantitative information about the influence of stress release and the penetration of drilling fluid in drillcore samples can only be gained by applying traced drilling fluid during the drilling process. Such investigations have been conducted at the Swedish Forsmark site (Waber et al. 2011) and the Finnish Olkiluoto site (Meier 2012, Meier et al. 2015, Eichinger et al. 2013). At both sites, sections of deep boreholes were drilled with NaI traced drilling fluid of known composition. The volume of penetrated drilling fluid in the investigated core samples was obtained by out-diffusion experiments. Modelling of the elution behaviour of the artificial tracer iodide and the natural tracer Cl revealed that the increase in water content caused by stress release makes about 2.4 % for isotropic granodiorite from the Forsmark site (Waber et al. 2011) and between 0.8 and 2.5 % and 5.0 and 8.9 % for anisotropic veined gneisses and isotropic TGG-gneiss, respectively, from the Olkiluoto site (Meier 2012, Meier et al. 2015, Eichinger et al. 2013). As a consequence, the penetration of drilling fluid in the newly created pore space depends on the rock type and may modify the obtained porewater chemistry outside the analytical uncertainty of the experimental procedures.

### ***Influence of the drilling disturbed zone***

In addition to stress release, the drilling process itself can disrupt the drill core samples due to the mechanical impact of the drill bit. The disruption induced by drilling is limited to the outermost rim of the drill core, termed the “drilling disturbed zone” (DDZ). It causes an enlargement of the existing and a creation of new pores and microcracks along the rim zone.

The quantification of the drilling disturbed zone is done utilising the tracer elution behaviour of out-diffusion experiments and transport 2-D modelling, similar as for the stress-release induced artefacts.

The DDZ was identified in crystalline drill cores from the Äspö underground laboratory and from the Forsmark and Olkiluoto investigation sites. For quartz-monzodiorite samples from the Äspö HRL in Sweden, Waber et al. (2011) found a DDZ of about 0.1 mm. These samples were stress released as they were collected from a short borehole close to an about 20 year old tunnel wall. Therefore, all induced enlargement of the pore space can be associated to the mechanical disruption during the drilling process. In granodioritic core samples from about 550 m b.s. in a deep borehole drilled at the Forsmark site, Waber et al. (2011) characterised the disrupted zone of up to 6 mm into the core. For veined gneiss and TGG-gneiss samples from Olkiluoto, (Meier et al. 2015, Eichinger et al. 2013) found a disrupted zone of 0.4–2.2 m and 1.0–1.8 mm, respectively. Newly created pore space by the drilling process appears thus related to a small rim portion of the entire drill core. Considering the large volume used in porewater out-diffusion experiments it thus appears that the perturbation of the pore space (and thus water-content measurements) in crystalline drill core samples is predominantly caused by stress release rather than by mechanical drilling damage.

In this study the influence of both processes is quantified by using uranine, which is added to the drilling fluid. Highly sophisticated analytical methods allow the quantification of uranine concentrations, which are released from the porewater in the ultra trace level (cf. Chapters 3.2.3, 7.1).

## **9.2 Uncertainties in bulk density determination**

Uncertainties in the determination of the bulk density of the large sized core samples are the exact determination of the wet and dry weight and the volume of the samples. The artefacts with respect to the determination of the exact wet and dry weight of the core samples and their control are described in detail in Chapter 4.2.

The volume of the cores is determined by measuring the diameter and length of the cores using a vernier calliper. As the experience from multiple deep boreholes from several locations showed, the diameter of the 10–12 cm cores is constant within a range of 0.05 cm. The measurement of the exact core length can be difficult, if the surface of the upper and lower lid of the cores is uneven. Care is taken that the top surfaces of the cylindrical core samples are straight sawn.

### 9.3 Uncertainties in the porewater Cl-, Br- and chlorine isotope determination and their control

Chlorine and bromine concentrations are calculated by mass balance equations based on the determined test water Cl- and Br-concentrations, the mass of test water and the mass of porewater.

The  $\delta^{37}\text{Cl}$  ratio measured on the experiment solutions directly corresponds to the porewater Cl isotope signature. This is because the attained equilibrium in the out-diffusion experiment with respect to total Cl is also expected to result in equilibrium with respect to the Cl isotopes (Gimmi and Waber 2004).

A prerequisite for the exact determination of the Br- and Cl-concentrations as well as the chlorine isotope signatures of porewater is the achievement of equilibrium with respect to Cl and Br during the out-diffusion experiments. The state of equilibration between porewater and the surrounding test water is controlled by the periodical taking of sub-samples, which are analysed for their Cl- and Br-concentrations. Equilibrium is achieved when the Cl- and Br-concentrations are constant within the analytical uncertainty ( $\pm 5\%$ ) for at least 20 days. The calculated Cl- and Br-concentrations are corrected for the mass and concentration of removed solution. Experience from multiple porewater studies in crystalline environments showed that for naturally saturated core samples with diameters of 5 cm equilibrium with respect to Cl and Br is reached after a half a year to a year at a temperature of 45 °C.

For the calculation of the porewater Cl- and Br-concentrations an exact determination of the mass of porewater is required, which is described before.

Another factor, which has influence on the calculation of the pore water tracer concentrations is the volume of test water, which can be influenced by evaporation or by a leakage during the sampling of the sub-samples. To evaluate these disturbing effects, the weights of the cylinders and the test water per se are determined exactly at the beginning and end of the out-diffusion experiments. Additionally, the masses of the removed sub-sample solution is monitored and taken into account.

The ingress of drilling fluid in by stress release and the formation of a drilling disturbed zone created pore space can lead to a dilution of the Cl- and Br-concentration of porewater. The proportion of drilling fluid in porewater can be evaluated by using NaI traced drilling fluid. Knowing the Cl-, Br- and I-concentrations of the drilling fluid, the porewater Cl-, and Br-concentrations can be corrected using mass balance equations. The dilution of the porewater chemistry is almost exclusively caused by the ingress of dilute drilling fluid in newly created pore space. The contact time between the drilling fluid and the core samples of drilling is generally too short to have a detectable influence due to diffusive exchange. Porewater studies in crystalline rocks from the Forsmark and Olkiluoto investigation sites show that the influence of infiltrated drilling fluid on the porewater Cl- and Br-concentrations is below 10 %, what is within the error range of the reported values (Waber et al. 2011, Meier 2012, Eichinger et al. 2013).

### 9.4 Uncertainties in the determination of porewater stable isotope compositions and their control

The low water content of crystalline rocks makes the diffusive isotope exchange technique very sensitive for artefacts induced during sampling, experiment and analyses. In addition, accurate determination of the stable isotope composition of porewaters requires knowledge about the salinity of porewater to adjust the water activity between porewater and test water in the experiment. Whereas some of the important parameters and processes can be controlled by strictly following a well-established sampling protocol (e.g. Waber and Smellie 2008), others such as salinity and porewater chemistry are commonly unknown and have to be estimated based on experience at least in previously non-explored areas.

As shown by Rogge (1997) and Rübél et al. (2002), the error of the calculated pore-water isotope composition depends predominately on the mass ratio between porewater and test water. The smallest error is obtained if this ratio becomes close to unity. To allow duplicate isotope measurements on the test water solutions a volume of about 2.5 mL are required. For crystalline rocks with a water content of 0.5 wt.% this corresponds to about a total rock mass of 800–1 000 g for the two exchange experiments, which are necessary to determine the  $\delta^{18}\text{O}$  and  $\delta^2\text{H}$  isotope signatures and the mass of porewater after isotope equilibration between porewater and test water.

In the following, the most common artefacts are briefly described that deviate the calculated isotope composition and water mass from that of the porewater isotope composition.

### **Influence of evaporation during sampling, preparation and experiment time**

Evaporation of porewater during sampling, preparation and experiment leads to higher  $\delta^{18}\text{O}$  and  $\delta^2\text{H}$  signatures following the Rayleigh fractionation. Significant evaporation of porewater can result in the precipitation of hydrated secondary salts, which can modify the isotope ratios of the left porewater. Evaporation occurring between the recovery of the cores and the preparation of the samples can be controlled according to the procedure described before. Evaporation of porewater during the experiments is controlled by taking the weights of the rocks before and after the diffusive isotope exchange experiments. Theoretically, the isotope ratios of porewater could in case of evaporation corrected according to the Rayleigh fractionation. However, the formation of secondary hydrated salt minerals and the resulting isotopic fractionation cannot be controlled, which hinders a thorough correction of the values.

Evaporation of test water during the experiments leads also to higher isotopic signatures, but not to the precipitation of solid salt phases.

The evaporation of test solution and porewater during the experiments as well as any water transfers within the closed experiments are controlled by taking the exact weights ( $\pm 0.001$  g) of the rock, test water and the entire closed experiment before and after equilibration.

### **Influence of incomplete equilibration between porewater and test water**

To assure isotope equilibration between the two reservoirs and account for the initially unknown diffusivity of the rock, the applied equilibration time should be chosen about three to four times as long as that calculated. It should be noted that evaporation from the glass container (i.e. open system) always describes a non-equilibrium (i.e. transient) state that cannot be quantified with respect to the water isotopes.

### **Artefacts induced by the salinity of porewater**

The isotope exchange between porewater in a rock sample and test water over the vapour phase depends on the water activity in these reservoirs and – in certain cases – the porewater composition. Differences in water activity will result in an unacceptable mass transfer of either test water to rock sample or vice versa. In case of Cl-rich porewater its chemistry should be matched in the test water in terms of the most abundant cation because of the differences in the hydration shells of Cl-complexes (e.g. NaCl vs. CaCl<sub>2</sub>) and related effects on the isotope composition of the free water molecules. For Cl-dominated porewater environments, de Haller et al. (2016) investigated this latter effect for a series of salinity and compositional ranges of natural and resaturated porewater in argillaceous rocks. Whereas the type of Cl-dominated pore-water compositions poses a major problem in the isotope analyses using conventional isotope ion ratio mass spectrometry, this problem appears at least partly overcome using the more recent cavity ring down spectroscopy (e.g. Mazurek et al. 2013). While for Cl-dominated, saline porewater environments in argillaceous rocks progress has been made in recent years, little is known about similar effects in SO<sub>4</sub>-dominated, saline environments. For a successful conduction of the isotope diffusive exchange technique in highly saline porewater environments in crystalline rocks with very low water contents and adaption of this method is still required.

In this context it should be mentioned that in the Scandinavian crystalline rocks subjected to porewater investigations, Cl<sup>-</sup> or HCO<sub>3</sub><sup>-</sup> are commonly the major anions and the total salinity surpassed that of seawater of in few samples (Waber and Smellie 2008, 2012, Eichinger 2009, Eichinger et al. 2006, 2013).

### **Artefacts induced by the ingress of drilling fluid**

Similar as the Cl- and Br-concentrations the porewater isotope composition can be modified by the ingress of drilling fluid into the drillcore during the drilling process. Such influence depends on the stress release of the drillcore and the drilling disturbed zone created during the contact time of drillcore

and drilling fluid. It can be evaluated using drilling fluid with known  $\delta^{18}\text{O}$  and  $\delta^2\text{H}$  signatures and additionally traced with an artificial tracer. This was evaluated for porewaters from crystalline rocks from the Olkiluoto investigation site (Meier et al. 2015, Eichinger et al. 2013). For these rocks it could be shown that a drilling fluid ingress of  $< 10\%$  of the total amount of porewater only leads to a very small shift of about  $0.02\text{‰}$  in the  $\delta^{18}\text{O}$  and  $\delta^2\text{H}$  pore-water signatures obtained by isotope diffusive exchange experiments. Such small deviation is within the error range of the pore-water values calculated from exchange experiments.

#### **Artefacts induced by the analyses of isotope signatures**

Under optimal conditions rather large masses of rock material are used for the exchange to allow test-water volumes of at least 3 mL in the exchange experiments. These volumes are not sufficient for repeat analyses of  $\delta^{18}\text{O}$  and  $\delta^2\text{H}$  in the applied test water using conventional mass spectrometry. Newer techniques such as the cavity ring down spectroscopy as applied in this study allow replicate measurements for  $\delta^{18}\text{O}$  and  $\delta^2\text{H}$  on such small volumes. More recently, these methods have also been tested for the exact determination of  $\delta^{18}\text{O}$  and  $\delta^2\text{H}$  in test water of salinity of  $> 4\text{ M}$  and of different composition ( $\text{NaCl}$ ,  $\text{CaCl}_2$ ; *cf.* Mazurek et al. 2013). Although certain problems such as memory effects also remain with this technique if not enough replicate analyses can be performed due to limitations in sample material, the analytical part commonly contributes the smallest portion if any at all to the artefacts inhibiting the derivation of the pore-water isotope composition by the isotope diffusive exchange technique.

## 10 Summary

Porewater investigations applying different indirect methods were successfully conducted on crystalline core samples taken between 71 and 350 m borehole length from borehole KFR121.

Potential major sampling-, preservation-, preparation-, experimental- and analytical artefacts, were carefully monitored during the investigation, and none were observed.

The gravimetrically determined water contents vary along the depth profile between 0.08 and 0.38 wt.%, corresponding to water-loss porosities between 0.22 and 0.94 Vol.%. Gravimetrically determined water contents agreed well with those determined by isotope diffusive exchange experiments. The bulk, wet density values are between 2.61 and 2.69 g/cm<sup>3</sup>.

Pore diffusion coefficients were determined by 1-dimensional diffusion modelling based on the fitting of Cl-elution curves, set up by taking periodic sub-samples from out-diffusion experiments. Elution curves could not be fitted by a single pore diffusion coefficient. All cores showed a faster diffusion in the outer rim of the cores and a slower diffusion in the inner parts. The average pore diffusion coefficients (10 °C) vary between  $0.4 \times 10^{-10}$  and  $0.6 \times 10^{-10}$  m<sup>2</sup>/s, corresponding to effective diffusion coefficients between  $0.9 \times 10^{-13}$  and  $4.3 \times 10^{-13}$  m<sup>2</sup>/s.

Additionally, elution curves for Na, K, Ca, Mg, F, SO<sub>4</sub> and partly Br could be set-up by taking periodically sub-samples from the out-diffusion experiments. The elution curves allow the evaluation of potential rock-water interactions during the experiments and serve as basis for future modelling of porewater compositions.

Out-diffusion experiments ran for more than 120 days. The analyses of time series samples showed that all experiments were in equilibrium with respect to Cl before they were terminated. Test water chemistries are mainly dominated by sodium, calcium, hydrogen carbonate, chloride and fluoride in varying proportions and concentrations.

The influence of drilling fluid contamination on the porewater Cl- and Br-concentration as well as on the porewater stable isotope signatures was evaluated by the analyses of uranine concentrations of the out-diffusion solutions. The applied drilling fluid was traced with uranine and its concentration was analysed in the in- and outflow water. The proportions of drilling fluid on the total volume of porewater varied between 3.5 Vol.% and 21.7 Vol.%.

Porewater Cl- and Br-concentrations were calculated using out-diffusion concentrations and the gravimetrically determined mass of porewater. They vary between 532 and 1 453 mg/kg H<sub>2</sub>O for Cl, and 2.1 and 6.9 mg/kg H<sub>2</sub>O for Br, resulting in Br·1 000/Cl mass ratios between 3.4 and 5.4.

The correction of the Cl- and Br-concentrations, which is based on the drilling fluid proportions, obtained by uranine measurements, result in slightly higher Cl- and Br-concentrations varying between 555 and 1 538 mg/kg H<sub>2</sub>O for Cl, and 2.2 and 7.3 mg/kg H<sub>2</sub>O for Br. For samples with drilling fluid contamination > 17 Vol.% (n = 3) the corrected Cl-concentrations are beyond the error calculations of the uncorrected values, whereas for Br it is only the case for the sample with a determined drilling fluid contamination of 22 Vol.%.

Porewater stable water isotope signatures were determined by isotope diffusive exchange experiments. Along the depth profile encountered by borehole KFR121, porewater δ<sup>18</sup>O signatures vary between -6.57 and -13.54 ‰ V-SMOW, and δ<sup>2</sup>H signatures between -59.9 and -121.5 ‰ V-SMOW. The drilling fluid corrected signatures are between -6.40 ‰ and -19.86 ‰ V-SMOW for δ<sup>18</sup>O and between -59.0 ‰ and -155.2 ‰ V-SMOW for δ<sup>2</sup>H. For samples with determined drilling fluid contaminations > 13 Vol.% (n = 5), the corrected isotope signatures are beyond the errors of the uncorrected values.



## References

SKB's (Svensk Kärnbränslehantering AB) publications can be found at [www.skb.com/publications](http://www.skb.com/publications).

**Crank J, 1975.** The Mathematics of Diffusion. Oxford: Oxford Science Publications.

**de Haller A, Hobbs M, Spangenberg J E, 2016.** Adapting the diffusive exchange method for stable isotope analysis of pore water to brine-saturated rocks. *Chemical Geology* 444, 37–48.

**Eichinger F, 2009.** Matrix porewater – fracture groundwater interaction in crystalline bedrock based on natural tracers: An archive of long-term hydrogeological evolution. PhD-thesis. University of Bern, Switzerland.

**Eichinger F L, Waber H N, Smellie J A T, 2006.** Characterisation of Matrix Porewater at the Olkiluoto Investigation Site, Finland. Posiva Working Report 2006-103, Posiva OY, Finland.

**Eichinger F, Hämmerli J, Waber H N, Diamond L W, Smellie J A T, 2013.** Chemistry and Dissolved Gases of Matrix Porewater and Fluid Inclusions in Olkiluoto Bedrock from Drillhole ONK-PH9. Posiva Working Report 2011-63, Posiva Oy, Finland.

**Gascoyne M, 2014.** Chlorine Isotopes and their Application to Groundwater Dating at Olkiluoto. Posiva Working report 2014-38, Posiva OY, Finland.

**Gimmi T, Waber H N, 2004.** Modelling of tracer profiles in porewater of argillaceous rocks in the Benken borehole: Stable water isotopes, chloride, and chlorine isotopes. Nagra Technical Report NTB 04-05, National Cooperative for the Disposal of Radioactive Waste, Switzerland.

**Gorbatsevich F F, 2003.** Decompaction mechanism of deep crystalline rocks under stress relief. *Tectonophysics*, 370, 121–128.

**Jacobsson L, Flansbjer M, Christiansson R, Janson T, 2007.** Measurement of micro crack volume in low porosity crystalline rocks. In 11th International Congress of Rock Mechanics, Lisbon 9–13 July 2007. Boca Raton, FL: Taylor & Francis, 7–10.

**Kowallis B J, Wang H F, 1983.** Microcrack study of granitic cores from Illinois deep borehole UPH 3. *Journal of Geophysical Research: Solid Earth* 88, 7373–7380.

**Lide D R, 1994.** CRC Handbook of chemistry and physics. 75th ed. Boca Raton, FL: CRC Press.

**Mazurek M, Oyama T, Eichinger F, De Haller A, 2013.** Squeezing of Porewater from Core Samples of DGR Boreholes: Feasibility Study. NWMO TR-2013-19, Nuclear Waste Management Organization, Canada.

**Meglis I L, Engelder T, Graham E, 1991.** The effect of stress-relief on ambient microcrack porosity in core samples from the Kent Cliffs (New York) and Moodus (Connecticut) scientific research boreholes. *Tectonophysics* 186, 163–173.

**Meier D B, 2012.** Matrix porewater in crystalline rocks at Olkiluoto, Finland: Chemical and transport properties and artefacts induced by drill core samples. Master's Thesis. University of Bern, Switzerland.

**Meier D B, Waber H N, Gimmi T, Eichinger F, Diamond L W, 2015.** Reconstruction of in situ porosity and porewater compositions of low-permeability crystalline rocks: Magnitude of artefacts induced by drilling and sample recovery. *Journal of Contaminant Hydrology* 183, 55–71.

**Morrow C, Lockner D, Hickman S, Rusanov M, Röckel T, 1994.** Effects of lithology and depth on the permeability of core samples from the Kola and KTB drill holes. *Journal of Geophysical Research: Solid Earth* 99, 7263–7274 (1978–2012).

**Ohlsson Y, Neretnieks I, 1995.** Literature survey of matrix diffusion theory and of experiments and data including natural analogues. SKB TR 95-12, Svensk Kärnbränslehantering AB.

**Rogge T, 1997.** Eine molekular-diffusive Methode zur Bestimmung des Porenwassergehaltes und der Zusammensetzung von stabilen Isotopen im Porenwasser von Gestein. Diploma thesis. University of Heidelberg, Germany. (In German.)

**Rübel A P, Sonntag C, Lippmann J, Pearson F J, Gautschi A, 2002.** Solute transport in formations of very low permeability: Profiles of stable isotope and dissolved noble gas contents of pore water in the Opalinus Clay. Mont Terri, Switzerland. *Geochimica et Cosmochimica Acta* 66, 1311–1321.

**Tullborg E-L, Larson S-Å, 2006.** Porosity in crystalline rocks – A matter of scale. *Engineering Geology* 84, 75–83.

**Waber H N, Smellie J A T, 2005.** SKB Site Investigations Forsmark – Borehole KFM06: Characterisation of porewater. Part I: Diffusion experiments. SKB P-05-196, Svensk Kärnbränslehantering AB.

**Waber H N, Smellie J A T, 2006.** Oskarshamn site investigations. Borehole KLX03: Characterisation of porewater. Part 2: Rock properties and diffusion experiments. SKB P-06-77, Svensk Kärnbränslehantering AB.

**Waber H N, Smellie J A T, 2008.** Characterisation of pore water in crystalline rock. *Applied Geochemistry* 23, 1834–1861.

**Waber H N, Gimmi T, Smellie J A T, 2011.** Effects of drilling and stress release on transport properties and porewater chemistry in crystalline rocks. *Journal of Hydrology* 405, 316–332.

**Waber H N, Smellie J A T, 2012.** Forsmark site characterisation: Borehole KFM22 and KFM23: Derivation of porewater data by diffusion experiments. SKB P-12-18, Svensk Kärnbränslehantering AB.

## Comparison of porewater results of core samples taken from borehole KFR121 with results obtained from boreholes KFM22 and KFM23

Previous porewater investigations were conducted within the Forsmark investigations on drillcores from several boreholes (Figure A1-1). The porewater data obtained from borehole KFR121 are following compared to porewater data sets from boreholes KFM22 and KFM23, which were drilled in the year 2011. Those two boreholes are located on the Forsmark investigation site, approximately 1.5 km south-west of borehole KFR121 (Figure A1-1). The results of porewater investigations on samples from the boreholes KFM22 and KFM23 are presented in Waber and Smellie (2012).

In the boreholes KFM22 and KFM23 core samples for porewater investigations were taken between -34 m and -89 m a.s.l.. In this depth zone only one core sample for porewater investigations was taken at -54 m a.s.l. from borehole KFR121.

The porewater Cl-concentration and  $\delta^{18}\text{O}$  and  $\delta^2\text{H}$  isotope signatures of the porewater sample taken at -54 m a.s.l. from borehole KFR121 are equal to those of porewater of a core sample taken at -53 m a.s.l. from borehole KFM23 (Figure A1-2). The Br-concentrations and Br·1 000/Cl ratio of the sample from KFR121 are higher than those of the sample from KFM23 at equal depth (Figure A1-2).

Porewater Cl- and Br-concentrations of core samples taken from borehole KFR121 below -90 m a.s.l. are lower than those of porewaters from KFM22 and KFM23 taken above -90 m a.s.l.. They follow the decreasing trend indicated by the Cl and Br depth profiles in boreholes KFM22 and KFM23.

Porewater Br·1 000/Cl ratios are varying widely in the depth profile encountered in boreholes KFM22 and KFM23 (Figure A1-2, A1-3). This variation continues also in the further course of the depth profile in borehole KFR121.

Considering the Br vs. Cl diagram, porewaters from boreholes KFM22 and KM23 plot on (1 sample), below (4 samples) or above (2 samples) the seawater dilution line, whereas porewaters from borehole KFR121 plot on (4 samples) or above (6 samples) the seawater dilution line (Figure A1-3). The wide variation of the porewater Br·1 000/Cl ratios indicates the preservation of different Cl- and Br-bearing sources.

The trend of decreasing  $\delta^{18}\text{O}$  and  $\delta^2\text{H}$  porewater isotope signatures over depth indicated in the profiles sampled in boreholes KFM22 and KFM23 is continuing in borehole KFM121 down to -100 m a.s.l. (Figure A1-1). Considering the also generally decreasing trend of porewater Cl-concentrations this indicates the increasing proportion of a preserved cold climatic fresh water component with increasing depth. In the bedrock section below -100 m a.s.l. encountered by borehole KFM121, the  $\delta^{18}\text{O}$  and  $\delta^2\text{H}$  porewater isotope signatures remain similar to the porewater Cl-concentrations at a low level and vary only slightly, indicating the presence of a cold climatic freshwater component down to a depth of -275 m a.s.l. (Figure A1-1). All porewater samples of all three boreholes plot close to the Global Meteoric Water Line on the  $\delta^{18}\text{O}$  vs.  $\delta^2\text{H}$  diagram (Figure A1-4).

Porewater from borehole KFR121 with Cl-concentrations below 1 100 mg/L as occurring in this borehole below -100 m a.s.l. show no correlation to the  $\delta^{18}\text{O}$  isotope signatures (Figure A1-5). Those are between -15.5 and -11.5 ‰ V-SMOW.

Porewaters taken above -100 m a.s.l. from boreholes KFR121, KFM22 and KFM23 show a correlation between  $\delta^{18}\text{O}$  isotope signatures and Cl-concentrations, concrete an increase of Cl-concentration with increasing  $\delta^{18}\text{O}$  isotope signatures (Figure A1-5).

These findings indicate that in low saline samples taken below -100 m a.s.l. a higher proportion of a cold-climatic water component is preserved than in porewaters taken above, in which a more saline component is more pronounced.

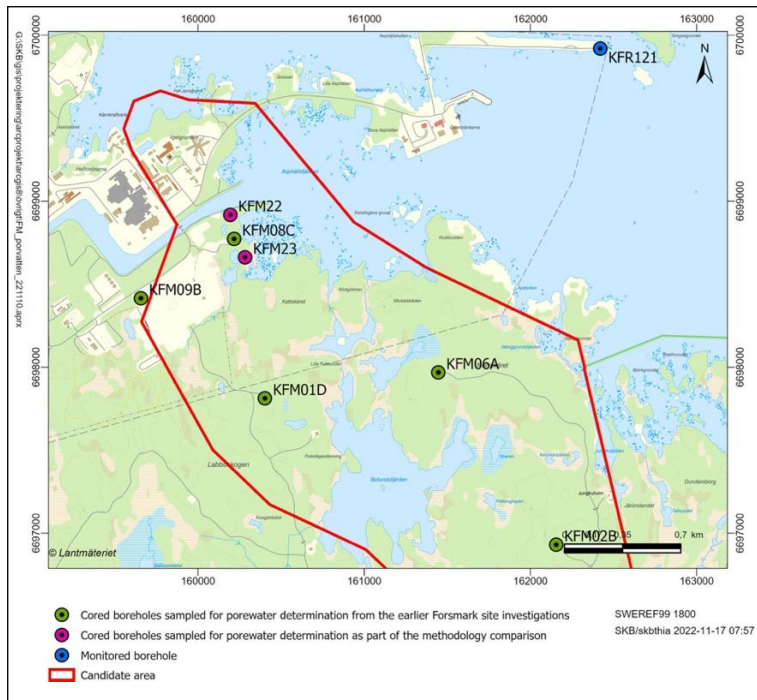


**Figure A1-1.** Overview of boreholes on the Forsmark site, from which samples for porewater investigations were taken (provided by SKB).

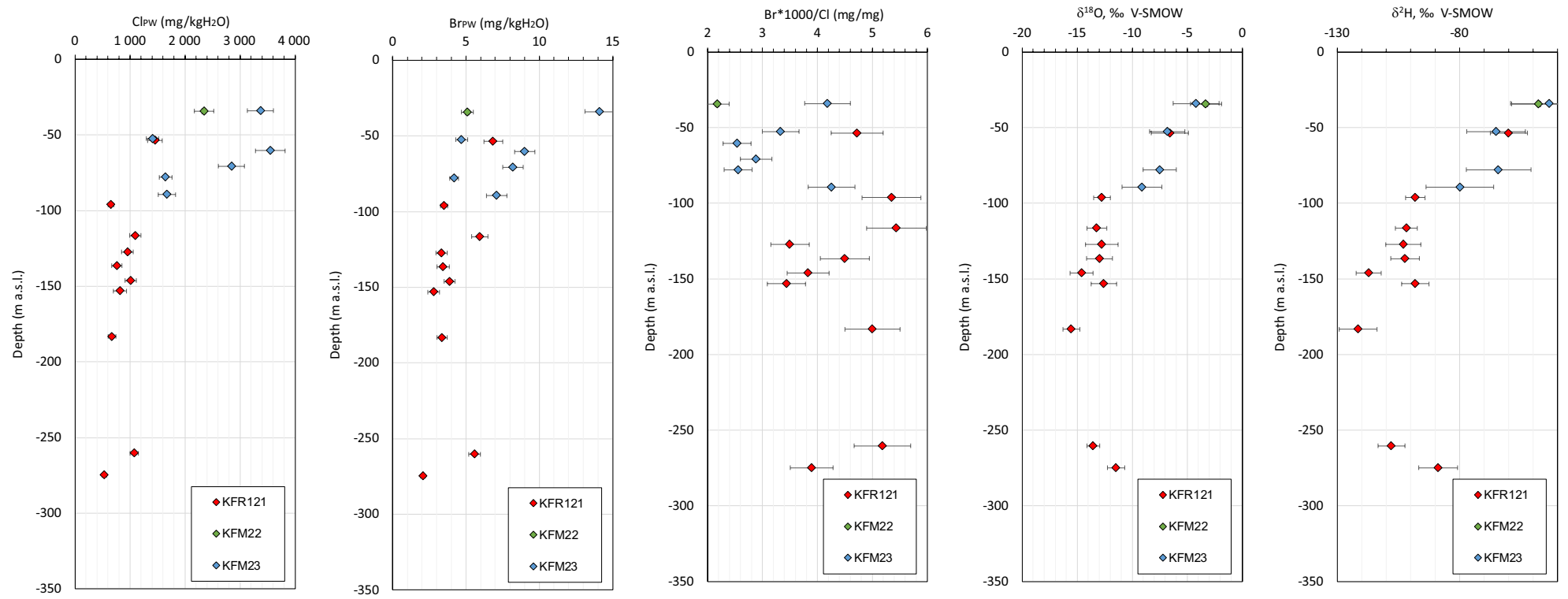


**Figure A1-2.** Porewater tracer depth profiles comparing data from boreholes KFR121, KFM22 and KFM23. Values of boreholes KFM22 and 23 are taken from Waber and Smellie (2012).

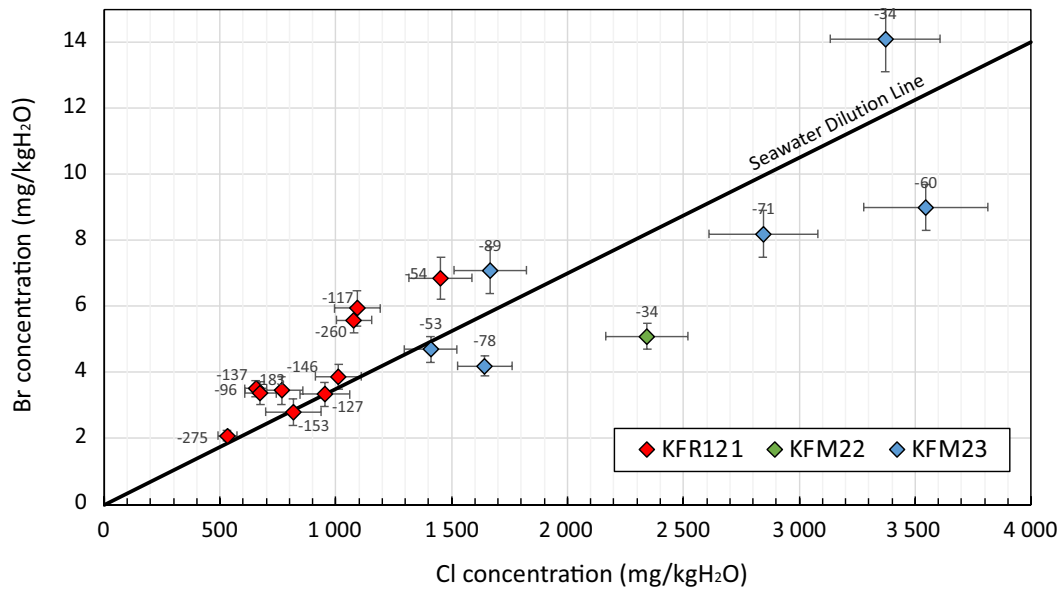


**Figure A1-3.** Bromide versus Chloride concentrations of porewaters of cores taken from boreholes KFR121, KFM22 and KFM23. Values of boreholes KFM22 and 23 are taken from Waber and Smellie (2012); the numbers mark the sampling depths above sea level.

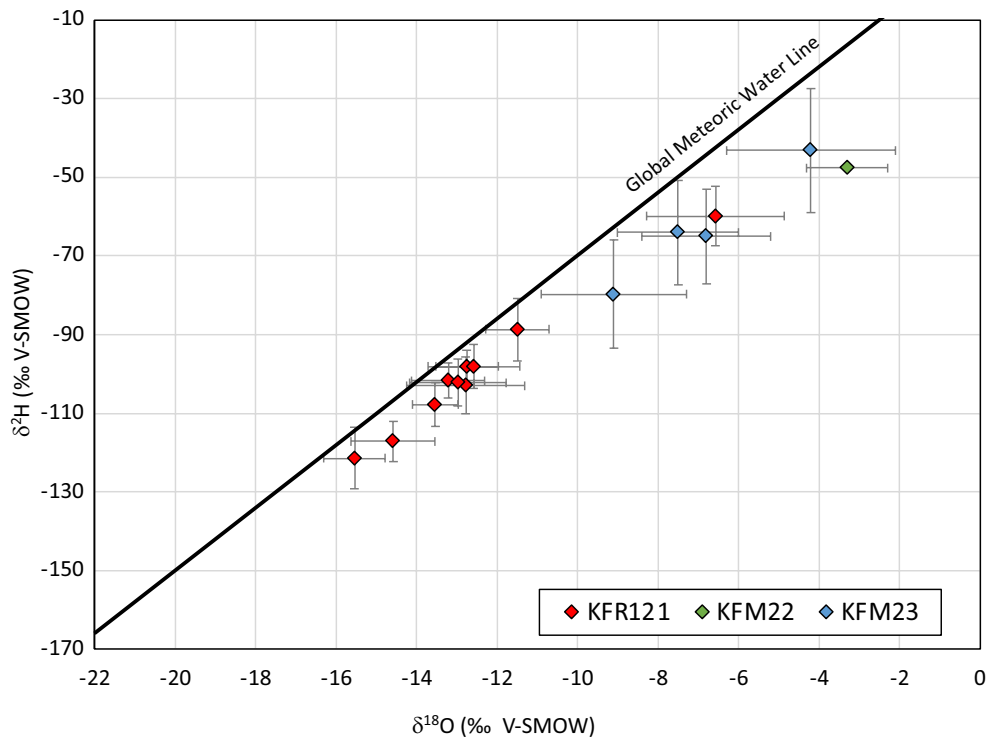


**Figure A1-4.**  $\delta^{18}\text{O}$  versus  $\delta^2\text{H}$  isotope signatures of porewaters of cores taken from boreholes KFR121, KFM22 and KFM23. Values of boreholes KFM22 and 23 are taken from Waber and Smellie (2012).

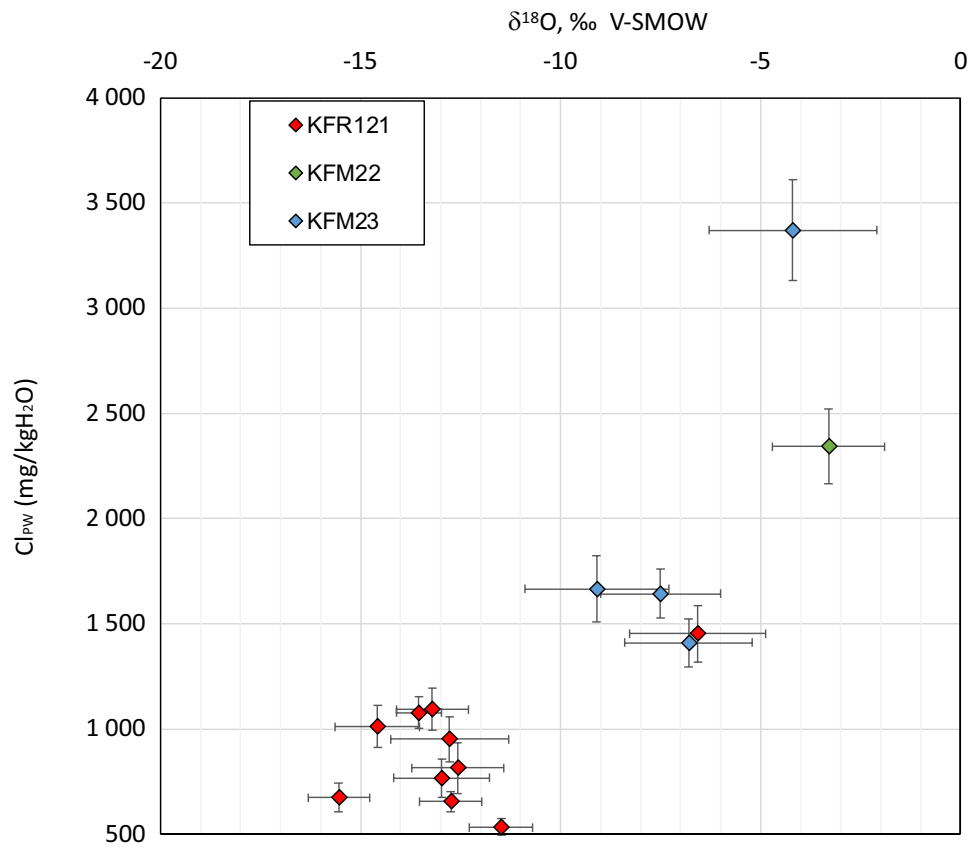


**Figure A1-5.**  $\delta^{18}\text{O}$  isotope signatures versus  $\text{Cl}$ -concentrations of porewaters of cores taken from boreholes KFR121, KFM22 and KFM23. Values of boreholes KFM22 and 23 are taken from Waber and Smellie (2012).



### Determination of $^{36}\text{Cl}/\text{Cl}$ ratios of porewater chloride extracted from core samples from borehole KFR121

$^{36}\text{Cl}$  in porewater may have three sources, which are a) cosmic radiation in the upper atmosphere and rain-out, b) spallation of K, Ca, and Ar in soil moisture and minerals and c) subsurface production by neutron activation of stable  $^{35}\text{Cl}$  from decay of naturally occurring radioelements (i.e. U, Th) and several rare earth elements like Gd and Sm in the bedrock. With time, the  $^{36}\text{Cl}$  will accumulate and decay until the rate of production equals the rate of decay (i.e. secular equilibrium) and this occurs in a closed system after a period of up to 1.5 million years (Gascoyne 2014).

To evaluate and quantify potential Cl-forming processes, which might have influence on the Cl-concentration of porewater, the  $^{36}\text{Cl}/\text{Cl}$  ratios of five out-diffusion test solutions were analysed by AMS at the ETH Zürich (a detailed description of the methods and results are given in the attached lab report).

Due to the non-destructive character of the out-diffusion experiments and the lack of any Cl-bearing minerals in the Forsmark bedrock, porewater is the only source for chloride in the out-diffusion test solutions.

The low chloride concentrations and low volumes of the out-diffusion test waters impeded the analyses. Two samples could only analysed by using a spike. So, the results are given in atoms per gram (at/g).

The  $^{36}\text{Cl}/\text{Cl}$  ratios and  $^{36}\text{Cl}$ -concentrations are all below the detection limit of  $< 0,005 \times 10^{-12}$  and  $< 5000$  at/g (Table A2-1). This indicates that the porewater Cl-concentrations are not influenced by any Cl-forming processes, as described in theory above.

**Table A2-1. Results of the determination of  $^{36}\text{Cl}/\text{Cl}$  ratios and  $^{36}\text{Cl}$ -concentrations of out-diffusion solutions extracting porewater from core samples from borehole KFR121.**

Sample	Hydroisotop Lab Nr.	Cl (TW) mg/l	$^{36}\text{Cl}/\text{Cl}$ ( $\times 10^{-12}$ ) -	$^{36}\text{Cl}$ at/g
KFR121 71.04–71.40	352825	9.1		< 5000
KFR121 150.25–150.66	352827	5.7		< 5000
KFR121 163.83–164.19	376658	4.0	< 0.005	
KFR121 187.58–187.94	376659	6.0	< 0.005	
KFR121 331.38–331.79	376660	16.4	< 0.005	



Eidgenössische Technische Hochschule Zürich  
Swiss Federal Institute of Technology Zurich

**Laboratory of Ion Beam Physics**

Dr. Christof Vockenhuber  
ETH Zurich  
Otto-Stern-Weg 5, HPK G31  
CH – 8093 Zürich

Tel. direct: + 41 44 633 3885  
Secretary: + 41 44 633 6507  
Fax: + 41 44 633 1067  
e-mail: vockenhuber@phys.ethz.ch

Dr. Florian Eichinger  
Hydroisotop GmbH  
Woelkestr. 9  
D-85301 Schweitenkirchen  
Germany  
e-mail: fe@hydroisotop.de

Zurich, April 14<sup>th</sup>, 2022

Dear Dr. Eichinger,

I'm pleased to send you the results of <sup>36</sup>Cl analysis of your water samples performed on the 6 MV EN-Tandem AMS facility at the Laboratory of Ion Beam Physics at ETH Zurich in April 2022:

sample	ETH label	<sup>36</sup> Cl conc. (at/ g)	err (%)	date	magazine
352825	CV4249	<5000		13.04.22	K220401
352827	CV4250	<5000		13.04.22	K220401

sample	ETH label	<sup>36</sup> Cl/ Cl final (10 <sup>-12</sup> )	err (%)	date	magazine
376658	CV4251	<0.005		13.04.22	K220401
376659	CV4252	<0.005		13.04.22	K220401
376660	CV4253	<0.005		13.04.22	K220401

Comments:

All five samples show <sup>36</sup>Cl levels in the blank range and only upper limits are given.

The <sup>36</sup>Cl concentration for samples 352825 and 352827 was determined by adding 3 mg of <sup>35</sup>Cl spike and from the isotopic ratios of <sup>37</sup>Cl/<sup>35</sup>Cl and <sup>36</sup>Cl/<sup>35</sup>Cl the <sup>36</sup>Cl concentration is calculated.

All measured ratios are within the valid range for <sup>36</sup>Cl analysis. Final <sup>36</sup>Cl/Cl ratios are corrected for machine blank and measured relative to 3 internal standard samples K382/4N.

The nominal <sup>36</sup>Cl/Cl ratio of the internal standard K382/4N is  $(17.36 \pm 0.35) \times 10^{-12}$ . The internal standard is calibrated against the primary standard KNSTD5000 (nominal <sup>36</sup>Cl/Cl ratio  $(5.00 \pm 0.10) \times 10^{-12}$ ) by K. Nishizumi. The half-life of <sup>36</sup>Cl is  $(3.01 \pm 0.02) \times 10^5$  years. A sample scatter of 1% was added to the final uncertainty.

Kind regards,

Dr. Christof Vockenhuber

## Error Calculations

### Gravimetric Water Content

The water content is calculated according to  $WC_{grav} = \frac{m_{pw}}{m_{core,wet}}$

Where  $WC_{grav}$  = gravimetric water content,  $m_{pw}$  = mass of porewater,  $m_{core,wet}$  = mass of the wet core sample.

### Error calculation after Gaussian error propagation

$$\sigma(WC_{grav}) = \sqrt{\left(dWC_{grav} dm_{PW} \times \sigma(m_{PW})\right)^2 + \left(dWC_{grav} dm_{core,wet} \times \sigma(m_{core,wet})\right)^2}$$

### Analytical errors (error of measurement)

$s(m_{pw})$  = difference between  $m_{core,dry\ surface}$  before and after drying + 0.05 g (= variations at end of drying);  
The constant of 0.05 g is the empirically derived uncertainty associated to the drying process of the surface, i.e. loss of water from the core surface.

$s(m_{core,wet})$  = difference between  $m_{core,dry\ surface}$  before and after experiment.

Both uncertainties include the mass difference of the individual cores before and after the experiments (cf. Appendix 2).

### Derivations

$$dWC_{grav} dm_{pw} = \frac{100}{m_{core,wet}}$$

$$dWC_{grav} dm_{core,wet} = \frac{-100 \times m_{pw}}{(m_{core,wet})^2}$$

### Water-Loss Porosity

The water-loss (connected porosity),  $\phi_{WL}$ , is calculated according to

$$\phi_{WL} = WC_{wet} \times \frac{\rho_{bulk,wet}}{\rho_{water}}$$

where  $WC_{wet}$  is the water content based on the wet weight of the rock sample and  $\rho_{bulk,wet}$  the bulk wet density of the rock. The density of water,  $\rho_{water}$ , is assumed to be 1 g/cm<sup>3</sup>.

The conversion of the formula leads to

$$\phi_{WL} = \frac{m_{pw} \times 100}{r^2 \times h \times \pi \times \rho_{water}}$$

where  $r$  = radius of the core pieces,  $h$  = height of the core.

### Error calculation after Gaussian error propagation

$$\sigma(\phi_{WL}) = \sqrt{\left(d\phi_{WL} dm_{PW} \times \sigma(m_{PW})\right)^2 + \left(d\phi_{WL} dr \times \sigma(r)\right)^2 + \left(d\phi_{WL} dh \times \sigma(h)\right)^2 + \left(d\phi_{WL} d\rho_{water} \times \sigma(\rho_{water})\right)^2}$$

### Analytical errors (error of measurement)

$s(m_{pw})$  = difference between  $m_{\text{core,dry surface}}$  before and after drying + 0.05 g (= variations at end of drying).

$s(r)$  = 0.02 cm.

$s(h)$  = 0.2 cm.

$s(\rho_{\text{water}})$  = 0.03 g/cm<sup>3</sup>.

### Derivations

$$d\phi dm_{pw} = \frac{100}{r^2 \times h \times \pi \times \rho_{\text{water}}}$$

$$d\phi dr = \frac{-m_{pw} \times 100 \times 2r \times h \times \pi \times \rho_{\text{water}}}{(r^2 \times h \times \pi \times \rho_{\text{water}})^2}$$

$$d\phi dh = \frac{-m_{pw} \times 100 \times r^2 \times \pi \times \rho_{\text{water}}}{(r^2 \times h \times \pi \times \rho_{\text{water}})^2}$$

$$d\phi dh = \frac{-m_{pw} \times 100 \times r^2 \times \pi \times h}{(r^2 \times h \times \pi \times \rho_{\text{water}})^2}$$

### Porewater Cl- and Br-concentrations

#### Calculations

$$C_{PW} = \frac{(m_{PW} + m_{TWi} - \sum^n m_s) \times C_{TW\infty} - (m_{TWi} \times C_{TWi}) + \sum^n m_s \times C_s}{m_{PW}}$$

where  $C_{pw}$  = porewater concentration;  $m_{pw}$  = mass of porewater;  $m_{TWi}$  = initial mass of test water;  $C_{TWi}$  = initial Cl-concentration of test water;  $m_s$  = mass of sub sample used for time series;  $C_s$  = Cl-concentration of sub sample used for time series.

#### Error calculation after Gaussian error propagation

$$\sigma(C_{PW}) = \sqrt{\left( \frac{dC_{PW}}{dm_{PW}} \times \sigma(m_{PW}) \right)^2 + \left( \frac{dC_{PW}}{dm_{TWi}} \times \sigma(m_{TWi}) \right)^2 + \left( \frac{dC_{PW}}{dC_{TW\infty}} \times \sigma(C_{TW\infty}) \right)^2 + \left( \frac{dC_{PW}}{dC_{TWi}} \times \sigma(C_{TWi}) \right)^2 + \left( \frac{dC_{PW}}{d(\sum m_s)} \times \sigma(\sum m_s) \right)^2 + \left( \frac{dC_{PW}}{d(\sum m_s \times c_s)} \times \sigma(\sum m_s \times c_s) \right)^2}$$

### Analytical errors (error of measurement)

$s(m_{PW})$  = difference between  $m_{\text{core,dry surface}}$  before and after drying + 0.05 g (= variations at end of drying).

$s(m_{TWi})$  = difference between  $m_{TWi} - m_s - m_{TW\infty} - 2\text{ml}$  (2 ml = remaining water in the cylinder).

$s(C_{TWi})$  = 5 % (Cl) and 10 % (Br) of the analysed concentration.

$s(C_{TW\infty})$  = 5 % (Cl) and 10 % (Br) of the analysed concentration.

$s(m_s)$  = 0.05 ml.

$s(C_s)$  = 5 % (Cl) and 10 % (Br) of the analysed concentration.

## Derivations

$$dC_{PW} dm_{PW} = \frac{C_{TW\infty} * m_{PW} - [C_{TW\infty} * (m_{PW} + m_{TWi}) - C_{TW} * m_{TWi}]}{m_{PW}^2}$$

$$dC_{PW} dm_{TWi} = \frac{(C_{TW\infty} - C_{TWi}) * m_{PW}}{m_{PW}^2}$$

$$dC_{PW} dC_{TW\infty} = \frac{(m_{PW} - m_{TWi}) * m_{PW}}{m_{PW}^2}$$

$$dC_{PW} dC_{TWi} = \frac{-m_{TWi} * m_{PW}}{m_{PW}^2}$$

$$\sigma\left(\sum(m_s)\right) = (Nr_s \times \sigma(m_s))$$

$$\sigma\left(\sum(m_s \times C_s)\right) = (Nr_s \times C_{s,ave} \times \sigma(m_s)) + (Nr_s \times m_s \times \sigma(C_s))$$

## Porewater Br/Cl mass ratios

Br·1 000/Cl porewater mass ratio = R

## Error calculation after Gaussian error propagation

$$\sigma(R) = \sqrt{(dRdC_{Br} \times \sigma(C_{Br}))^2 + (dRdC_{Cl} \times \sigma(C_{Cl}))^2}$$

## Analytical errors (error of measurement)

s(C<sub>Cl</sub>) = Error of porewater Cl-concentration calculated according to AIII-3.

s(C<sub>Br</sub>) = Error of porewater Br-concentration calculated according to AIII-3.

## Derivations

$$dRdC_{Br} = \frac{1000}{C_{Cl}}$$

$$dRdC_{Cl} = \frac{-1000 \times C_{Br}}{C_{Cl}^2}$$

## Isotope Signatures of Porewater

### Calculation

$$C_{PW} = \frac{C_{TW\infty(Std1)} \times m_{TW(Std2)} \times m_{Rock(Std1)} \times (C_{TW\infty(Std2)} - C_{TW^0(Std2)}) - C_{TW\infty(Std2)} \times m_{TW(Std1)} \times m_{Rock(Std2)} \times (C_{TW\infty(Std1)} - C_{TW^0(Std1)})}{m_{TW(Std2)} \times m_{Rock(Std1)} \times (C_{TW\infty(Std2)} - C_{TW^0(Std2)}) - m_{TW(Std1)} \times m_{Rock(Std2)} \times (C_{TW\infty(Std1)} - C_{TW^0(Std1)})}$$

$m_{PW}$  = mass of porewater (g).

$m_{TW}$  = mass of test water (g).

$C_{TW}$  = isotopic signature of test water at the beginning of the experiment (‰).

$C_{TW\infty}$  = isotopic signature of test water after equilibration (‰).

*Std 1* = Experiment 1 applying standard 1.

*Std 2* = Experiment 2 applying standard 2.

## Error calculation after Gaussian error propagation

$$\sigma(C_{PW}) = \sqrt{\left( (dC_{PW} dm_{TW(Std1)} \times \sigma(m_{TW(Std1)}))^2 + (dC_{PW} dm_{TW(Std2)} \times \sigma(m_{TW(Std2)}))^2 + \right. \\ \left. + (dC_{PW} dC_{TW(Std1)} \times \sigma(C_{TW(Std1)}))^2 + (dC_{PW} dC_{TW(Std2)} \times \sigma(C_{TW(Std2)}))^2 + \right. \\ \left. + (dC_{PW} dC_{TW\infty(Std1)} \times \sigma(C_{TW\infty(Std1)}))^2 + (dC_{PW} dC_{TW\infty(Std2)} \times \sigma(C_{TW\infty(Std2)}))^2 \right)}$$

### Analytical errors (error of measurement)

$$s(m_{TW(Std1)}) = 0.002 \text{ g.}$$

$$s(m_{TW(Std2)}) = 0.002 \text{ g.}$$

$$s(C_{TW(Std1)}) = 0.1 \text{ ‰ for } ^{18}\text{O} \text{ and } 1.0\text{‰ for } ^2\text{H.}$$

$$s(C_{TW(Std2)}) = 0.1 \text{ ‰ for } ^{18}\text{O} \text{ and } 1.0\text{‰ for } ^2\text{H.}$$

$$s(C_{TW\infty(Std1)}) = 0.1 \text{ ‰ for } ^{18}\text{O} \text{ and } 1.0\text{‰ for } ^2\text{H.}$$

$$s(C_{TW\infty(Std2)}) = 0.1 \text{ ‰ for } ^{18}\text{O} \text{ and } 1.0\text{‰ for } ^2\text{H.}$$

### Derivations

$$dC_{PW} dm_{TW(Std1)} = \frac{(C_{TW(Std1)} - C_{TW\infty(Std1)}) \times C_{TW\infty(Std2)}}{(m_{TW(Std1)} \times (C_{TW(Std1)} - C_{TW\infty(Std1)}) - (C_{TW(Std2)} - C_{TW\infty(Std2)}) \times m_{TW(Std2)})} - \\ \frac{((C_{TW(Std1)} - C_{TW\infty(Std1)}) \times C_{TW\infty(Std2)} \times m_{TW(Std1)} - (C_{TW(Std2)} - C_{TW\infty(Std2)}) \times C_{TW\infty(Std1)} \times m_{TW(Std2)}) \times (C_{TW(Std1)} - C_{TW\infty(Std1)})}{(m_{TW(Std1)} \times (C_{TW(Std1)} - C_{TW\infty(Std1)}) - (C_{TW(Std2)} - C_{TW\infty(Std2)}) \times m_{TW(Std2)})^2}$$

$$dC_{PW} dm_{TW(Std2)} = \frac{-(C_{TW(Std2)} - C_{TW\infty(Std2)}) \times C_{TW\infty(Std1)}}{(m_{TW(Std1)} \times (C_{TW(Std1)} - C_{TW\infty(Std1)}) - (C_{TW(Std2)} - C_{TW\infty(Std2)}) \times m_{TW(Std2)})} + \\ + \frac{((C_{TW(Std1)} - C_{TW\infty(Std1)}) \times C_{TW\infty(Std2)} \times m_{TW(Std1)} - (C_{TW(Std2)} - C_{TW\infty(Std2)}) \times C_{TW\infty(Std1)} \times m_{TW(Std2)}) \times (C_{TW(Std2)} - C_{TW\infty(Std2)})}{(m_{TW(Std1)} \times (C_{TW(Std1)} - C_{TW\infty(Std1)}) - (C_{TW(Std2)} - C_{TW\infty(Std2)}) \times m_{TW(Std2)})^2}$$

$$dC_{PW} dC_{TW(Std1)} = \frac{C_{TW\infty(Std2)} \times m_{TW(Std1)}}{(m_{TW(Std1)} \times (C_{TW(Std1)} - C_{TW\infty(Std1)}) - (C_{TW(Std2)} - C_{TW\infty(Std2)}) \times m_{TW(Std2)})} - \\ - \frac{((C_{TW(Std1)} - C_{TW\infty(Std1)}) \times C_{TW\infty(Std2)} \times m_{TW(Std1)} - (C_{TW(Std2)} - C_{TW\infty(Std2)}) \times C_{TW\infty(Std1)} \times m_{TW(Std2)}) \times m_{TW(Std1)}}{(m_{TW(Std1)} \times (C_{TW(Std1)} - C_{TW\infty(Std1)}) - (C_{TW(Std2)} - C_{TW\infty(Std2)}) \times m_{TW(Std2)})^2}$$

$$\begin{aligned}
dC_{PW}dC_{TW(Std2)} &= \frac{-C_{TW\infty(Std1)} \times m_{TW(Std2)}}{(m_{TW(Std1)} \times (C_{TW(Std1)} - C_{TW\infty(Std1)}) - (C_{TW(Std2)} - C_{TW\infty(Std2)}) \times m_{TW(Std2)})} + \\
&+ \frac{((C_{TW(Std1)} - C_{TW\infty(Std1)}) \times C_{TW\infty(Std2)} \times m_{TW(Std1)} - (C_{TW(Std2)} - C_{TW\infty(Std2)}) \times C_{TW\infty(Std1)} \times m_{TW(Std2)}) \times m_{TW(Std1)}}{(m_{TW(Std1)} \times (C_{TW(Std1)} - C_{TW\infty(Std1)}) - (C_{TW(Std2)} - C_{TW\infty(Std2)}) \times m_{TW(Std2)})^2} \\
dC_{PW}dC_{TW\infty(Std1)} &= \frac{-(C_{TW\infty(Std2)} \times m_{TW(Std1)} + (C_{TW(Std2)} - C_{TW\infty(Std2)}) \times m_{TW(Std2)})}{(m_{TW(Std1)} \times (C_{TW(Std1)} - C_{TW\infty(Std1)}) - (C_{TW(Std2)} - C_{TW\infty(Std2)}) \times m_{TW(Std2)})} + \\
&+ \frac{((C_{TW(Std1)} - C_{TW\infty(Std1)}) \times C_{TW\infty(Std2)} \times m_{TW(Std1)} - (C_{TW(Std2)} - C_{TW\infty(Std2)}) \times C_{TW\infty(Std1)} \times m_{TW(Std2)}) \times m_{TW(Std1)}}{(m_{TW(Std1)} \times (C_{TW(Std1)} - C_{TW\infty(Std1)}) - (C_{TW(Std2)} - C_{TW\infty(Std2)}) \times m_{TW(Std2)})^2} \\
dC_{PW}dC_{TW\infty(Std2)} &= \frac{(m_{TW(Std1)} \times (C_{TW(Std1)} - C_{TW\infty(Std1)}) + C_{TW\infty(Std1)} \times m_{TW(Std2)})}{(m_{TW(Std1)} \times (C_{TW(Std1)} - C_{TW\infty(Std1)}) - (C_{TW(Std2)} - C_{TW\infty(Std2)}) \times m_{TW(Std2)})} - \\
&- \frac{((C_{TW(Std1)} - C_{TW\infty(Std1)}) \times C_{TW\infty(Std2)} \times m_{TW(Std1)} - (C_{TW(Std2)} - C_{TW\infty(Std2)}) \times C_{TW\infty(Std1)} \times m_{TW(Std2)}) \times m_{TW(Std2)}}{(m_{TW(Std1)} \times (C_{TW(Std1)} - C_{TW\infty(Std1)}) - (C_{TW(Std2)} - C_{TW\infty(Std2)}) \times m_{TW(Std2)})^2}
\end{aligned}$$

## Calculation of Water Contents by Isotope Diffusive Exchange

### Calculation

$$WC_{IsoEx} = \left[ \frac{m_{TW(Std2)} \times m_{Rock(Std1)} \times (C_{TW^0(Std2)} - C_{TW\infty(Std2)}) + m_{TW(Std1)} \times m_{Rock(Std2)} \times (C_{TW\infty(Std1)} - C_{TW^0(Std1)})}{m_{Rock(Std1)} \times m_{Rock(Std2)} \times (C_{TW\infty(Std2)} - C_{TW\infty(Std1)})} \right] \times 100$$

$m_{PW}$  = mass of porewater (g).

$m_{TW}$  = mass of test water (g).

$C_{TW}$  = isotopic signature of test water at the beginning of the experiment (‰).

$C_{TW\infty}$  = isotopic signature of test water after equilibration (‰).

*Std 1* = Experiment 1 applying standard 1.

*Std 2* = Experiment 2 applying standard 2.

### Error calculation after Gaussian error propagation

$$\sigma(m_{PW}) = \sqrt{\begin{aligned} & (dm_{PW} dm_{TW(Std1)} \times \sigma(m_{TW(Std1)}))^2 + (dm_{PW} dm_{TW(Std2)} \times \sigma(m_{TW(Std2)}))^2 + \\ & + (dm_{PW} dC_{TW(Std1)} \times \sigma(C_{TW(Std1)}))^2 + (dm_{PW} dC_{TW(Std2)} \times \sigma(C_{TW(Std2)}))^2 + \\ & + (dm_{PW} dC_{TW\infty(Std1)} \times \sigma(C_{TW\infty(Std1)}))^2 + (dm_{PW} dC_{TW\infty(Std2)} \times \sigma(C_{TW\infty(Std2)}))^2 \end{aligned}}$$

### Analytical errors (error of measurement)

$$\begin{aligned}s(m_{TW(Std1)}) &= 0.002 \text{ g.} \\s(m_{TW(Std2)}) &= 0.002 \text{ g.} \\s(C_{TW(Std1)}) &= 0.1 \text{ ‰ for } ^{18}\text{O} \text{ and } 1.0\text{‰ for } ^2\text{H.} \\s(C_{TW(Std2)}) &= 0.1 \text{ ‰ for } ^{18}\text{O} \text{ and } 1.0\text{‰ for } ^2\text{H.} \\s(C_{TW\infty(Std1)}) &= 0.1 \text{ ‰ for } ^{18}\text{O} \text{ and } 1.0\text{‰ for } ^2\text{H.} \\s(C_{TW\infty(Std2)}) &= 0.1 \text{ ‰ for } ^{18}\text{O} \text{ and } 1.0\text{‰ for } ^2\text{H.}\end{aligned}$$

### Derivations

$$dm_{PW} dm_{TW(Std1)} = \frac{(C_{TW(Std1)} - C_{TW\infty(Std1)})}{(C_{TW\infty(Std1)} - C_{TW\infty(Std2)})}$$

$$dm_{PW} dm_{TW(Std2)} = \frac{-(C_{TW(Std2)} - C_{TW\infty(Std2)})}{(C_{TW\infty(Std1)} - C_{TW\infty(Std2)})}$$

$$dm_{PW} dC_{TW(Std1)} = \frac{m_{TW(Std1)}}{(C_{TW\infty(Std1)} - C_{TW\infty(Std2)})}$$

$$dm_{PW} dC_{TW(Std2)} = \frac{-m_{TW(Std2)}}{(C_{TW\infty(Std1)} - C_{TW\infty(Std2)})}$$

$$dm_{PW} dC_{TW\infty(Std1)} = \left( \frac{-1}{(C_{TW\infty(Std1)} - C_{TW\infty(Std2)})} - \frac{(C_{TW(Std1)} - C_{TW\infty(Std1)})}{(C_{TW\infty(Std1)} - C_{TW\infty(Std2)})^2} \right) \times m_{TW(Std1)} + (C_{TW(Std2)} - C_{TW\infty(Std2)}) \times m_{TW(Std2)}$$

$$dm_{PW} dC_{TW\infty(Std2)} = \left( \frac{(C_{TW(Std1)} - C_{TW\infty(Std1)}) \times m_{TW(Std1)}}{(C_{TW\infty(Std1)} - C_{TW\infty(Std2)})^2} + \frac{1}{(C_{TW\infty(Std1)} - C_{TW\infty(Std2)})^2} - \frac{(C_{TW(Std2)} - C_{TW\infty(Std2)})}{(C_{TW\infty(Std1)} - C_{TW\infty(Std2)})^2} \right) \times m_{TW(Std2)}$$

# Analytical Raw Data

## Calculation of Water Content Values – Raw Data

**Table A4-1. Drying time series and water contents of extra core pieces of core samples taken from borehole KFR121.**

Sample	Set-up date	m (wet) g	17.06.20	01.07.20	15.07.20	29.07.20	11.08.20	25.08.20	08.09.20	23.09.20
<b>Drying time (days)</b>			7	21	35	49	62	76	90	105
KFR121 71.04–71.40 A	10.06.20	62.454	62.393	62.387	62.378	62.380				
KFR121 71.04–71.40 B	10.06.20	91.586	91.426	91.409	91.403	91.399	91.395	91.394		
KFR121 124.60–124.97 A	10.06.20	112.837	112.671	112.655	112.649	112.646	112.641	112.640		
KFR121 124.60–124.97 B	10.06.20	97.764	97.536	97.493	97.481	97.469	97.462	97.457	97.452	97.453
<b>Drying time (days)</b>			<b>29.06.20</b>	<b>13.07.20</b>	<b>27.07.20</b>	<b>10.08.20</b>	<b>24.08.20</b>	<b>07.09.20</b>	<b>23.09.20</b>	
			7	21	35	49	63	77		
KFR121 150.25–150.66 A	22.06.20	103.060	102.965	102.958	102.952	102.95				
KFR121 150.25–150.66 B	22.06.20	74.052	73.986	73.979	73.979					
KFR121 163.83–164.19 A	22.06.20	132.660	132.481	132.458	132.444	132.438	132.435	132.433		
KFR121 163.83–164.19 B	22.06.20	64.227	64.188	64.184	64.183					
KFR121 175.42–175.75 A	22.06.20	148.994	148.815	148.785	148.769	148.762	148.753	148.752		
KFR121 175.42–175.75 B	22.06.20	60.478	60.420	60.415	60.413					
KFR121 187.58–187.94 A	22.06.20	130.125	129.914	129.903	129.898	129.896				
KFR121 187.58–187.94 B	22.06.20	71.141	71.051	71.046	71.044					
KFR121 196.40–196.81 A	22.06.20	94.311	94.243	94.239	94.236	94.234				
KFR121 196.40–196.81 B	22.06.20	64.303	64.260	64.254	64.253					
KFR121 234.33–234.75 A	22.06.20	136.754	136.555	136.539	136.529	136.527				
KFR121 234.33–234.75 B	22.06.20	94.879	94.762	94.756	94.753	94.753				
KFR121 331.38–331.79 A	22.06.20	153.649	153.047	153.036	153.03	153.028				
KFR121 331.38–331.79 B	22.06.20	87.352	87.071	87.062	87.055	87.053				
KFR121 349.57–349.95 A	22.06.20	136.052	135.785	135.769	135.763	135.759	135.757			
KFR121 349.57–349.95 B	22.06.20	164.928	164.444	164.407	164.401	164.395	164.385	164.379	164.379	

**Table A4-1. Continued.**

Sample	Set-up date	m wet g	m dry g	m (PW) g	Water content wet weight wt. %	Water content dry weight wt. %
KFR121 71.04–71.40 A	10.06.20	62.454	62.378	0.076	0.12	0.12
KFR121 71.04–71.40 B	10.06.20	91.586	91.394	0.192	0.21	0.21
KFR121 124.60–124.97 A	10.06.20	112.837	112.64	0.197	0.17	0.17
KFR121 124.60–124.97 B	10.06.20	97.764	97.452	0.312	0.32	0.32
KFR121 150.25–150.66 A	22.06.20	103.060	102.95	0.110	0.11	0.11
KFR121 150.25–150.66 B	22.06.20	74.052	73.979	0.073	0.10	0.10
KFR121 163.83–164.19 A	22.06.20	132.660	132.433	0.227	0.17	0.17
KFR121 163.83–164.19 B	22.06.20	64.227	64.183	0.044	0.07	0.07
KFR121 175.42–175.75 A	22.06.20	148.994	148.752	0.242	0.16	0.16
KFR121 175.42–175.75 B	22.06.20	60.478	60.413	0.065	0.11	0.11
KFR121 187.58–187.94 A	22.06.20	130.125	129.896	0.229	0.18	0.18
KFR121 187.58–187.94 B	22.06.20	71.141	71.044	0.097	0.14	0.14
KFR121 196.40–196.81 A	22.06.20	94.311	94.234	0.077	0.08	0.08
KFR121 196.40–196.81 B	22.06.20	64.303	64.253	0.050	0.08	0.08
KFR121 234.33–234.75 A	22.06.20	136.754	136.527	0.227	0.17	0.17
KFR121 234.33–234.75 B	22.06.20	94.879	94.753	0.126	0.13	0.13
KFR121 331.38–331.79 A	22.06.20	153.649	153.028	0.621	0.40	0.41
KFR121 331.38–331.79 B	22.06.20	87.352	87.053	0.299	0.34	0.34
KFR121 349.57–349.95 A	22.06.20	136.052	135.757	0.295	0.22	0.22
KFR121 349.57–349.95 B	22.06.20	164.928	164.379	0.549	0.33	0.33

**Table A4-2. Drying time series and water contents of core pieces used for isotope diffusive exchange experiments of core samples taken from borehole KFR121.**

Sample		Date start drying	Drying times (days)	m (cryst. dish) g	m (cryst+ rock) g	03.09.20	17.09.20	01.10.20	16.10.20	29.10.20	12.11.20	26.11.20	10.12.20
KFR121 71.04–71.40	LAB	20.08.20	28	89.837	320.253	320.000	319.999						
KFR121 71.04–71.40	ICE	20.08.20	28	91.797	322.606	322.350	322.351						
KFR121 124.60–124.97	LAB	20.08.20	28	92.884	314.849	314.495	314.497						
KFR121 124.60–124.97	ICE	20.08.20	112	90.689	313.027	312.487	312.475	312.459	312.449	312.440	312.435	312.426	312.428
KFR121 150.25–150.66	LAB	20.08.20	28	87.506	390.347	389.977	389.98						
KFR121 150.25–150.66	ICE	20.08.20	28	88.790	389.976	389.642	389.644						
KFR121 163.83–164.19	LAB	20.08.20	28	91.514	309.950	309.714	309.716						
KFR121 163.83–164.19	ICE	20.08.20	28	88.635	307.588	307.403	307.405						
KFR121 175.42–175.75	LAB	20.08.20	28	81.569	295.971	295.715	295.713						
KFR121 175.42–175.75	ICE	20.08.20	28	88.669	303.338	303.127	303.127						
KFR121 187.58–187.94	LAB	20.08.20	28	88.329	316.131	315.83	315.838						
KFR121 187.58–187.94	ICE	20.08.20	28	83.843	310.617	310.372	310.374						
KFR121 196.40–196.81	LAB	20.08.20	28	86.929	409.991	409.908	409.91						
KFR121 196.40–196.81	ICE	20.08.20	28	87.17	410.207	409.706	409.708						
KFR121 234.33–234.75	LAB	20.08.20	28	85.211	378.452	378.037	378.04						
KFR121 234.33–234.75	ICE	20.08.20	70	91.408	384.172	383.784	383.78	383.771	383.76	383.758			
KFR121 331.38–331.79	LAB	20.08.20	28	89.012	308.27	307.447	307.445						
KFR121 331.38–331.79	ICE	20.08.20	28	88.736	307.227	306.66	306.658						
KFR121 349.57–349.95	LAB	20.08.20	112	88.822	271.131	270.666	270.655	270.641	270.631	270.623	270.619	270.608	370.611
KFR121 349.57–349.95	ICE	20.08.20	84	85.978	268.212	267.728	267.721	267.706	367.699	267.690	267.690		

**Table A4-2. Continued.**

Sample		Date start drying	Drying times (days)	Mass dry g	m rock wet g	m rock dry g	m (PW) g	WCwet, wt. %	WCdry, wt. %
KFR121 71.04–71.40	LAB	20.08.20	28	319.999	230.416	230.162	0.254	0.11	0.11
KFR121 71.04–71.40	ICE	20.08.20	28	322.350	230.809	230.553	0.256	0.11	0.11
KFR121 124.60–124.97	LAB	20.08.20	28	314.495	221.965	221.611	0.354	0.16	0.16
KFR121 124.60–124.97	ICE	20.08.20	112	312.426	222.338	221.737	0.601	0.27	0.27
KFR121 150.25–150.66	LAB	20.08.20	28	389.977	302.841	302.471	0.370	0.12	0.12
KFR121 150.25–150.66	ICE	20.08.20	28	389.642	301.186	300.852	0.334	0.11	0.11
KFR121 163.83–164.19	LAB	20.08.20	28	309.714	218.436	218.200	0.236	0.11	0.11
KFR121 163.83–164.19	ICE	20.08.20	28	307.403	218.953	218.768	0.185	0.08	0.08
KFR121 175.42–175.75	LAB	20.08.20	28	295.713	214.402	214.144	0.258	0.12	0.12
KFR121 175.42–175.75	ICE	20.08.20	28	303.127	214.669	214.458	0.211	0.10	0.10
KFR121 187.58–187.94	LAB	20.08.20	28	315.830	227.802	227.501	0.301	0.13	0.13
KFR121 187.58–187.94	ICE	20.08.20	28	310.372	226.774	226.529	0.245	0.11	0.11
KFR121 196.40–196.81	LAB	20.08.20	28	409.908	323.062	322.979	0.083	0.03	0.03
KFR121 196.40–196.81	ICE	20.08.20	28	409.706	323.037	322.536	0.501	0.16	0.16
KFR121 234.33–234.75	LAB	20.08.20	28	378.037	293.241	292.826	0.415	0.14	0.14
KFR121 234.33–234.75	ICE	20.08.20	70	383.758	292.764	292.350	0.414	0.14	0.14
KFR121 331.38–331.79	LAB	20.08.20	28	307.445	219.258	218.433	0.825	0.38	0.38
KFR121 331.38–331.79	ICE	20.08.20	28	306.658	218.491	217.922	0.569	0.26	0.26
KFR121 349.57–349.95	LAB	20.08.20	112	270.608	182.309	181.786	0.523	0.29	0.29
KFR121 349.57–349.95	ICE	20.08.20	84	267.690	182.234	181.712	0.522	0.29	0.29

**Table A4-3. Drying time series and water contents of full diameter core pieces used for out-diffusion experiments of core samples taken from borehole KFR121.**

Sample	Date start drying	m wet surface g	m dry surface g	m wet surface g	m dry surface g	29.10.20 g	12.11.20 g	26.11.20 g	11.12.20 g	25.12.20 g	08.01.21 g	22.01.21 g	05.02.21 g	19.02.21 g
<b>Drying time (days)</b>						6	20	34	49	63	77	91	105	119
KFR121 71.04–71.40	23.10.20	786.890	786.890	786.924	322.351	786.119	785.852	785.761	785.718	785.684	785.660	785.652	785.623	785.622
KFR121 124.60–124.97	23.10.20	776.026	776.026	776.084	314.497	774.233	773.931	773.863	773.819	773.778	773.774	773.772		
KFR121 150.25–150.66	23.10.20	825.508	825.508	825.660	389.98	824.752	824.678	824.643	824.64	824.631	824.622	824.627		
KFR121 163.83–164.19	23.10.20	780.309	780.309	780.367	309.716	779.896	779.762	779.72	779.707	779.689	779.672	779.674		
KFR121 175.42–175.75	23.10.20	788.053	788.053	788.077	295.713	787.662	787.481	787.388	787.329	787.281	787.246	787.234	787.194	787.192
KFR121 187.58–187.94	23.10.20	780.832	780.832	780.931	315.838	779.97	779.845	779.817	779.81	779.802	779.786	779.794		
KFR121 196.40–196.81	23.10.20	802.280	802.280	802.356	409.91	801.874	801.711	801.656	801.637	801.614	801.605	801.607		
KFR121 234.33–234.75	23.10.20	799.855	799.855	799.883	378.04	799.083	798.777	798.68	798.644	798.611	798.605	798.609		
KFR121 331.38–331.79	23.10.20	755.140	755.140	755.271	307.445	752.777	752.519	752.475	752.47	752.446	752.436	752.438		
KFR121 349.57–349.95	23.10.20	790.287	790.287	790.478	267.721	788.744	788.544	788.473	788.452	788.430	788.414	788.416		

**Table A4-3. Continued.**

Sample	Date start drying	m (dry) g	m (PW) b.e. g	m (PW) a.e. g	Δm (PW) a.e.–b.e.	WC wet b.e. wt. %	WC wet a.e. wt. %	WC dry b.e. wt. %	WC dry a.e. wt. %
<b>Drying time (days)</b>									
KFR121 71.04–71.40	23.10.20	785.622	1.268	1.252	-0.016	0.16	0.16	0.16	0.16
KFR121 124.60–124.97	23.10.20	773.772	2.254	2.239	-0.015	0.29	0.29	0.29	0.29
KFR121 150.25–150.66	23.10.20	824.622	0.886	0.937	0.051	0.11	0.11	0.11	0.11
KFR121 163.83–164.19	23.10.20	779.672	0.637	0.650	0.013	0.08	0.08	0.08	0.08
KFR121 175.42–175.75	23.10.20	787.192	0.861	0.846	-0.015	0.11	0.11	0.11	0.11
KFR121 187.58–187.94	23.10.20	779.786	1.046	1.063	0.017	0.13	0.14	0.13	0.14
KFR121 196.40–196.81	23.10.20	801.605	0.675	0.687	0.012	0.08	0.09	0.08	0.09
KFR121 234.33–234.75	23.10.20	798.605	1.250	1.242	-0.008	0.16	0.16	0.16	0.16
KFR121 331.38–331.79	23.10.20	752.436	2.704	2.668	-0.036	0.36	0.35	0.36	0.35
KFR121 349.57–349.95	23.10.20	788.414	1.873	1.909	0.036	0.24	0.24	0.24	0.24

### Calculation of Bulk Wet and Dry Density – Raw Data

**Table A4-4. Measured core parameter and calculation of density.**

Sample	m (core a.e.) wet g	m (core) dry g	diameter core cm	height core cm	Volume core ccm	bulk, wet density g/ccm	bulk, dry density g/ccm
KFR121 71.04–71.40	786.924	785.622	4.50	18.51	294.39	2.67	2.67
KFR121 124.60–124.97	776.084	773.772	4.49	18.7	296.09	2.62	2.61
KFR121 150.25–150.66	825.660	824.622	4.50	19.44	309.18	2.67	2.67
KFR121 163.83–164.19	780.367	779.672	4.51	18.29	292.18	2.67	2.67
KFR121 175.42–175.75	788.077	787.192	4.51	18.43	294.42	2.68	2.67
KFR121 187.58–187.94	780.931	779.786	4.50	18.28	290.73	2.69	2.68
KFR121 196.40–196.81	802.356	801.605	4.51	18.65	297.94	2.69	2.69
KFR121 234.33–234.75	799.883	798.605	4.50	18.88	300.27	2.66	2.66
KFR121 331.38–331.79	755.271	752.436	4.51	18.07	288.67	2.62	2.61
KFR121 349.57–349.95	790.478	788.414	4.51	18.98	303.21	2.61	2.60

## Isotope Diffusive Exchange Experiments – Raw Data

**Table A4-5. Experimental raw data of isotope diffusive exchange experiments.**

Sample		Date experiment start	Date experiment end	Standard	Weight container g	Weight container and rock g	Cryst. dish g	Cryst. dish + H <sub>2</sub> O g	Total weight container g	Weight rock g	Weight test solution g
KFR121 71.04–71.40	LAB	10.06.20	09.08.20	KFR121-LAB	523.774	754.260	14.481	15.573	770.230	230.486	1.492
KFR121 124.60–124.97	LAB	10.06.20	09.08.20		521.480	743.581	13.796	15.298	758.876	222.101	1.502
KFR121 150.25–150.66	LAB	22.06.20	21.08.20		528.302	831.257	12.983	14.492	845.738	302.955	1.509
KFR121 163.83–164.19	LAB	22.06.20	21.08.20		520.309	738.751	14.346	15.850	754.598	218.442	1.504
KFR121 175.42–175.75	LAB	22.06.20	21.08.20		521.377	735.815	13.892	15.405	751.216	214.438	1.513
KFR121 187.58–187.94	LAB	22.06.20	21.08.20		513.331	741.147	14.891	16.410	757.551	227.816	1.519
KFR121 196.40–196.81	LAB	22.06.20	21.08.20		523.281	846.417	14.713	16.225	862.633	323.136	1.512
KFR121 234.33–234.75	LAB	22.06.20	21.08.20		524.191	817.488	14.911	16.421	833.895	293.297	1.510
KFR121 331.38–331.79	LAB	22.06.20	21.08.20		515.286	734.891	14.380	15.888	750.771	219.605	1.508
KFR121 349.57–349.95	LAB	22.06.20	21.08.20		514.521	696.975	12.967	14.482	711.454	182.454	1.515
KFR121 71.04–71.40	ICE	10.06.20	09.08.20	KFR121-ICE	522.361	753.200	14.632	16.157	769.354	230.839	1.525
KFR121 124.60–124.97	ICE	10.06.20	09.08.20		522.373	744.753	12.969	14.466	759.209	222.380	1.497
KFR121 150.25–150.66	ICE	22.06.20	21.08.20		521.113	822.406	14.061	15.579	837.964	301.293	1.518
KFR121 163.83–164.19	ICE	22.06.20	21.08.20		515.182	734.356	14.436	15.946	750.298	219.174	1.510
KFR121 175.42–175.75	ICE	22.06.20	21.08.20		515.061	729.781	14.105	15.609	745.386	214.720	1.504
KFR121 187.58–187.94	ICE	22.06.20	21.08.20		513.331	740.540	14.370	15.901	756.439	227.209	1.531
KFR121 196.40–196.81	ICE	22.06.20	21.08.20		523.281	841.322	13.141	14.661	855.975	318.041	1.520
KFR121 234.33–234.75	ICE	22.06.20	21.08.20		524.191	813.915	13.893	15.394	829.305	289.724	1.501
KFR121 331.38–331.79	ICE	22.06.20	21.08.20		515.286	731.162	13.998	15.513	746.661	215.876	1.515
KFR121 349.57–349.95	ICE	22.06.20	21.08.20		514.521	697.323	15.003	16.503	713.823	182.802	1.500

**Table A4-5. Continued.**

Sample		Date experiment start	Date experiment end	Standard	Total weight container after experiment g	Weight test solution after experiment g	Weight container and rock after experiment g	Weight test solution after experiment g	Weight rock after experiment g	mass (PW) g	mass TW+PW after exp. g
KFR121 71.04–71.40	LAB	10.06.20	09.08.20	KFR121-LAB	770.244	15.883	754.348	1.402	230.574	0.254	1.656
KFR121 124.60–124.97	LAB	10.06.20	09.08.20		758.891	15.227	743.650	1.431	222.170	0.354	1.785
KFR121 150.25–150.66	LAB	22.06.20	21.08.20		845.755	14.390	831.353	1.407	303.051	0.37	1.777
KFR121 163.83–164.19	LAB	22.06.20	21.08.20		754.617	15.758	738.846	1.412	218.537	0.236	1.648
KFR121 175.42–175.75	LAB	22.06.20	21.08.20		751.229	15.316	735.904	1.424	214.527	0.258	1.682
KFR121 187.58–187.94	LAB	22.06.20	21.08.20		757.567	16.312	741.245	1.421	227.914	0.301	1.722
KFR121 196.40–196.81	LAB	22.06.20	21.08.20		862.655	16.128	846.523	1.415	323.242	0.083	1.498
KFR121 234.33–234.75	LAB	22.06.20	21.08.20		833.912	16.334	817.570	1.423	293.379	0.415	1.838
KFR121 331.38–331.79	LAB	22.06.20	21.08.20		750.785	15.862	734.912	1.482	219.626	0.825	2.307
KFR121 349.57–349.95	LAB	22.06.20	21.08.20		711.474	14.420	697.047	1.453	182.526	0.523	1.976
KFR121 71.04–71.40	ICE	10.06.20	09.08.20	KFR121-ICE	769.367	16.064	753.289	1.432	230.928	0.256	1.688
KFR121 124.60–124.97	ICE	10.06.20	09.08.20		759.225	14.386	744.825	1.417	222.452	0.601	2.018
KFR121 150.25–150.66	ICE	22.06.20	21.08.20		837.982	15.481	822.487	1.420	301.374	0.334	1.754
KFR121 163.83–164.19	ICE	22.06.20	21.08.20		750.320	15.856	734.449	1.420	219.267	0.185	1.605
KFR121 175.42–175.75	ICE	22.06.20	21.08.20		745.403	15.515	729.872	1.410	214.811	0.211	1.621
KFR121 187.58–187.94	ICE	22.06.20	21.08.20		756.455	15.815	740.628	1.445	227.297	0.245	1.690
KFR121 196.40–196.81	ICE	22.06.20	21.08.20		855.992	14.553	841.425	1.412	318.144	0.501	1.913
KFR121 234.33–234.75	ICE	22.06.20	21.08.20		829.318	15.306	814.003	1.413	289.812	0.414	1.827
KFR121 331.38–331.79	ICE	22.06.20	21.08.20		746.675	15.473	731.192	1.475	215.906	0.569	2.044
KFR121 349.57–349.95	ICE	22.06.20	21.08.20		713.838	16.434	697.391	1.431	182.870	0.522	1.953

**Table A4-6. Results of  $\delta^{18}\text{O}$  and  $\delta^2\text{H}$  analyses of isotope diffusive exchange test solutions.**

Sample		Initial $\delta^{18}\text{O}$ TW	Initial $\delta^2\text{H}$ TW	Final $\delta^{18}\text{O}$ TW	Final $\delta^2\text{H}$ TW
		(‰) VSMOW	(‰) VSMOW	(‰) VSMOW	(‰) VSMOW
KFR121 71.04–71.40	LAB	-10.22	-73.8	-9.72	-71.9
KFR121 124.60–124.97	LAB	-10.22	-73.8	-10.77	-78.9
KFR121 150.25–150.66	LAB	-10.22	-73.8	-10.78	-79.0
KFR121 163.83–164.19	LAB	-10.22	-73.8	-10.53	-77.3
KFR121 175.42–175.75	LAB	-10.22	-73.8	-10.62	-77.9
KFR121 187.58–187.94	LAB	-10.22	-73.8	-10.90	-80.5
KFR121 196.40–196.81	LAB	-10.22	-73.8	-10.59	-77.5
KFR121 234.33–234.75	LAB	-10.22	-73.8	-11.29	-83.0
KFR121 331.38–331.79	LAB	-10.22	-73.8	-11.15	-83.2
KFR121 349.57–349.95	LAB	-10.22	-73.8	-10.51	-77.1
KFR121 71.04–71.40	ICE	-32.00	-247.7	-28.58	-221.9
KFR121 124.60–124.97	ICE	-32.00	-247.7	-27.80	-216.3
KFR121 150.25–150.66	ICE	-32.00	-247.7	-28.51	-220.8
KFR121 163.83–164.19	ICE	-32.00	-247.7	-29.68	-230.6
KFR121 175.42–175.75	ICE	-32.00	-247.7	-29.21	-226.7
KFR121 187.58–187.94	ICE	-32.00	-247.7	-29.32	-227.8
KFR121 196.40–196.81	ICE	-32.00	-247.7	-29.03	-225.1
KFR121 234.33–234.75	ICE	-32.00	-247.7	-28.72	-223.4
KFR121 331.38–331.79	ICE	-32.00	-247.7	-26.89	-209.5
KFR121 349.57–349.95	ICE	-32.00	-247.7	-27.30	-212.3

## Out-Diffusion Experiments – Raw Data

**Table A4-7. Raw data of out-diffusion experiments.**

Sample		KFR121 71.04–71.40	KFR121 124.60–124.97	KFR121 150.25–150.66	KFR121 163.83–164.19	KFR121 175.42–175.75
<b>Start experiment</b>		<b>10.06.20</b>	<b>10.06.20</b>	<b>22.06.20</b>	<b>22.06.20</b>	<b>22.06.20</b>
Initial Rock Mass (as received, +/- mountain wet)	g	786.890	776.026	825.508	780.309	788.053
Initial Rock Mass (start experiment)	g	786.890	776.026	825.508	780.309	788.053
Final Rock Mass (resaturated)	g	786.874	776.011	825.559	780.322	788.038
Uptake of water	g	-0.016	-0.015	0.051	0.013	-0.015
Saturation	%	100.002	100.002	99.994	99.998	100.002
Core diameter	cm	4.50	4.49	4.50	4.51	4.50
Core length	cm	18.51	18.7	19.44	18.29	18.43
Volume of Rock sample	cm <sup>3</sup>	294.39	296.09	309.18	292.18	294.42
Density (calculated from volume and mass)	g/cm <sup>3</sup>	2.67	2.62	2.67	2.67	2.68
Mass of Rock (calculated from volume and density)		786.89	776.03	825.51	780.31	788.05
<b>Masses before experiment</b>						
Mass cylinder	g	217.335	215.069	216.704	216.199	214.466
Mass cylinder + core	g	1004.282	991.156	1042.208	996.504	1002.480
Mass cylinder + core + H <sub>2</sub> O	g	1188.825	1178.807	1225.594	1178.664	1179.712
Initial water mass	ml	184.604	187.719	183.381	182.144	177.232
Ratio Exp. Water : Rock		0.235	0.242	0.222	0.233	0.225
<b>End experiment</b>		<b>23.10.20</b>	<b>23.10.20</b>	<b>23.10.20</b>	<b>23.10.20</b>	<b>23.10.20</b>
Final Water Mass (measured, not all recoverable)	ml	171.642	174.638	158.950	170.243	164.485
Time Experiment	days	135	135	123	123	123
<b>Volume of samples for CI-measurements</b>						
Sample A	ml	0.5	0.5	0.5	0.5	0.5
Sample B	ml	0.5	0.5	0.5	0.5	0.5
Sample C	ml	0.5	0.5	0.5	0.5	0.5
Sample D	ml	0.5	0.5	0.5	0.5	0.5
Sample E	ml	0.5	0.5	0.5	0.5	0.5
Sample F	ml	1.5	1.5	1.5	1.5	1.5
Sample G	ml	0.5	0.5	0.5	0.5	0.5
Sample H	ml	0.5	0.5	0.5	0.5	0.5
Sample I	ml	0.5	0.5	0.5	0.5	0.5
Sample K	ml	0.5	0.5	0.5	0.5	0.5
Sample L	ml	0.5	0.5	0.5	0.5	0.5
Sample M	ml	0.5	0.5	0.5	0.5	0.5
Sample N	ml	0.5	0.5	0.5	0.5	0.5
Sample O	ml	0.5	0.5	0.5	0.5	0.5
<b>Total volume subsamples</b>		<b>8.0</b>	<b>8.0</b>	<b>8.0</b>	<b>8.0</b>	<b>8.0</b>

**Table A4-7. Continued.**

Sample		KFR121 187.58–187.94	KFR121 196.40–196.81	KFR121 234.33–234.75	KFR121 331.38–331.79	KFR121 349.57–349.95
<b>Start experiment</b>		<b>10.06.20</b>	<b>10.06.20</b>	<b>22.06.20</b>	<b>23.06.20</b>	<b>23.06.20</b>
Initial Rock Mass (as received, +/- mountain wet)	g	780.832	802.280	799.855	755.140	790.287
Initial Rock Mass (start experiment)	g	780.832	802.280	799.855	755.140	790.287
Final Rock Mass (resaturated)	g	780.849	802.292	799.847	755.104	790.323
Uptake of water	g	0.017	0.012	-0.008	-0.036	0.036
Saturation	%	99.998	99.999	100.001	100.005	99.995
Core diametre	cm	4.50	4.51	4.50	4.51	4.51
Core length	cm	18.28	18.65	18.88	18.07	18.98
Volume of Rock sample	cm <sup>3</sup>	290.73	297.94	300.27	288.67	303.21
Density (calculated from volume and mass)	g/cm <sup>3</sup>	2.69	2.69	2.66	2.62	2.61
Mass of Rock (calculated from volume and density)		780.83	802.28	799.86	755.14	790.29
<b>Masses before experiment</b>						
Mass cylinder	g	213.970	217.193	212.862	212.970	214.532
Mass cylinder + core	g	994.805	1019.412	1012.685	968.097	1004.837
Mass cylinder + core + H <sub>2</sub> O	g	1176.071	1204.043	1200.804	1140.678	1193.137
Initial water mass	ml	184.604	187.719	183.381	182.144	177.232
Ratio Exp.Water : Rock		0.232	0.230	0.235	0.229	0.238
<b>End experiment</b>		<b>23.10.20</b>	<b>23.10.20</b>	<b>23.10.20</b>	<b>23.10.20</b>	<b>23.10.20</b>
Final Water Mass (measured, not all recoverable)	ml	169.384	172.352	175.967	159.846	175.470
Time Experiment	days	123	123	123	122	122
<b>Volume of samples for CI-measurements</b>						
Sample A	ml	0.5	0.5	0.5	0.5	0.5
Sample B	ml	0.5	0.5	0.5	0.5	0.5
Sample C	ml	0.5	0.5	0.5	0.5	0.5
Sample D	ml	0.5	0.5	0.5	0.5	0.5
Sample E	ml	0.5	0.5	0.5	0.5	0.5
Sample F	ml	1.5	1.5	1.5	1.5	1.5
Sample G	ml	0.5	0.5	0.5	0.5	0.5
Sample H	ml	0.5	0.5	0.5	0.5	0.5
Sample I	ml	0.5	0.5	0.5	0.5	0.5
Sample K	ml	0.5	0.5	0.5	0.5	0.5
Sample L	ml	0.5	0.5	0.5	0.5	0.5
Sample M	ml	0.5	0.5	0.5	0.5	0.5
Sample N	ml	0.5	0.5	0.5	0.5	0.5
Sample O	ml	0.5	0.5	0.5	0.5	0.5
<b>Total volume subsamples</b>		<b>8.0</b>	<b>8.0</b>	<b>8.0</b>	<b>8.0</b>	<b>8.0</b>



SKB is responsible for managing spent nuclear fuel and radioactive waste produced by the Swedish nuclear power plants such that man and the environment are protected in the near and distant future.

**skb.se**